

AD A109278

LEVEL

(1)

*General Elec. Co. - Greenville, Ohio*  
OPERATION ACOUSTIC DESIGN TECHNOLOGY

PROJECT \_\_\_\_\_ T.M. NO. 72-349

G. E. CLASS II

TITLE: (ANALYTICAL MODELS FOR NEARFIELD  
JET NOISE CALCULATIONS II

(USAF Contract No. F33615-71-C-1662)

PREPARED BY C.Y. Chen 6/6/72

APPROVED BY P.R. Knott 6/6/72  
DATE

DTIC  
SELECTED  
JAN 6 1982  
H

DISTRIBUTION STATEMENT A  
Approved for public release;  
Distribution Unlimited

81 7 27 088

# TABLE OF CONTENTS

	<u>Page</u>
Table of Contents . . . . .	i
Abstract . . . . .	ii
1. Introduction . . . . .	1
2. Mathematical Formulation . . . . .	3
3. Methods of Calculation . . . . .	7
3.1 Near Field Sound Pressure Prediction Based on Mean Flow and Turbulence Parameters (Detail Aero-Acoustic Method) . . . . .	7
3.2 Near Field Sound Pressure Prediction Based on Velocity Profile (Velocity Profile Method) . . . . .	8
4. Discussion of Results . . . . .	11
4.1 Analytical and Experimental Comparison - Full Scale Jet Engine . . . . .	11
4.2 Analytical and Experimental Comparisons - Scale Model Hot Jets . . . . .	12
4.3 Investigation of Acoustic Models Composing Different Quadrupoles . . . . .	13
4.4 Effect of Initial Turbulence Levels . . . . .	15
4.5 Contour Plots . . . . .	17
5. Summary and Conclusions . . . . .	18
Symbols . . . . .	20
References . . . . .	21
Figures . . . . .	23 - 72

81 7 27 088

# ABSTRACT

Three analytical models for near field noise calculation are formulated for subsonic and supersonic jet flows. Evaluation of these models in comparison with nearfield noise measurements from a full scale jet engine and scale model hot jets is presented. The use of compositions of different quadrupoles as prediction models is demonstrated.

The effect of initial turbulence level on the near noise field was studied by the use of the analytical models. The results of the study indicate that an increase of the turbulence level in the jet exit plane causes an increase in sound pressure level for high frequencies. The effect of the turbulence level is negligible for low frequency sound.

Accession For	
NTIS GPO&I	<input checked="" type="checkbox"/>
DTIC TAB	<input type="checkbox"/>
Unannounced	<input type="checkbox"/>
Justification	<i>Per</i>
<i>FL-182 on file</i>	
By	
Distribution	
Available in	
and/or	
Dist	
<i>A</i>	

## ANALYTICAL MODELS FOR NEARFIELD JET NOISE CALCULATIONS

### 1. Introduction

The intense noise generated from the jet exhaust not only causes annoyance to the general public in the far field but also presents serious problems for health hazard to personnel, and for structural fatigue damage in the immediate vicinity of the exhaust. There have been a great number of investigations for the far sound field of the jet. However, the investigations for the near sound field are relatively few (References 1 to 11). Consequently the near field is far less understood. The lack of knowledge is also due to the more complicated nature of the near sound field which includes not only outwardly propagating waves but also local reciprocated motions and pressure fluctuations.

The near sound field of a jet, for practical purposes, can be considered as a region within twenty to thirty diameters from the jet exhaust nozzle. More precise definitions are the induction near field at distances less than a wave length from the source and the geometric near field at distances from the source that are less than the order of the geometric extent of the source. In many situations, both induction and geometric near fields overlap each other and for practical purposes a region within 20 to 30 diameters from the jet exhaust includes both types of near field.

The near and far sound field of a jet display quite different properties. For example, the familiar far-field sound pressure dependence on the inverse square of distance and the simple relationship between the sound pressure and intensity  $I = P^2 / \rho_0 a_0$  are no longer valid for the near field. In the far field, the distances from the observation point to different parts of the source distribution in the jet flow field are approximately the same. In the near field, the spatial distribution of sources along the jet flow becomes extremely important because distances are different from different parts of the jet flow to the observer.

Experimental investigations (References 1 to 5) have provided some useful information on the sound pressure spectra and constant sound pressure contours

of the near noise field of jets under particular operating conditions. To predict near noise field, there exist semi-empirical methods based on near-field noise measurement from full scale jet engines (Reference 6) and based on tests from scale model hot jets (Reference 5). These methods may give crude estimates for the near noise field of a jet. However, there is definitely the lack of basic understanding of the near noise field and therefore, the lack of an accurate prediction procedure.

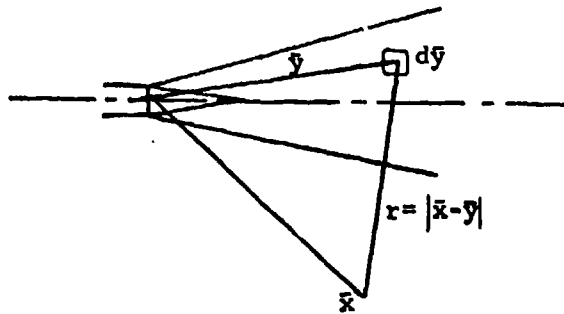
The present investigation is an attempt to formulate an analytical prediction method for the near noise field of a jet based on the fundamental characteristics of the quadrupole distributions explored by Franz (Reference 7). Within the limitation of the quadrupole theory, the present study is restricted to subsonic and supersonic jet flows without shock waves. The other noise generation mechanisms for supersonic flow such as shock wave and Mach wave are not considered here.

## 2. Mathematical Formulation

Starting from Lighthill's fundamental solution to the inhomogeneous wave equations governing the distribution of quadrupoles, the density fluctuations  $\rho(\bar{x}, t)$  at time  $t$  and point  $\bar{x}$  in the medium outside of a turbulent region can be written as

$$\rho(\bar{x}, t) = \frac{1}{4\pi c_0^2} \int \frac{\partial^2}{\partial x_i \partial x_j} \frac{T_{ij}(\bar{y}, t - r/c_0)}{r} d\bar{y} \quad (1)$$

where  $T_{ij}(\bar{y}, t - r/c_0)$  is the quadrupole strength per unit volume at the retarded time  $t - r/c_0$  and at  $\bar{y}$  in the turbulent region. (See sketch below)



By using the relation between density fluctuations and pressure fluctuations  $p = c_0^2 \rho$ , and carrying out the double differentiation, the instantaneous sound pressure due to the distribution of quadrupoles becomes

$$p(\bar{x}, t) = \frac{1}{4\pi} \int \left[ \frac{r_j r_l}{r^2} \left( \frac{\ddot{T}_{ij}}{rc_0^2} + \frac{3\dot{T}_{ij}}{r^2 c_0} + \frac{3T_{ij}}{r^3} \right) - \delta_{ij} \left( \frac{\dot{T}_{ij}}{r^2 c_0} + \frac{T_{ij}}{r^3} \right) \right] d\bar{y} \quad (2)$$

where  $r_{ij} = x_i - y_j$ ,  $\delta_{ij}$  is the Kronecker delta and dots denote partial differentiation with respect to time. In this form, the far-field (or radiation field) sound pressure term in  $\ddot{T}_{ij}/r$ , the "induction near-field" sound pressure terms in  $\dot{T}_{ij}/r^2$  and the terms in  $T_{ij}/r^3$  for the "transition region" are explicitly displayed. In the far-sound field, where the distance  $r$  is large compared with the wave length, the term  $\ddot{T}_{ij}/r$  dominates and the remaining terms are negligible. In the near-sound field, however, all the terms are to be retained.

Under the assumptions that the turbulence is essentially steady and the distance  $r$  is large compared to the eddy size, Franz (Reference 7) shows that the mean-square sound pressures due to the distribution of different types of quadrupoles can be written in terms of the radiated acoustic power  $P$  as:

$$\overline{p^2} = \frac{\rho_o c_o P}{4\pi r^2} (15 \sin^2 \theta \cos^2 \theta \cos^2 \phi) \left( 1 + 3 \frac{c_o^2}{r^2 \omega^2} + 5 \frac{c_o^4}{r^4 \omega^4} \right) \quad (3)$$

for lateral quadrupole,

$$\begin{aligned} \overline{p^2} = \frac{\rho_o c_o P}{4\pi r^2} (5 \cos^4 \theta) & \left[ 1 + \frac{c_o^2}{r^2 \omega^2} \left( 3 - \frac{4}{\cos^2 \theta} + \frac{1}{\cos^4 \theta} \right) \right. \\ & \left. + \frac{c_o^4}{r^4 \omega^4} \left( 9 - \frac{6}{\cos^2 \theta} + \frac{1}{\cos^4 \theta} \right) \right] \end{aligned} \quad (4)$$

for longitudinal quadrupole, and

$$\overline{p^2} = \frac{\rho_o c_o P}{4\pi r^2} \left( 1 + 2 \frac{c_o^2}{r^2 \omega^2} + 12 \frac{c_o^4}{r^4 \omega^4} \right) \quad (5)$$

for quadrupole radiation from isotropic turbulence.

These expressions were obtained based on a small flow velocity so that the effect of source convection do not appear. For non-negligible convection speed, the correct expressions can be written as (Appendix C of Reference 7)

$$\begin{aligned} \overline{p^2} = & \frac{\rho_o c_o P}{4\pi r^2} (15 \sin^2 \theta \cos^2 \phi) \left\{ \cos^2 \theta + \frac{c_o^2}{r^2 \omega^2} (3 Q^2 \cos^2 \theta - 6 M_c Q \cos \theta \right. \\ & \left. + 4 M_c^2) + \frac{c_o^4}{r^4 \omega^4} (9 Q^4 \cos^2 \theta - 18 M_c Q^3 \cos \theta + 9 M_c^2 Q^2) \right\} C^{-5} \end{aligned} \quad (6)$$

for lateral quadrupole,

$$\begin{aligned} \overline{p^2} = & \frac{\rho_o c_o P}{4\pi r^2} \left\{ \cos^4 \theta + \frac{c_o^2}{r^2 \omega^2} [3 Q^2 \cos^4 \theta - 12 M_c Q \cos^3 \theta \right. \\ & - (4 - 9 M_c^2) \cos^2 \theta + 6 M_c \cos \theta + 1] + \frac{c_o^4}{r^4 \omega^4} [9 Q^4 \cos^4 \theta \\ & - 36 M_c Q^3 \cos^3 \theta - 6(1 - 9 M_c^2) Q^2 \cos^2 \theta \\ & \left. + 12(1 - 3 M_c^2) Q M_c \cos \theta + (1 - 3 M_c^2)^2] \right\} C^{-5} \end{aligned} \quad (7)$$

for longitudinal quadrupole,

$$\overline{p^2} = \frac{\rho_o c_o P}{4\pi r^2} \left( 1 + 2 \frac{c_o^2}{r^2 \omega^2} + 12 \frac{c_o^4}{r^4 \omega^4} \right) C^{-5} \quad (8)$$

for quadrupole radiation from isotropic turbulence, where

$$C = [(1 - M_c \cos \theta)^2 + \left(\frac{\omega l}{c_0}\right)^2]^{1/2}$$

$$Q = \frac{1 - M_c}{[(1 - M_c \cos \theta)^2 + \left(\frac{\omega l}{c_0}\right)^2]^{1/2}}$$

The factor C used here which is obtained by Ffowcs Williams (Reference 13) for high-speed flow replaces Franz' original form  $1 - M_c \cos \theta$ . The convection factors  $C^{-5}$  in Equations (6) and (7) also replace  $C^{-6}$  of Franz' forms to account for the increased number C of eddies whose sound arrives at the field point simultaneously (Reference 14). It is easy to see when  $M_c$  is small compared to unity, both C and Q approach unity and Equations (6), (7), and (8) reduce to Equations (3), (4), and (5). Thus, Equations (6) to (8) are valid for both low-speed and high-speed flows.

Applications of the above theoretical results to predict the near noise field of a jet require further approximation of the quantities involved which will be discussed in the next section.

### 3. Methods of Calculation

The mean square sound pressures given above can be considered as contributions due to unit volume of jet flow. The idealized structure of a turbulent jet may be divided into several regions. The initial region consists of a potential core enclosed by a mixing region of strong shear. Downstream of it are the transition region and the fully developed turbulent region. Different parts of the jet may be considered to generate sound by different types of quadrupoles. In the present investigation, each type of quadrupole is considered as an acoustic model for prediction, assuming the entire jet flow represented by one type of quadrupole. This is followed by investigation of compositions of different quadrupoles for different parts of the jet.

The utility of the theoretical results given in Section 2 depends on the ability to estimate the quantities involved in the equations. The following are two methods for carrying out the computation.

#### 3.1 Near Field Sound Pressure Prediction Based on Mean Flow and Turbulence Parameters (Detail Aero-acoustic Method)

To express the near-field sound pressure in terms of mean flow and turbulence parameters throughout the entire jet flow, the following approximations are made:

$$\omega = 1.1 u' / l \quad (9)$$

$$P = \beta_1 \frac{\rho^2 u'^4 U^4}{\rho_0 c_0^5 l} \quad (10)$$

where  $l$  is the scale of turbulence,  $\beta_1$  the proportional constant,  $u'$  and  $U$  the rms value of the fluctuation velocity and mean flow velocity respectively. The approximation (10) for the radiated sound power per unit volume of jet has been shown to be a good representation (Reference 15). When  $\theta$  is measured from the exhaust axis of a circular jet and when the observation point is at least several jet diameter from the jet, the term  $\cos^2 \phi$  in (6) may be replaced by its average value, namely  $1/2$ , and the  $r$  value can be approximated by:

$$r = \sqrt{(X-x)^2 + (Y-y)^2}$$

where  $(X,Y)$ ,  $(x,y)$  are coordinates for the observation and source positions respectively,  $X$  and  $x$  being distances from jet exit along jet axis and  $Y,y$  being radial distances. Thus, the sound pressure observed at  $(X,Y)$  can be obtained by integrating over the source coordinates  $(x,y)$ , (for details, see Reference 15).

### 3.2 Near Field Sound Pressure Prediction Based on the Mean Velocity Profile (Velocity Profile Method)

Another approach, for the near field sound pressure prediction, based on the mean velocity profile only will be described below. Two basic assumptions are made. The first assumption is that the radiated acoustic power obeys Lighthill's eighth power law

$$P \sim \frac{\rho_o U^8}{c_o^5 l} \quad (11)$$

for unit volume of jet. The second assumption is that the radiated sound frequency  $\omega$  satisfies the empirical sound source-location relationship:

$$\frac{fD}{U_o} = \left( \alpha \frac{x}{D} \right)^{-\beta} \quad (12)$$

where

$$f = \omega/2\pi$$

$\alpha$ ,  $\beta$  are empirical constants ( $\alpha \doteq 1.22$   $\beta \doteq 1.25$ , for conical nozzles, see References 1 and 12).

The mean-square sound pressure due to per unit length of jet can be written, for the case of isotropic turbulence, as

$$\frac{d \bar{p}^2}{dx} \sim \frac{\rho_o^2}{4\pi c_o^4} \int \frac{U^8}{r^2 l} \left( 1 + 2 \frac{c_o^2}{r^2 \omega^2} + 12 \frac{c_o^4}{r^4 \omega^4} \right) C^{-5} da(x) \quad (13)$$

where  $a(x)$  is the cross-section area of the jet at  $x$ ,  $C$  is the convection factor:

$$C = [(1 - M_c \cos \theta)^2 + \eta M_c^2]^{1/2}$$

$$M_c = \xi U/c$$

$$l \sim x$$

where  $\eta$  and  $\xi$  are experimental constants.

Since

$$\frac{d \bar{p}^2}{df} = \frac{d \bar{p}^2}{dx} \frac{dx}{df}$$

the mean-square sound pressure per unit frequency becomes

$$\frac{d \bar{p}^2}{df} = K \frac{\rho_o^2}{4\pi c_o^4} \frac{1}{Bf} \int_0^{r_j} \frac{U^8}{r^2} \left( 1 + 2 \frac{c_o^2}{r^2 \omega^2} + 12 \frac{c_o^4}{r^4 \omega^4} \right) \bar{C}^5 2\pi y dy \quad (14)$$

for a circular jet,  $r_j$  being the distance from the jet axis to the jet edge.  
In non-dimensional form:

$$\frac{\frac{d}{f} \frac{p^2}{U_o^8}}{\left(\frac{fD}{U_o}\right)} = \frac{1}{\beta \left(\frac{fD}{U_o}\right)} \int_0^{2r_j/D} \frac{\tilde{U}^8}{\tilde{r}^2} \left(1 + 2 \frac{c_o^2}{r^2 \omega^2} + 12 \frac{c_o^4}{r^4 \omega^4}\right) \tilde{C}^5 2\pi \tilde{y} d\tilde{y} \quad (15)$$

where:

$$\begin{aligned} \tilde{U} &= U/U_o & \tilde{x} &= x/D & \tilde{X} &= X/D \\ \tilde{r} &= r/D & \tilde{y} &= 2y/D & \tilde{Y} &= Y/D \end{aligned}$$

Equation (15) represents the non-dimensional mean-square sound pressure per unit frequency in terms of the mean velocity profile for the case of isotropic turbulence. For lateral and longitudinal quadrupoles, similar expressions can be obtained.

#### 4. Discussion of Results

Correlations of the theoretical results and the experimental data will be reported in this section. Applications of the analytical models obtained in Section 2 to predict near-field sound pressure levels of full scale jet engines and scale model hot jets will be discussed. Predicted effect of initial turbulence levels at the jet exit plane on the near noise field will also be demonstrated.

Of the two methods of calculation discussed in Section 3, the method based on mean flow and turbulence parameters (Section 3.1) was used for the majority the calculations. The more simple method of calculation based on the mean velocity profile (Section 3.2) has given compatible results to the detail aero-acoustic method, however, the effects of turbulence intensity could not be accounted for explicitly in this model. In Figures 1 and 2 the two methods of computation are seen to yield similar prediction trends for both subsonic and supersonic jet flows.

##### 4.1 Analytical & Experimental Comparisons - Full Scale Jet Engine

A detailed analytical and experimental comparisons of sound pressure spectra for a full-scale GE4 engine were obtained at a typical take-off condition of SST and B1 aircraft with a jet exit Mach number of 1.46, a velocity of 3300 feet per second, a total temperature of 3000° R. For the near field acoustic predictions an assumed initial turbulence level of 15% was used.

The experimental arrangement of the twenty-seven near-field microphone locations (all within twenty jet nozzle diameters) are shown in Figure 3. The measured sound pressure level spectra at all microphone locations shown as circles in Figures 4(a) through 4(n). The curves shown in each Figure are the three analytical predictions - the quadrupole radiation from isotropic turbulence and the lateral and longitudinal quadrupoles. These spectrum curves show that at certain locations, one particular model may compare better with the measurements than the others. A close examination of the results reveals that in the jet exit plane (at microphone locations 2, 8, 15) the isotropic turbulence model follows well the data trend and with comparable sound level magnitudes. In fact, the isotropic turbulence model predicts the spectrum

shapes quite well at all the microphone locations. In general, the isotropic turbulence model overpredicts at the locations with angles to the jet axis less than  $90^\circ$ , and underpredicts at the locations with angles to the jet axis greater than  $90^\circ$  (i.e., microphones 3, 4, 5, 6, 9, 10, 11, 12, 16, 17, 18, 19, 20).

For the microphone locations along the jet exhaust plume, such as microphones 22 through 27, the longitudinal quadrupole model appears to be the best prediction. It is interesting to see that the spectrum shapes and the frequency peaks are well predicted by both the longitudinal and the lateral quadrupoles at microphones 23, 24, 26, 27 which are located 12 to 20 diameters downstream of the nozzle exit. However, at these locations the lateral quadrupole tends to overpredict the peak SPL while the longitudinal quadrupole underpredicts slightly. At locations closer to the jet exit plane (i.e., microphone 22 and 25 which are within 8 diameters from jet exit) the predicted spectrum peaks from both the quadrupole models wrongly shift to the lower frequencies while the spectrum decay rate at higher frequencies remains valid.

It is worthwhile to note that the large jumps of measured sound pressure level of 10 dB or more across the 1/3 octave band centered at 160 Hz occur at several locations (microphones 3, 4, 5, 6, 10, 11, 12, 19, 20). The model scale near-field measurements at G.E. obtained recently (Reference 16) has shown shock noise contributions to near-sound field to be of this order at these locations. The current acoustic near-field models do not account for shock noise effects, but it is expected that appropriate corrections for shock noise could be incorporated into the current model.

#### 4.2 Analytical & Experimental Comparisons - Scale Model Hot Jets

Near-field noise measurements of scale model hot jets conducted recently at G.E. (Reference 16) were obtained at 10 microphone locations (Figure 5). A typical shock-free supersonic data ( $M = 1.3559$ ,  $T_t = 2407^\circ \text{ R}$ , Reading 4, see Chapter IV of Reference 16), was used for comparisons with the three analytical acoustic models. For the model scale predictions an initial turbulence level of 5 percent was assumed. Typical results are presented in Figures 6(a) to (e). The isotropic turbulence model predicts well the SPL magnitudes and spectrum shapes in the jet exit plane (microphones 6 and 9) and locations upstream (microphones 7 and 10). In fact, the spectrum shapes are predicted quite well at all locations by the isotropic turbulence model,

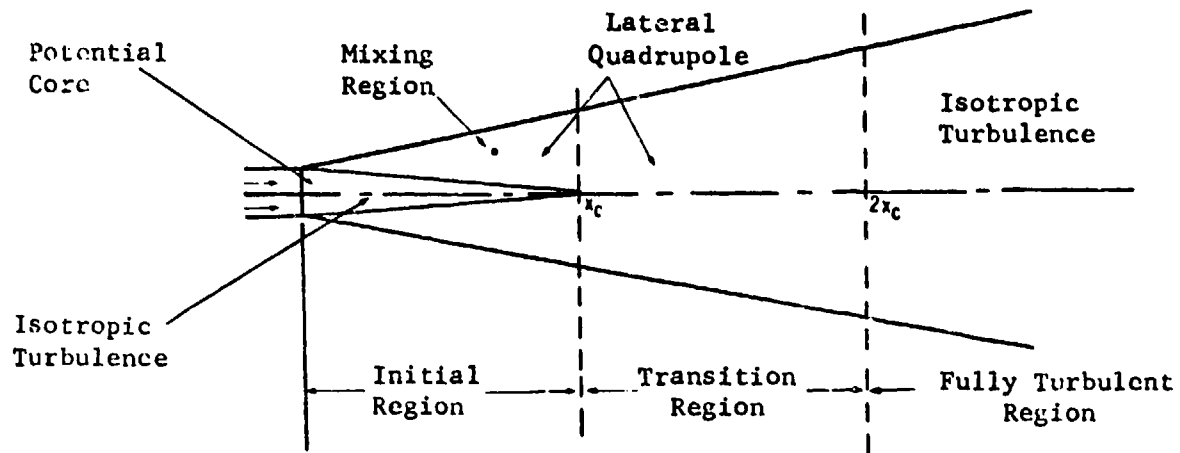
over-predicting at locations downstream of the nozzle exit and underpredicting upstream of it. Both lateral and longitudinal quadrupole models predict the peak frequency in the spectrum and the rate of decay in the high frequency range at locations farther downstream of the nozzle exit (microphones 1, 3 and 4) while only the longitudinal quadrupole model gives comparable sound pressure levels. At locations close to the jet plume, within 10 diameters from the nozzle exit (microphones 2 and 5), all three models overpredict the peak sound pressure levels. These observations essentially confirm the findings given in Subsection 4.1 where the full scale GE4 engine acoustic data was used to compare with the predictions.

#### 4.3 Investigation of Acoustic Models Composing Different Quadrupoles

Each of the three analytical models discussed in Section 2 has been evaluated by comparing with measurements (see sub-section 4.1 and 4.2). In order to improve the predictions obtained by the use of individual models, composite acoustic models were considered. The structure of a turbulent jet is divided into several regions: the initial region (consisting of a potential core enclosed by a mixing region of strong shear), the transition region, (just downstream of the potential core) and the fully turbulent (or similarity) region. Different parts of the jet may be considered to generate sound by different acoustic sources. The following are two preliminary composite acoustic models which were examined in this study.

##### Composite Acoustic Model I

The isotropic turbulence model is used in the potential core and the fully turbulent region (see sketch below). The lateral quadrupole which is usually considered to be predominant in any region with large mean shear is used in the mixing region enclosing the potential core and in the transition region which is approximately one core length downstream of the potential core.



#### Composite Acoustic Model II

The lateral quadrupole is used in the mixing region and the isotropic turbulence model is used elsewhere of the jet flow.

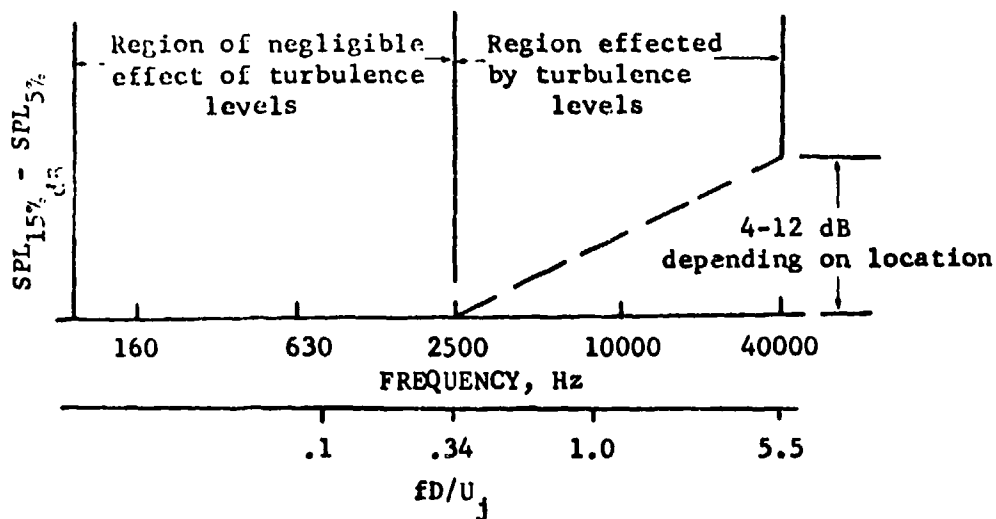
The predictions with these two composite acoustic models were obtained for a supersonic jet of Mach number  $M = 1.3559$ ,  $T_t = 2407^\circ \text{ R}$ , and an assumed value of  $u'/U_j = .05$ . The results are given in Figures 7(a) through (e). The prediction by composite acoustic model I (represented by solid lines) was found to be almost the same as that given by the lateral quadrupole model, except at low frequencies ( $f < 1000 \text{ Hz}$ ) where the isotropic turbulence model is dominant. For the composite acoustic model II, (represented by dashed lines) the isotropic turbulence model is seen to be dominant for frequencies below 2500 Hz. Although a great improvement in near-field prediction was not obtained by the new models examined, this study clearly demonstrates the possibility of changing the acoustic characteristics by the change of the composition of the quadrupole models, and that improvements to the predictions are possible through a properly selected model.

#### 4.4 Effect of Initial Turbulence Levels

##### Scale Model Hot Jet

In order to investigate the effect of the initial turbulence levels on the near-field noise, the predictions were performed (for the same jet flow conditions as discussed in Subsection 4.2;  $M = 1.3559$ ,  $T_t = 2400^\circ \text{ R}$ ), except at an assumed turbulence level of 15% instead of 5%.

Figures 8(a) through (e) show the predicted results with an assumed 15 percent initial turbulence intensity at the jet exit. It is generally expected that the higher the turbulence level in the jet flow the greater the sound pressure level it produces. Comparing the SPL spectra at the corresponding microphone locations (e.g. Figure 6(a) comparing with Figure 8(a)) one sees that the higher turbulence level (15%) produces the greater SPL only for high frequencies. A negligible effect of initial turbulence levels on SPL was found for frequencies lower than 2500 Hz (or  $fd/U_j < 0.34$ ). The effect on higher frequency SPL is more pronounced as the frequency increases. The sketch below gives a rough idea how SPL changes with turbulence level and with frequency.



From the above sketch the maximum increase in SPL ( $u'/U_j = 15\%$  compared with 5%) is seen to vary from 4 to 12 dB, depending on microphone locations. At locations close to the jet exit and immediately downstream of it (microphones 5, 6, 8 and 9), the effect of initial turbulence is very strong (10-12 dB). Since at these locations the high frequency sound either dominates or becomes important with almost a flat spectrum curve in the high frequencies, the effect of turbulence level is certainly not negligible. For the locations far from the jet exit (microphones 1, 2, 3, 4), the effect of the initial turbulence level on the overall sound pressure seems to be minimal.

#### Full Scale Engine

The effect of turbulence level for a full scale GE4 engine at 18 near-field microphone locations was also examined. (See Figure 3 for microphone arrangement). For the six microphone locations along the jet plume, the longitudinal quadrupole model was chosen to calculate the SPL spectra. Figure 9(a) through (c), the predictions (the solid lines are calculated with an assumed turbulence level  $u'/U_j = .15$ , the dashed lines with  $u'/U_j = .05$ ) compared with the measurements are shown. At these locations, the effect of turbulence level is seen to be minimal except for high frequencies ( $f > 2000$  Hz or  $fd/U_j > 2.3$ ). In general, the predictions are in good agreement with the observed data, except at two locations (microphone #22 and 25) close to the jet plume where in the low frequency spectra the predictions deviate from the data.

Predictions with the isotropic turbulence model with the assumed turbulence levels of 5 and 15 percent (i.e.  $u'/U_j = .05$  and  $.15$ ) at microphone locations 1 through 12 are shown in Figure 9(d) to (i). The increase of turbulence level is seen to increase the sound pressure levels for these locations at all frequencies. In the case of a smaller jet (diameter = 4.55 inches) the effect of turbulence level is negligible for frequencies below 2500 Hz as discussed above. Since a more meaningful frequency parameter may be the Strouhal number  $fd/U_j$ ;  $fd/U_j = .34$  from the smaller jet would correspond to  $f \sim 300$  Hz for the full scale engine, below which the effect of turbulence may be negligible. Thus, the effect of turbulence is seen to be more important for almost all frequencies for a full scale jet engine.

#### 4.5 Contour Plots

Due to the complicated nature of the near jet noise field, the sound pressure distributions in the vicinity of the jet exhaust can be best visualized on the contour plots. Several contour plots were obtained (Figures 10 through 17) using General Electric's automatic computation system with a CALCOMP plotter and compared with the jet engine data described in Subsection 4.1 and 4.4. In Figure 10, the measured OASPL's are shown at each microphone location together with the constant SPL contours. The corresponding predictions from the three acoustic models are shown in Figures 11 to 13. The isotropic turbulence model is seen to predict well the contour shapes. The OASPL magnitudes are well predicted close to  $90^\circ$  from jet axis; it overpredicted (4 to 10 dB) downstream of the nozzle exit, and it underpredicted (4 to 7 dB) upstream of the nozzle exit. Although the lateral and longitudinal quadrupole models (Figure 12 and Figure 13) fail to predict the overall contour shapes, it is interesting to note that the lateral quadrupole model shows the same peculiar loop as the measurements around  $X/D = 7.5$ ,  $Y/D = 10$ .

In Figures 14 through 17, four more contour plots for 1/3 octave SPL's are presented. If the sound source for a particular frequency band is considered to be located where the maximum sound pressure occurs, the source location for these particular bands can be obtained approximately.

They are:

$X/D = 14$	for 1/3 octave band centered at 100 Hz
$X/D = 8$	for 1/3 octave band centered at 400 Hz
$X/D = 5$	for 1/3 octave band centered at 1600 Hz
$X/D = 3$	for 1/3 octave band centered at 6300 Hz

This shows that the high frequency sound is generated close to the nozzle exit and the low-frequency sound is generated further downstream.

## 5. Summary and Conclusions

Three analytical models for near field noise prediction have been formulated for subsonic and supersonic jet flows. These analytic acoustic models have been fully evaluated with near field measurements from full scale engine and scale model hot jets (with the emphasis on the supersonic jet flows). The use of a spatial composition of quadrupoles as a prediction model has also been demonstrated. The near noise field of the jet is very complicated because it includes not only outwardly propagating waves but also local reciprocated motions and pressure fluctuations. In spite of this complicated nature, the present investigation has shown a good deal of success in predicting near-field noise on a spectral basis as well as on an overall SPL basis.

From the experimental and analytical comparisons of sound pressure level spectra for supersonic jet flows, the important findings are:

- (1) In general, the isotropic turbulence model predicts well the sound pressure spectrum shapes. It predicts the sound pressure levels quite well in the nozzle exit plane and for most angular positions downstream of the nozzle ( $\theta < 90^\circ$ ); the model underpredicts at angular positions upstream of it ( $\theta < 90^\circ$ ; where shock waves are known to influence the sound levels but were not taken into account in the present prediction model).
- (2) Both the lateral and the longitudinal quadrupole models predict the spectrum shapes and peak noise frequencies at locations with angles to the jet axis less than  $45^\circ$ . The longitudinal quadrupole model gives the best level comparisons at these locations.
- (3) At locations close to  $135^\circ$  from jet axis, all three acoustic models give good correlations with experimental data. The longitudinal model is seen to be the best.
- (4) At locations with angles to the jet axis less than  $45^\circ$  and within a distance of 10 diameters from jet exit, all three models overpredict the peak noise levels but the longitudinal quadrupole model agrees very well in the upper frequency spectrum with measurements.

The predicted effect of initial turbulence level on the near field noise shows that the increase of the turbulence level in the jet exit plane causes the increase in sound pressure level for high-frequency range of the spectrum. The effect of turbulence level is negligible for low frequencies. This can be explained by noting that the change of initial turbulence level of the jet has strong effects on the flow field in the initial mixing region where the high-frequency sound is generated and has little effects on the flow field further downstream where the low-frequency sound is generated.

A preliminary investigation for acoustic models composing different quadrupoles for different parts of the jet flow demonstrates the possibility of improvement in the near field jet noise prediction by various compositions of the quadrupole models.

The present analysis does not take into account the noise contribution due to the presence of shock waves from which the shock tones and shock-related broad band noise originate. To obtain a practical prediction method for near-noise field in which shock waves are usually present, screech and shock-turbulence interaction must be accounted for.

It is recommended that further investigation of near-field noise be directed to the following:

- (1) Composition of different acoustic models for different parts of the jet flow should be studied to obtain a more reliable prediction method.
- (2) Measurements of various turbulence levels at jet exit plane be obtained in conjunction with near field noise data so that the effect of turbulence level on near noise field can be ascertained.
- (3) Shock-wave contributions to the near-field noise should be more closely studied and their contributions should be accounted for in near-field and far-field acoustic models.

## DEFINITION OF SYMBOLS

### Symbols

$c_o$	Ambient speed of sound
$C$	Convection factor $C = [(1-M_c \cos \theta)^2 + (\frac{\omega l}{c_o})^2]^{1/2}$
$D$	Jet exit diameter
$f$	Frequency, cps or Hz
$K$	Empirical constant, Equations (14-15)
$l$	scale of turbulence
$M_c$	Convection Mach number $M_c = .63 U/c_o$
$P$	Sound pressure
$P$	Radiated sound power
$Q$	$Q = (1-M_c)/[(1-M_c \cos \theta)^2 + (\frac{\omega l}{c_o})^2]^{1/2}$
$r$	Distance from source point to observation point, $r =  \bar{x} - \bar{y} $
$t$	Time
$T_{ij}$	Strength of quadrupole or instantaneous 'Reynolds stress' $T_{ij} = \rho V_i V_j + p_{ij} - C_o \rho \delta_{ij}$ , $V_i$ being the velocity components, $p_{ij}$ the stress between adjacent elements of gas
$U$	Local mean velocity
$U_o$	Mean velocity at jet exit
$u'$	fluctuating velocity
$x_i$	Component of observation point vector $\bar{x}$ , $i = 1, 2, 3$
$y_i$	Component of source point vector $\bar{y}$ , $i = 1, 2, 3$
$\alpha$	Empirical constant in Equation (12)
$\beta$	Empirical constant in Equation (12)
$\beta_1$	Proportional constant
$\theta$	Angle with jet exhaust axis
$\rho$	Gas density
$\phi$	Azimuth angle in spherical polar coordinates
$\omega$	Radian frequency ( $\omega = 2 \pi f$ )

## References

1. Howes, Walton L., Callaghan, Edmund E., Coles, Willard D. and Mull, Harold R.: "Near Noise Field of a Jet-Engine Exhaust." NACA Rept. 1338, 1957 (Supersedes NACA TN's 3763 and 3764)
2. Wolfe, M.O.W.: "Near Field Jet Noise." Report 113, NATO AGARD. April-May 1957.
3. Hermes, P.H. and Smith, D.L.: "Measurement and Analyses of the J57-P21 Noise Field," AFFDL-TDR-66-147, 1967.
4. Morgan, L.C., Sutherland, and K.J. Young, "The Use of Acoustic Scale Models for Investigating Near Field Noise of Jet and Rocket Engines," WADD TR-61-178, April 1961.
5. Plumblee, H. E., Ballentine, J.R., and Passinas B., "Near Field Noise Analyses of Aircraft Propulsion Systems with Emphasis on Prediction Techniques for Jets," WADC-TR-58-343, August 1967.
6. Franken, Peter A., and Kerwin, E.M. Jr., "Methods of Flight Vehicle Noise Predictions," WADC-TR-58-343, November 1958.
7. Franz, G. J., "The Near-Sound Field of Turbulence," David Taylor Model Basin, Report 986, AD 630684, October 1959.
8. Dahlen, H., "Über Akustische Nahfelder von Triebwerksstrahlen," (On Near Acoustic Field of Jets), Jahrbuch 1962 der WGLR, Wissenschaftlichen Gesellschaft für Luftfahrt, Braunschweig, West Germany.
9. Lassiter, L.W. and Hubbard, H. H., "The Near Noise Field of Static Jets and Some Model Studies of Devices for Noise Reduction." NACA Rept. 1261 1956.
10. Ollerhead, J.B., "On the Prediction of the Near Field Noise of Supersonic Jets," NASA CR-857, August 1967.
11. Eldred, K.M., et al., "Suppression of Jet Noise with Emphasis on the Near Field," TR-ASD-TDR-62-578, Flight Dynamics Laboratory, Wright-Patterson AFB, Ohio, 1953.

12. Lee, R., et al., "Research Investigation of the Generation and Suppression of Jet Noise," General Electric Company, Flight Propulsion Laboratory, January, 1961.
13. Ffowcs Williams, J.E., "The Noise from Turbulence Convected at High Speed," Proc. Royal Soc. A255, pp. 469-503, 1953.
14. Ffowcs Williams, J.E., "Some Thoughts on the Effect of Aircraft Motion and Eddy Convection on the Noise from Air Jets," Univ. Southampton Aero. Astro. Rept. No. 155, 1960.
15. Benzakein, M.J., Chen, C.Y., Knott, P.R., "A Computational Technique for Jet Aerodynamic Noise," AIAA 4th Fluid and Plasma Dynamics Conference, Palo Alto, California, June 21-23, 1971.
16. Benzakein, M.J. and Knott, P.R., "Supersonic Exhaust Noise Velocity Model", Technical Report for AFAPL/TBC, General Electric Company, Evendale, Ohio, May, 1972. (To be released).

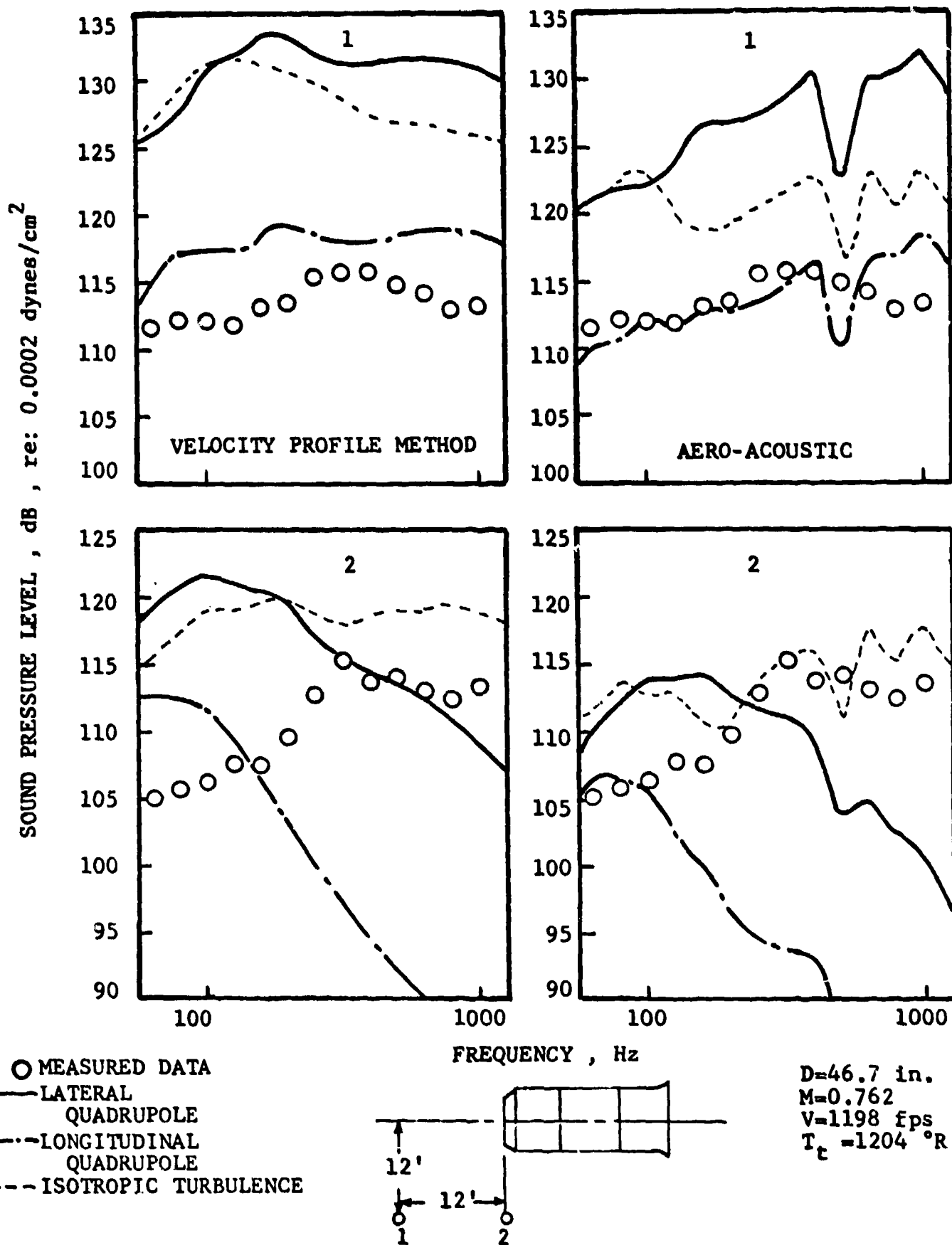


FIGURE 1 - 1/3 OCTAVE BAND FREQUENCY SPECTRA  
COMPARISON OF PREDICTION AND MEASUREMENTS

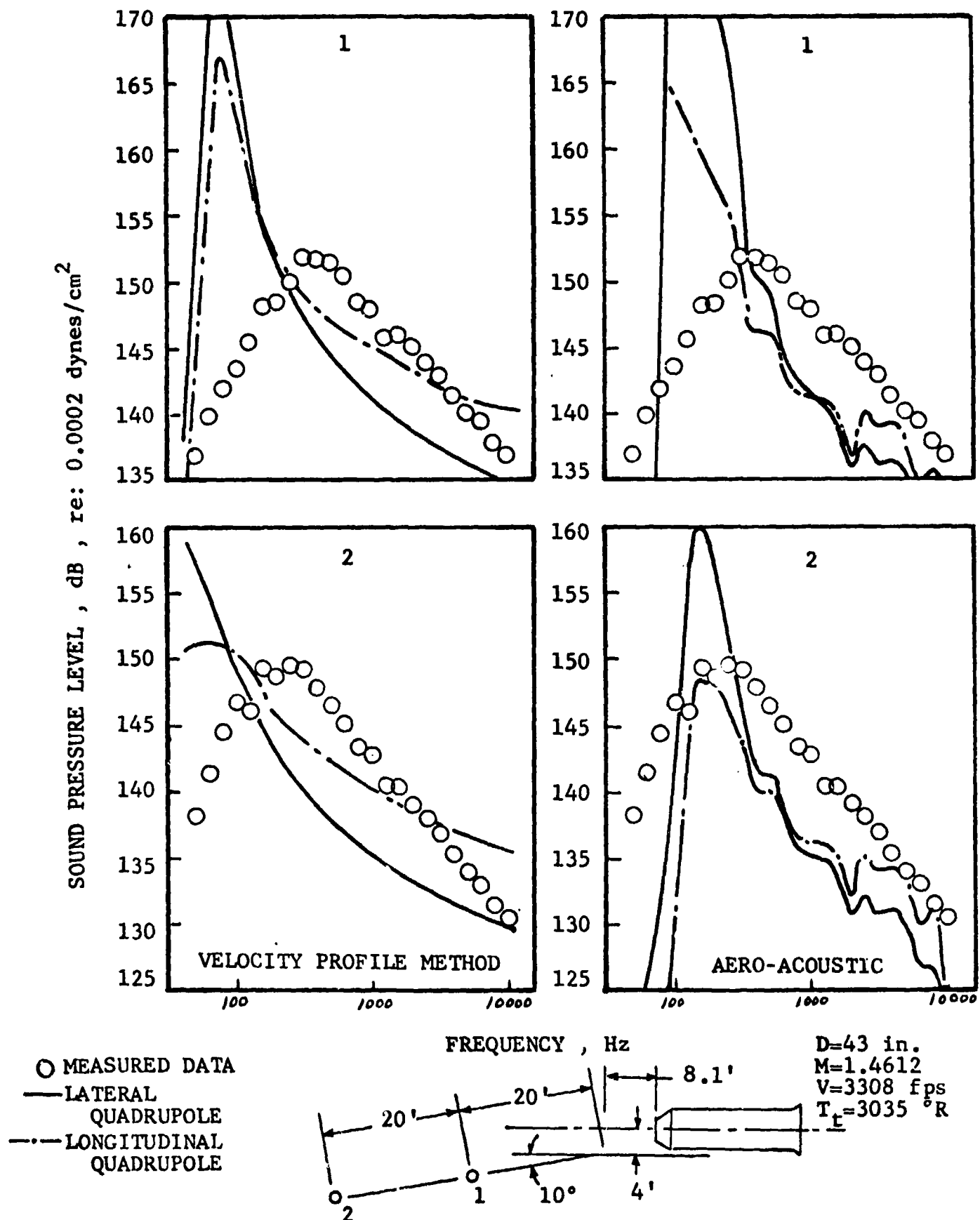
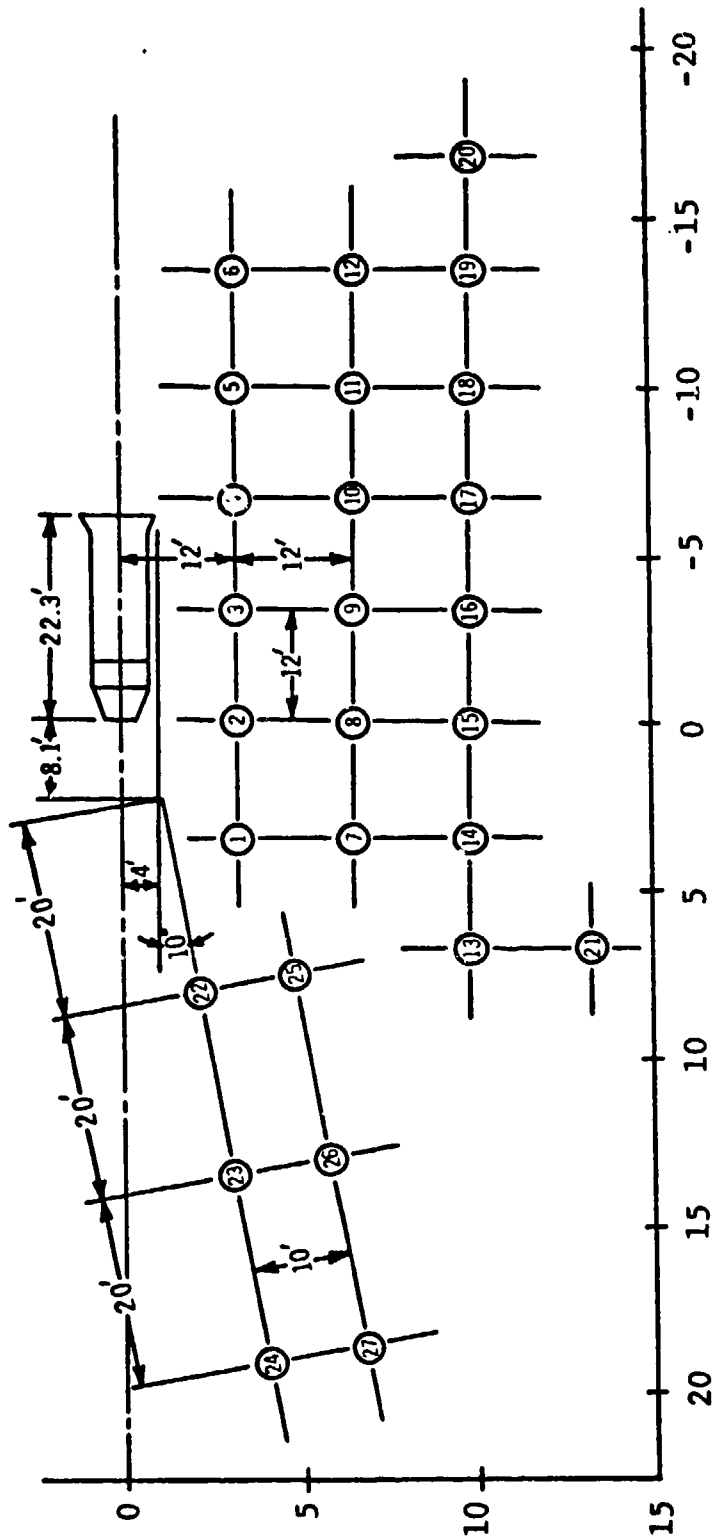


FIGURE 2 -

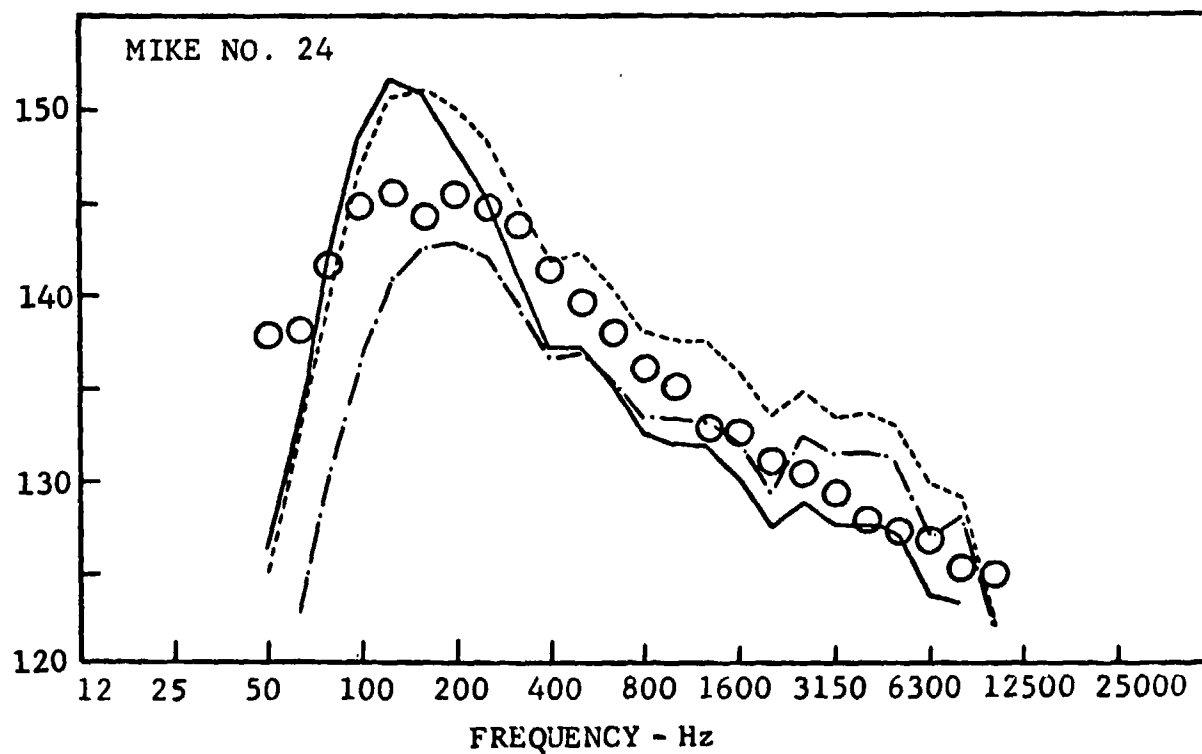
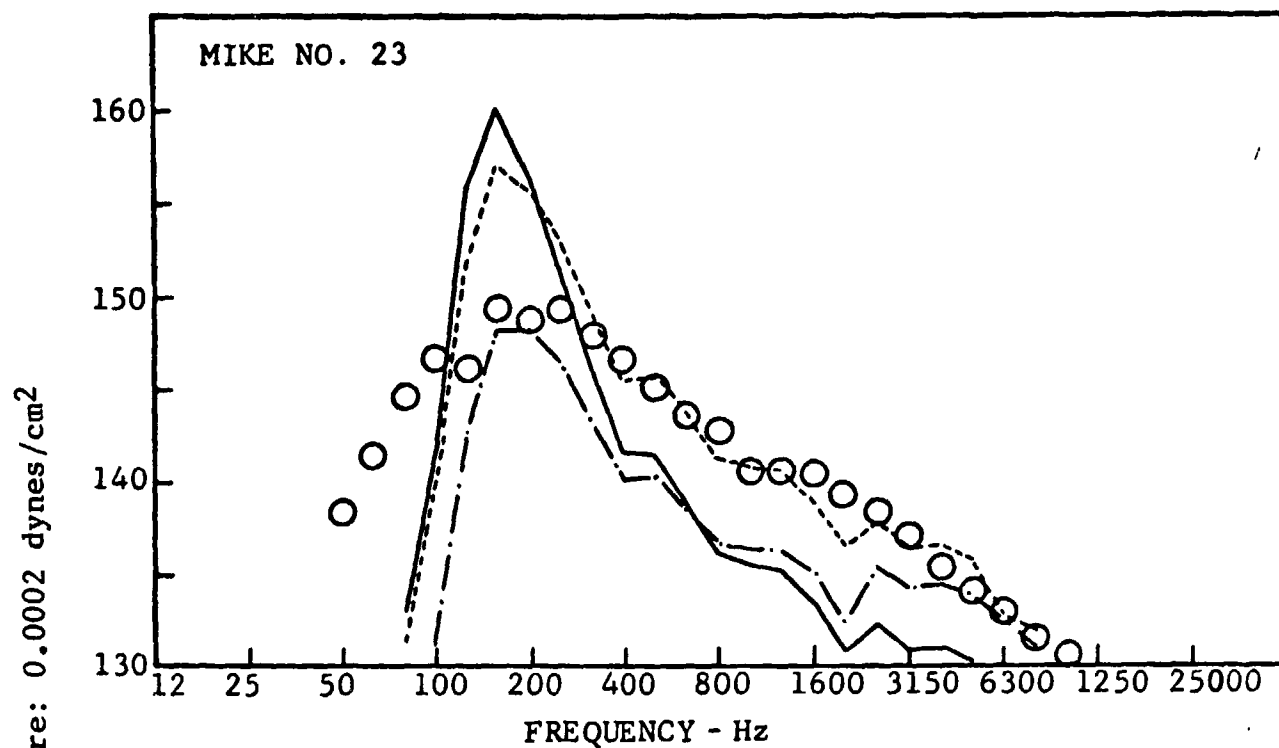
1/3 OCTAVE BAND FREQUENCY SPECTRA  
COMPARISON OF PREDICTION AND MEASUREMENTS

Y/D, RADIAL DISTANCE IN DIAMETERS



X/D, AXIAL DISTANCE IN DIAMETERS

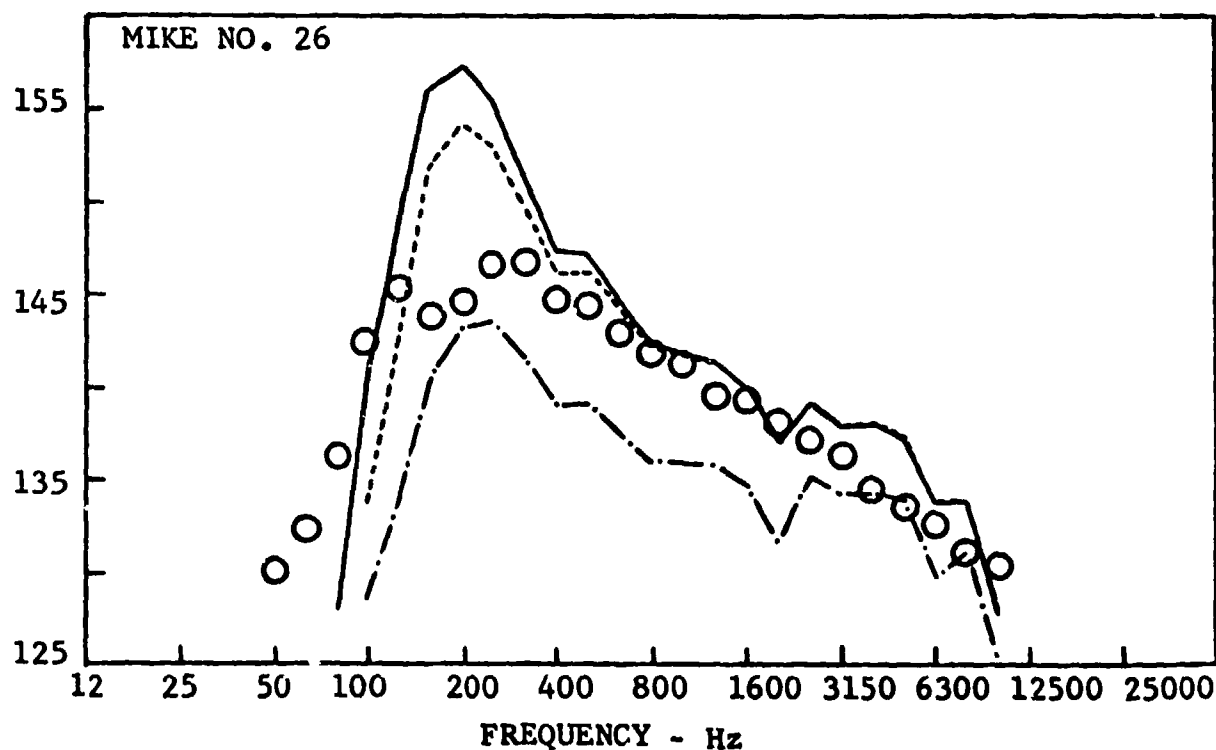
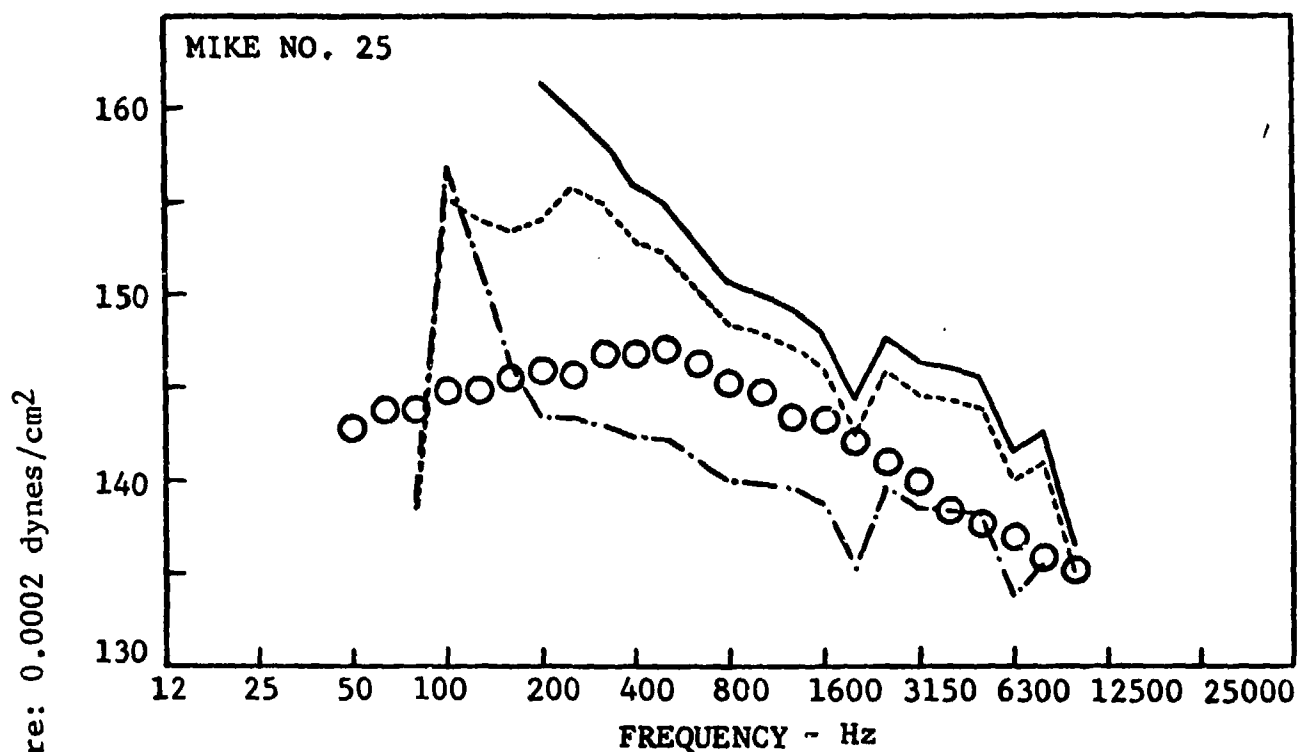
FIGURE 3 - NEAR FIELD MICROPHONE LOCATIONS (  $D = 43$  inches )



○ MEASURED DATA  
 --- ISOTROPIC TURBULENCE  
 — LATERAL QUADRUPOLE  
 - - - LONGITUDINAL QUADRUPOLE

D = 43 INCHES  
 M = 1.4612  
 V = 3300 fps  
 $T_t = 3035^{\circ}R$

FIGURE 4(a) - 1/3 OCTAVE BAND FREQUENCY SPECTRA.  
 COMPARISON OF PREDICTION AND MEASUREMENTS.



○ MEASURED DATA  
 --- ISOTROPIC TURBULENCE  
 — LATERAL QUADRUPOLE  
 - - - LONGITUDINAL QUADRUPOLE

D = 43 INCHES  
 M = 1.4612  
 V = 3300 fps  
 T<sub>c</sub> = 3035 °R

FIGURE 4(b) - 1/3 OCTAVE BAND FREQUENCY SPECTRA.  
 COMPARISON OF PREDICTION AND MEASUREMENTS.

○ MEASURED DATA  
 --- ISOTROPIC TURBULENCE  
 — LATERAL QUADRUPOLE  
 - - - LONGITUDINAL QUADRUPOLE

D = 43 INCHES  
 M = 1.4612  
 U<sub>j</sub> = 3300 fps  
 T<sub>t</sub> = 3035 °R

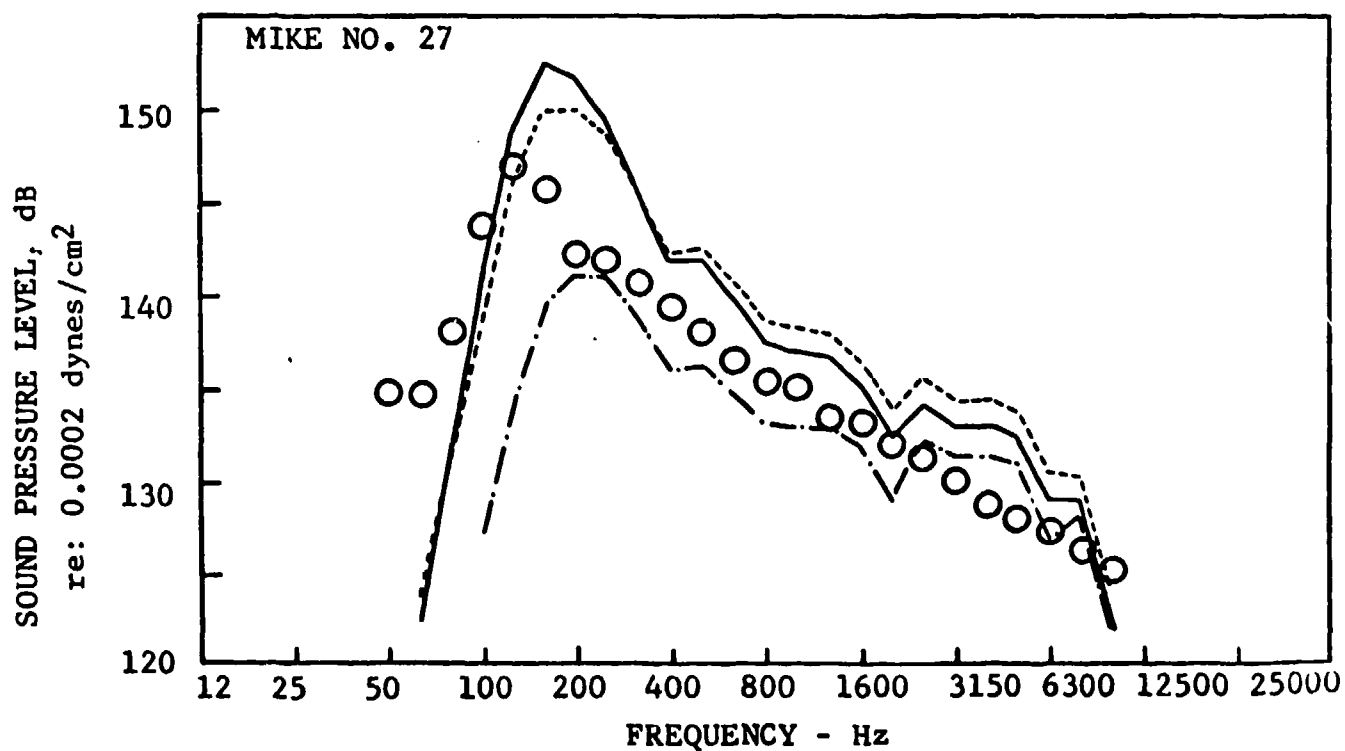
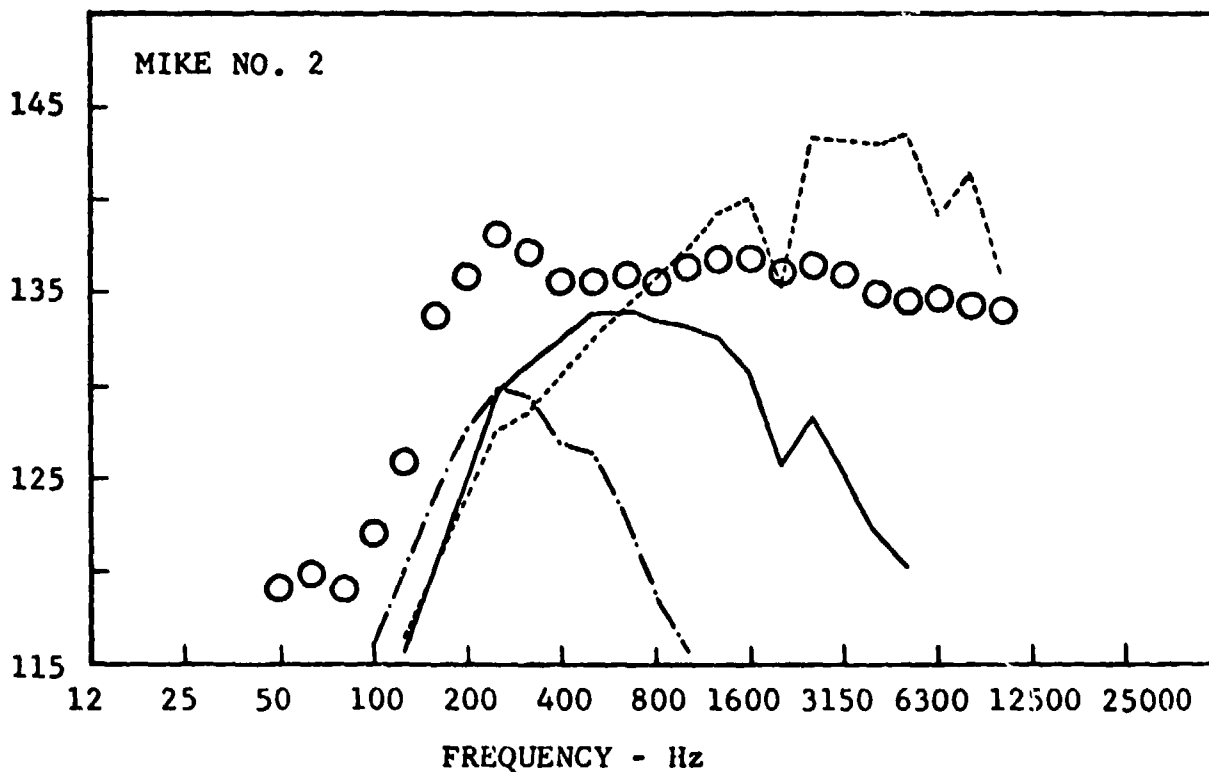
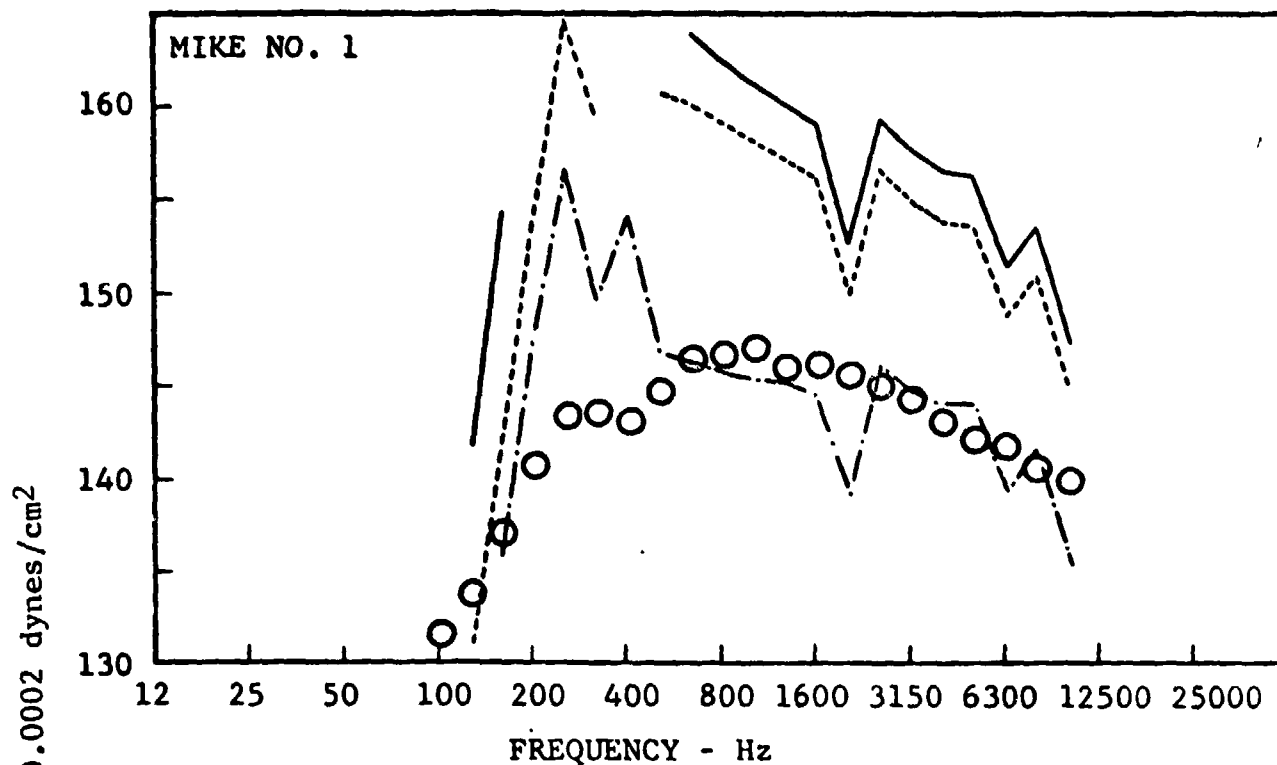


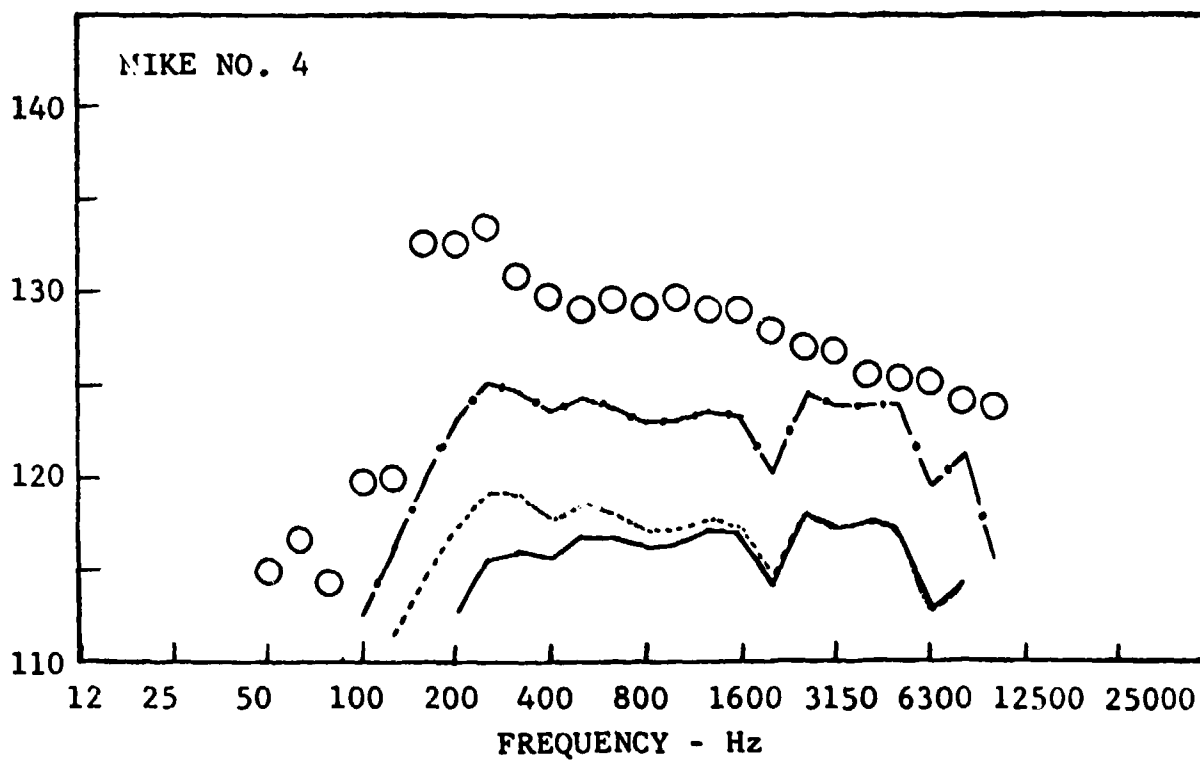
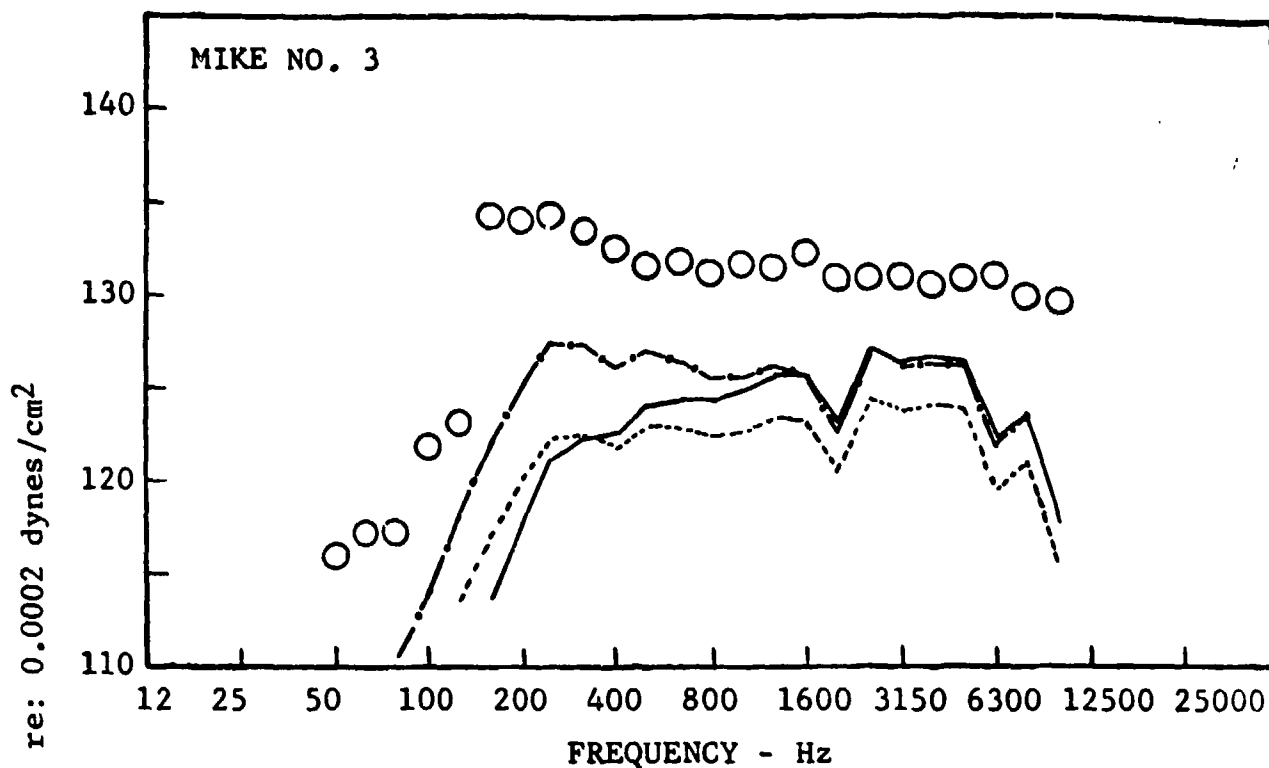
FIGURE 4(c) - 1/3 OCTAVE BAND FREQUENCY SPECTRA.  
 COMPARISON OF PREDICTION AND MEASUREMENTS.



○ MEASURED DATA  
 --- ISOTROPIC TURBULENCE  
 — LATERAL QUADRUPOLE  
 - - - LONGITUDINAL QUADRUPOLE

D = 43 INCHES  
 M = 1.4612  
 V = 3300 fps  
 T<sub>t</sub> = 3035 °R

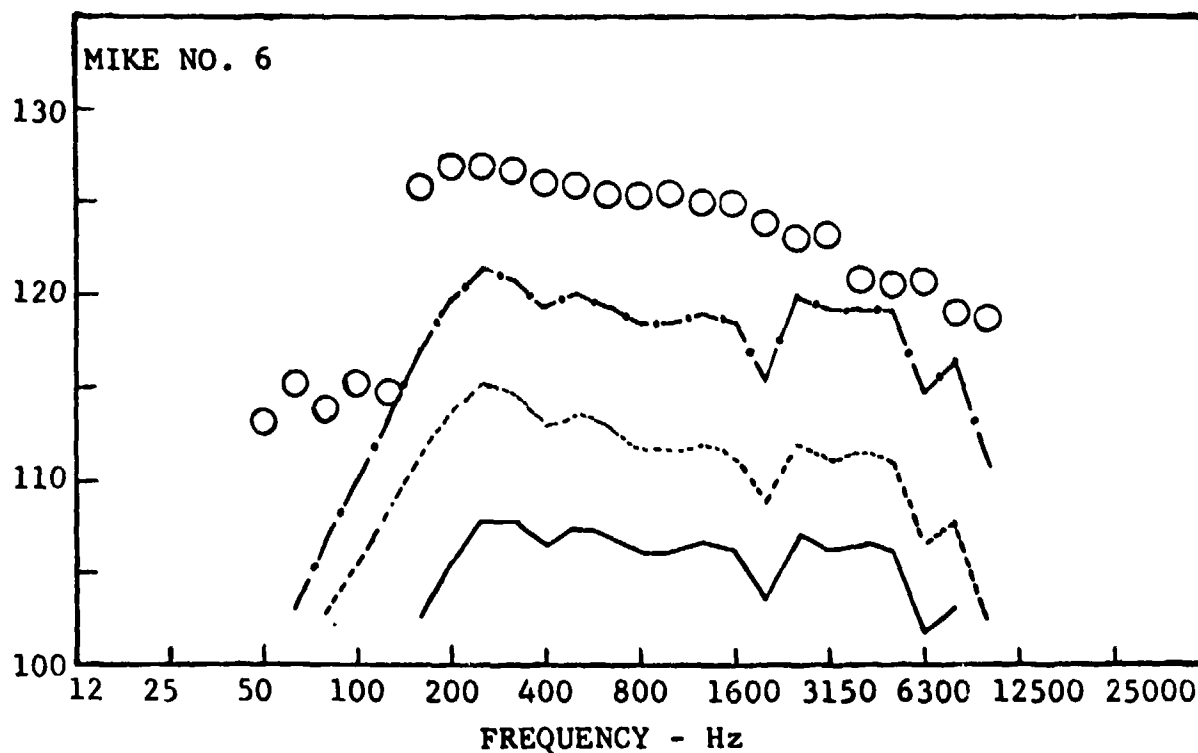
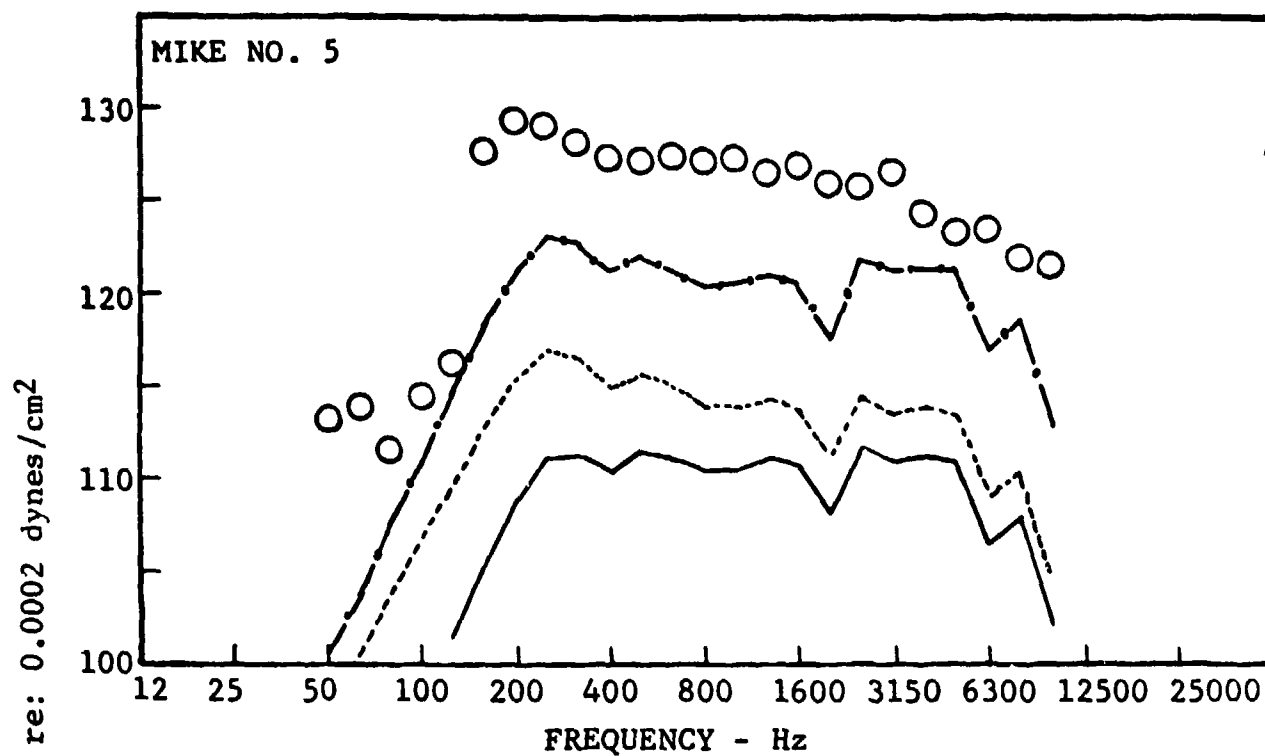
FIGURE 4(d) - 1/3 OCTAVE BAND FREQUENCY SPECTRA.  
 COMPARISON OF PREDICTION AND MEASUREMENTS.



○ MEASURED DATA  
 --- ISOTROPIC TURBULENCE  
 — LATERAL QUADRUPOLE  
 -.- LONGITUDINAL QUADRUPOLE

D = 43 INCHES  
 M = 1.4612  
 V = 3300 fps  
 T<sub>t</sub> = 3035 °R

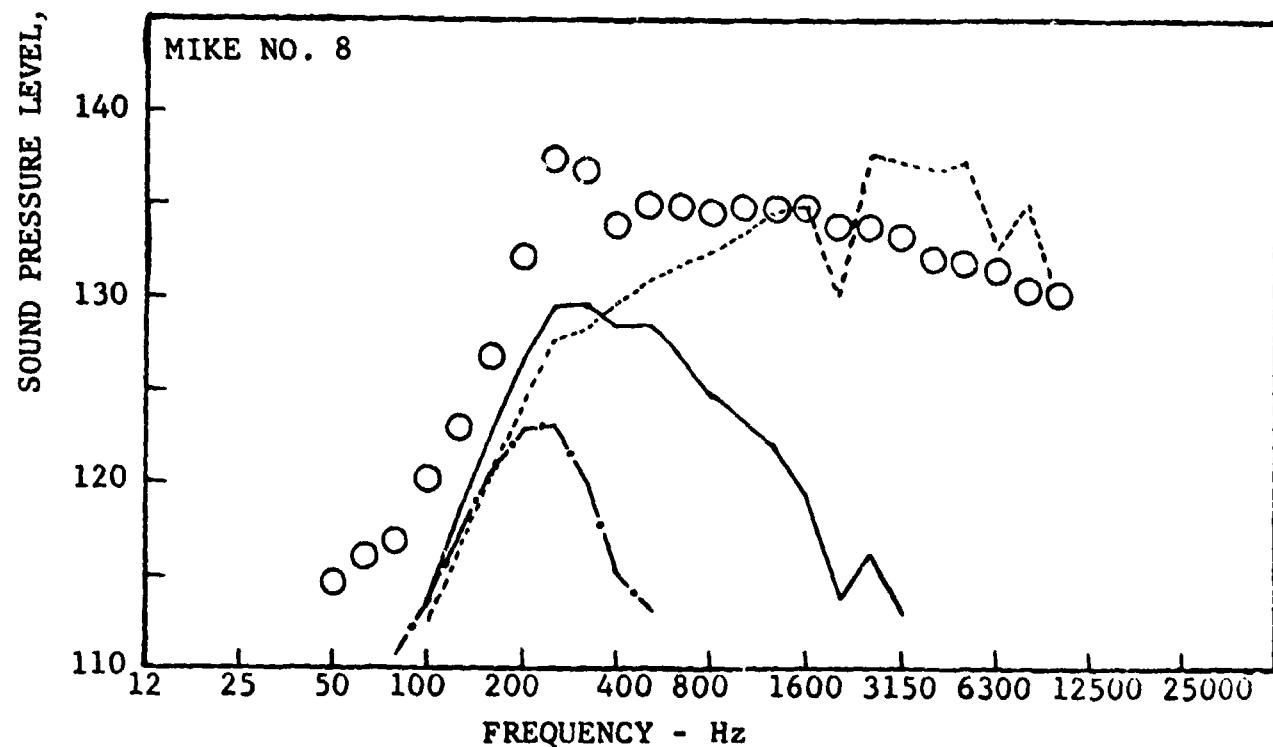
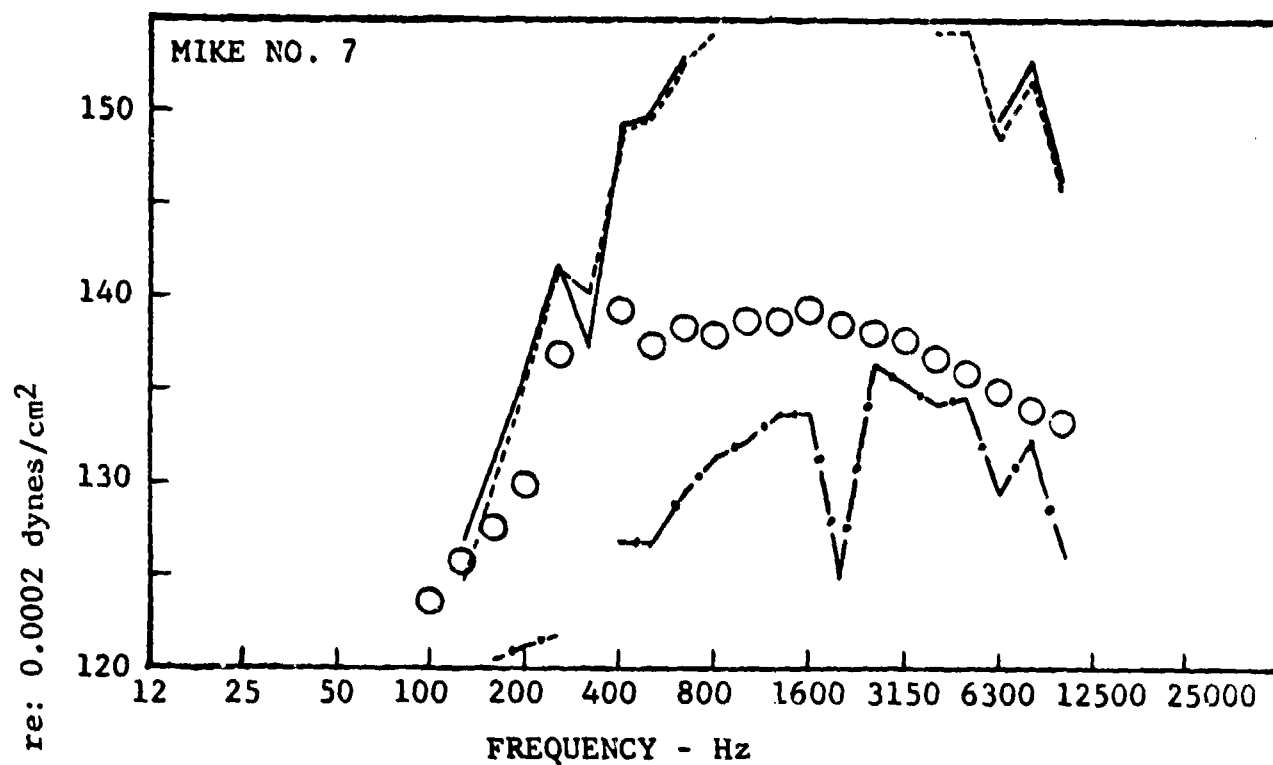
FIGURE 4(e) - 1/3 OCTAVE BAND FREQUENCY SPECTRA.  
 COMPARISON OF PREDICTION AND MEASUREMENTS.



○ MEASURED DATA  
 --- ISOTROPIC TURBULENCE  
 — LATERAL QUADRUPOLE  
 - - - LONGITUDINAL QUADRUPOLE

D = 43 INCHES  
 M = 1.4612  
 V = 3300 fps  
 T<sub>t</sub> = 3035 °R

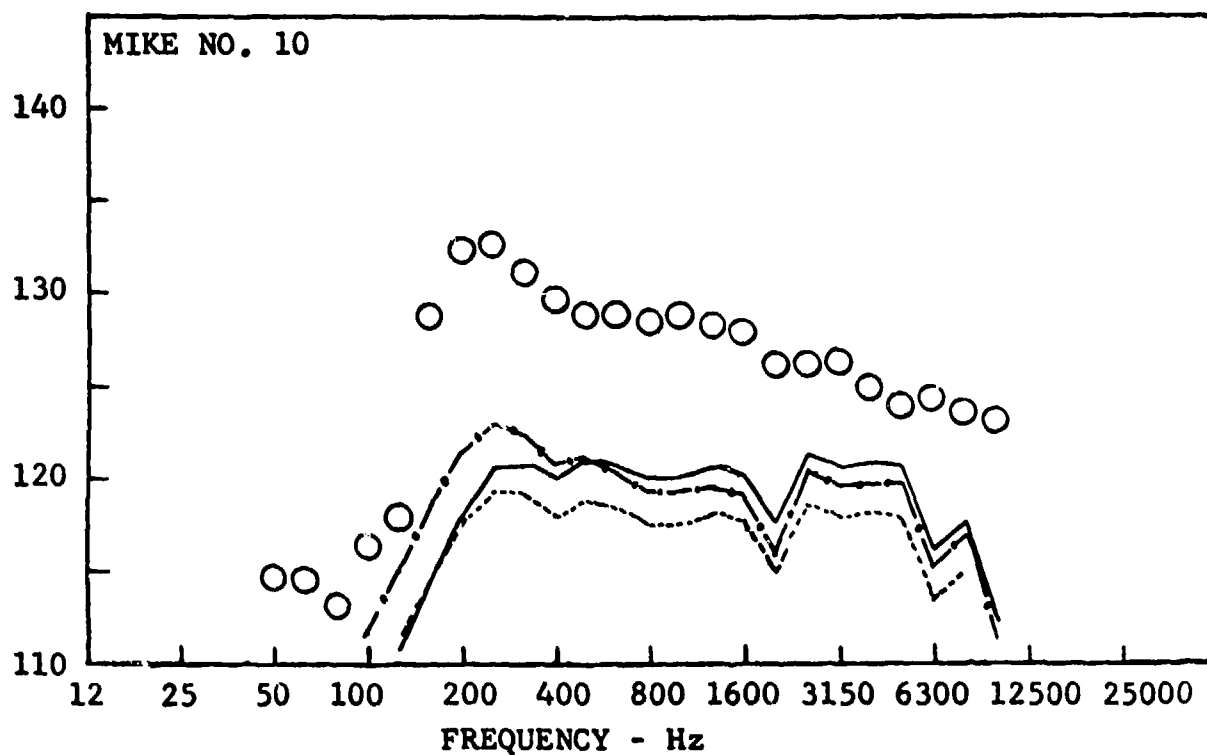
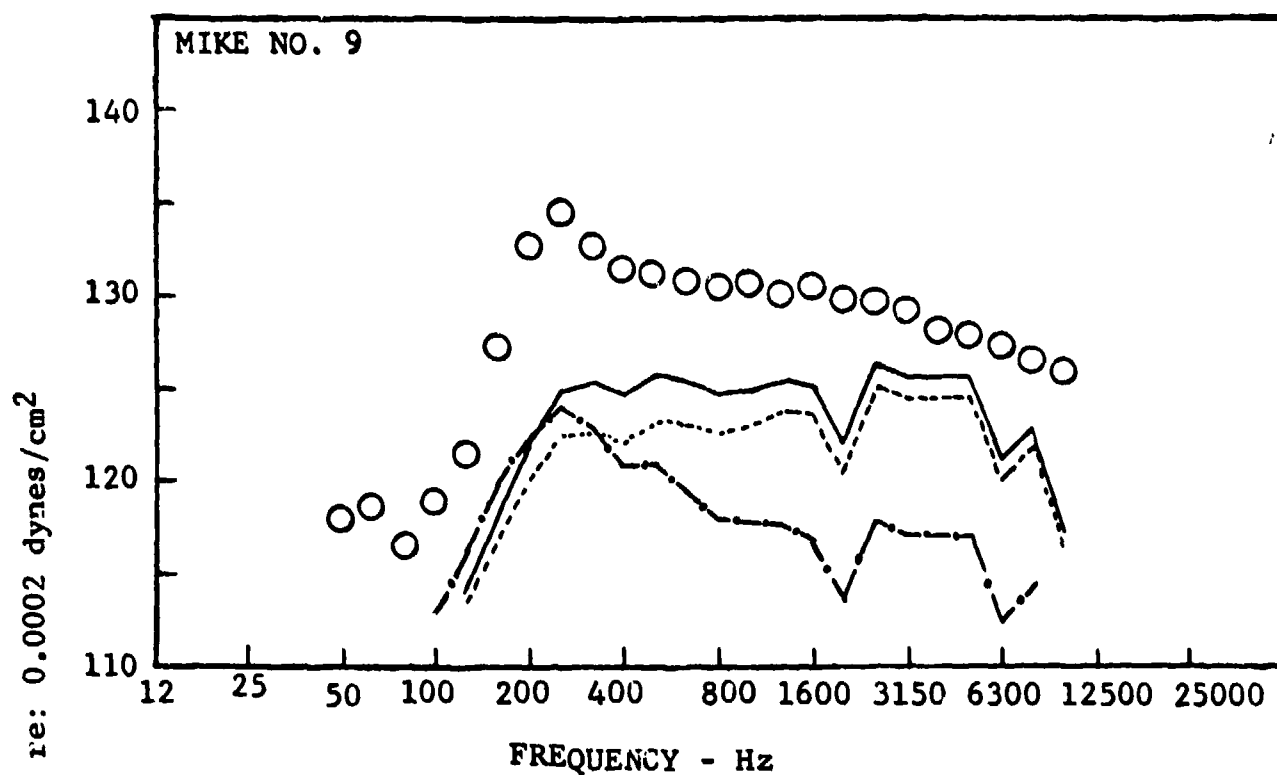
FIGURE 4(f) - 1/3 OCTAVE BAND FREQUENCY SPECTRA.  
 COMPARISON OF PREDICTION AND MEASUREMENTS.



○ MEASURED DATA  
 --- ISOTROPIC TURBULENCE  
 — LATERAL QUADRUPOLE  
 -.- LONGITUDINAL QUADRUPOLE

D = 43 INCHES  
 M = 1.4612  
 V = 3300 fps  
 T<sub>t</sub> = 3035 °R

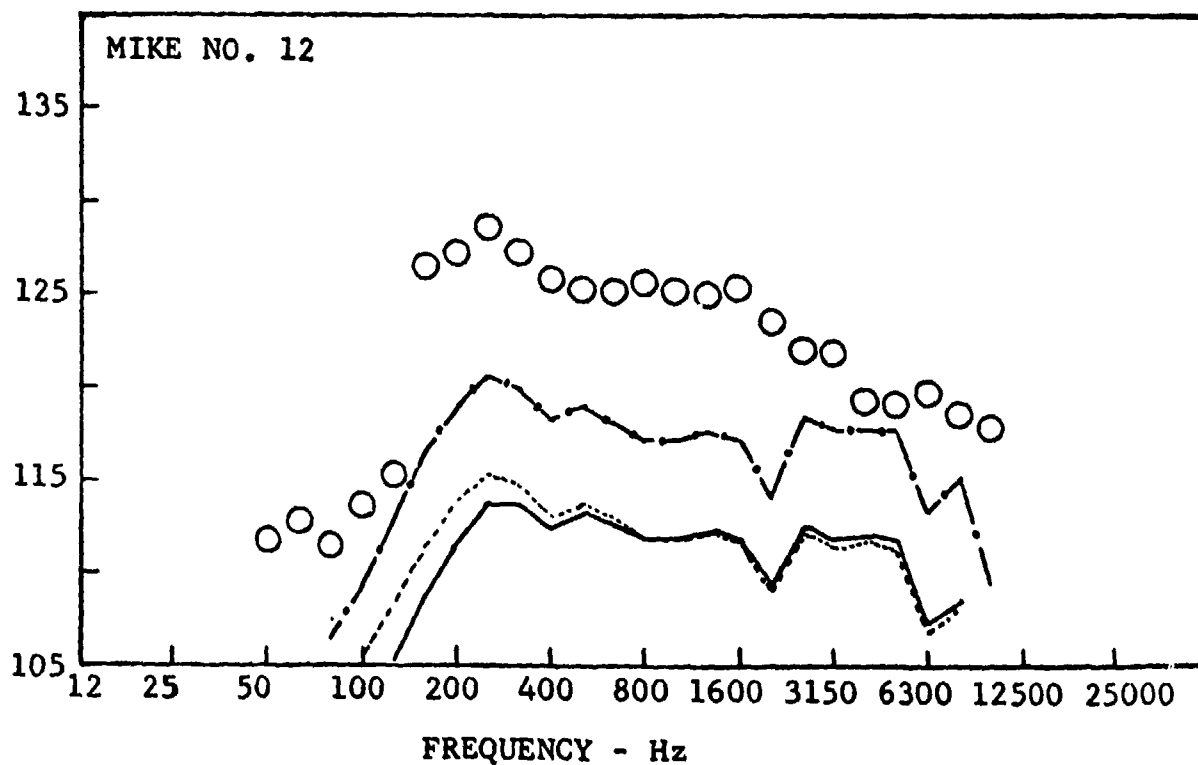
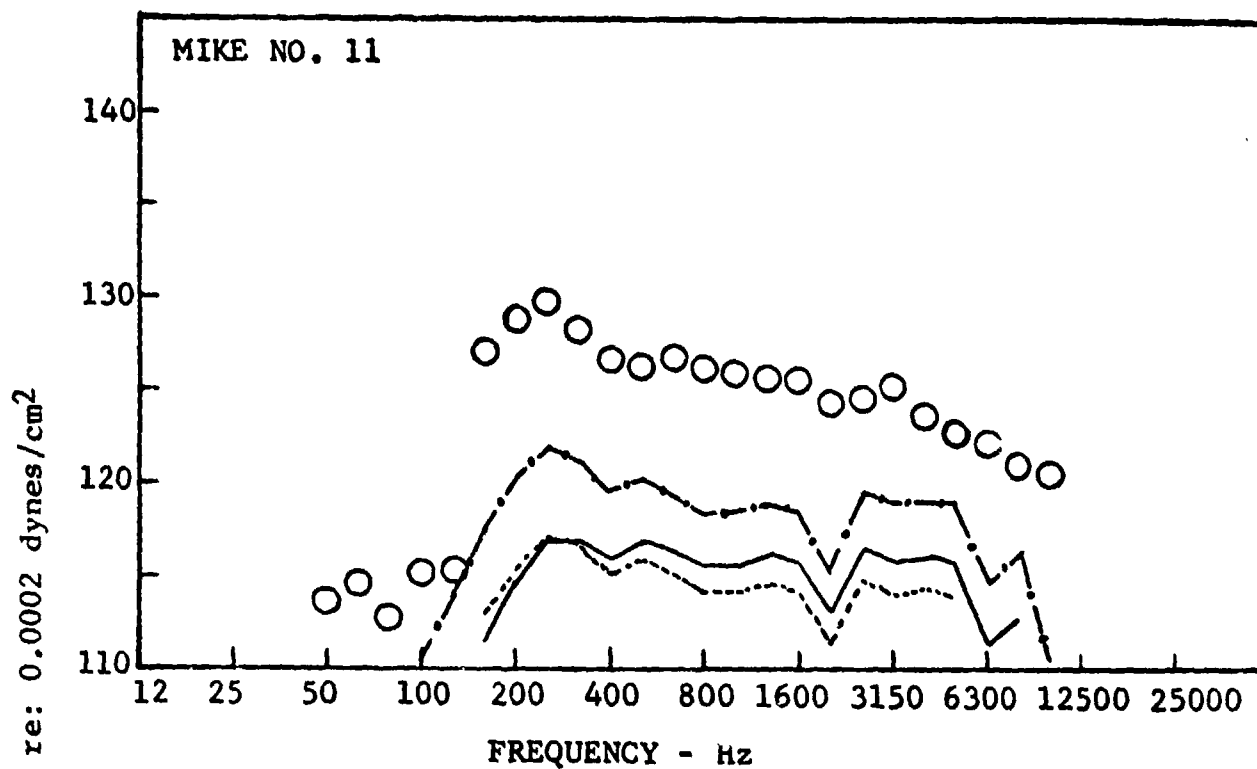
FIGURE 4(g) - 1/3 OCTAVE BAND FREQUENCY SPECTRA.  
 COMPARISON OF PREDICTION AND MEASUREMENTS.



○ MEASURED DATA  
 --- ISOTROPIC TURBULENCE  
 — LATERAL QUADRUPOLE  
 -·- LONGITUDINAL QUADRUPOLE

D = 43 INCHES  
 M = 1.4612  
 V = 3300 fps  
 T<sub>t</sub> = 3035 °R

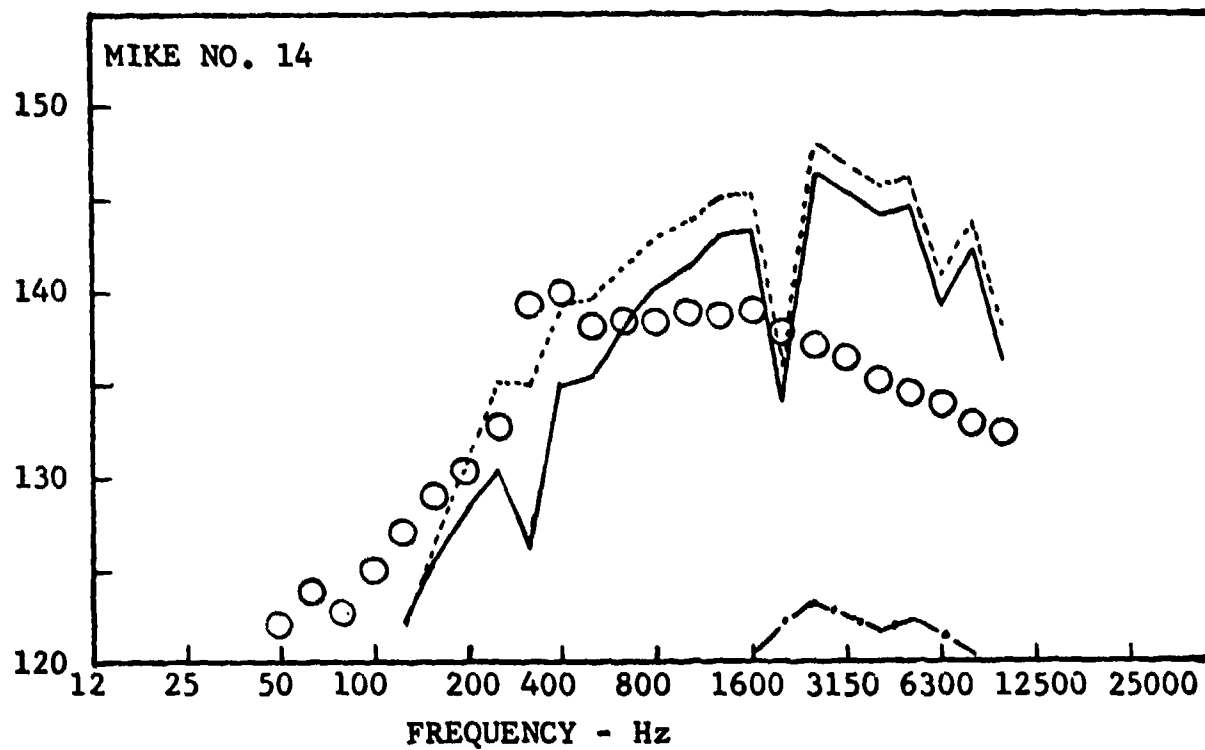
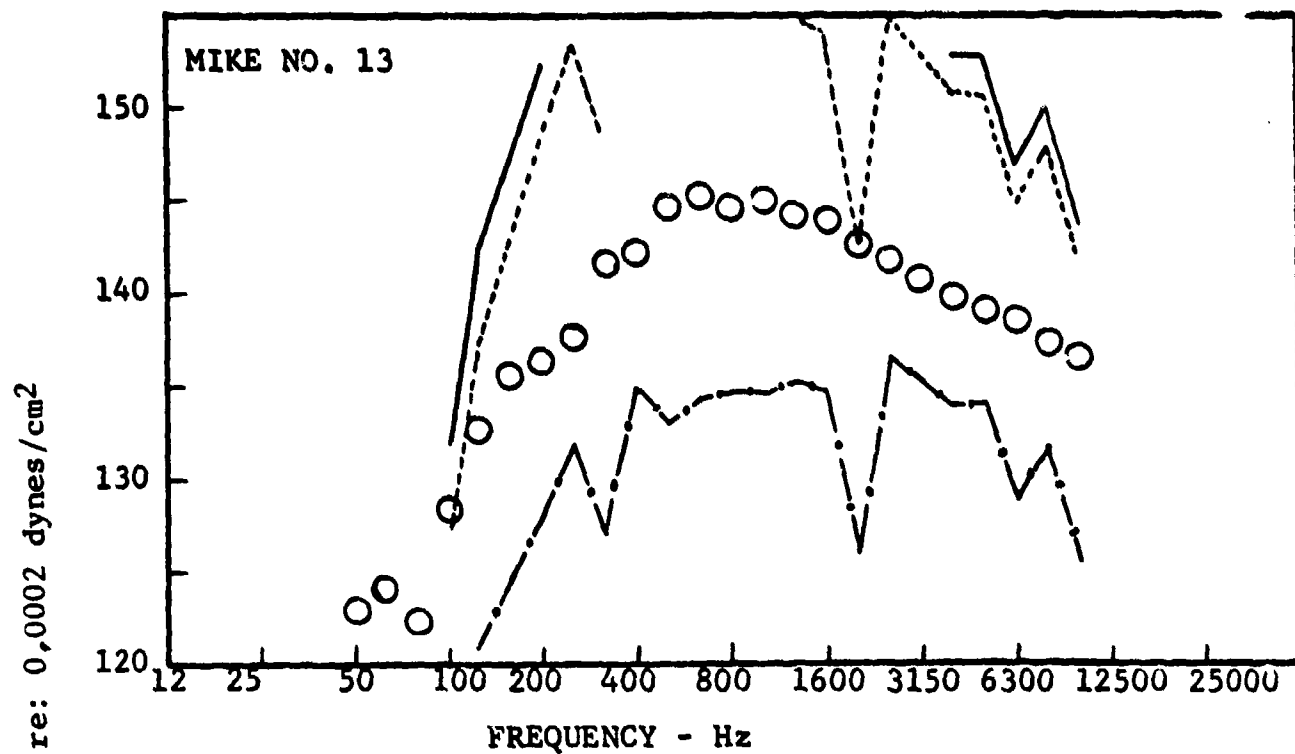
FIGURE 4(h) - 1/3 OCTAVE BAND FREQUENCY SPECTRA.  
 COMPARISON OF PREDICTION AND MEASUREMENTS.



○ MEASURED DATA  
 --- ISOTROPIC TURBULENCE  
 — LATERAL QUADRUPOLE  
 - - - LONGITUDINAL QUADRUPOLE

D = 43 INCHES  
 M = 1.4612  
 V = 3300 fps  
 T<sub>t</sub> = 3035 °R

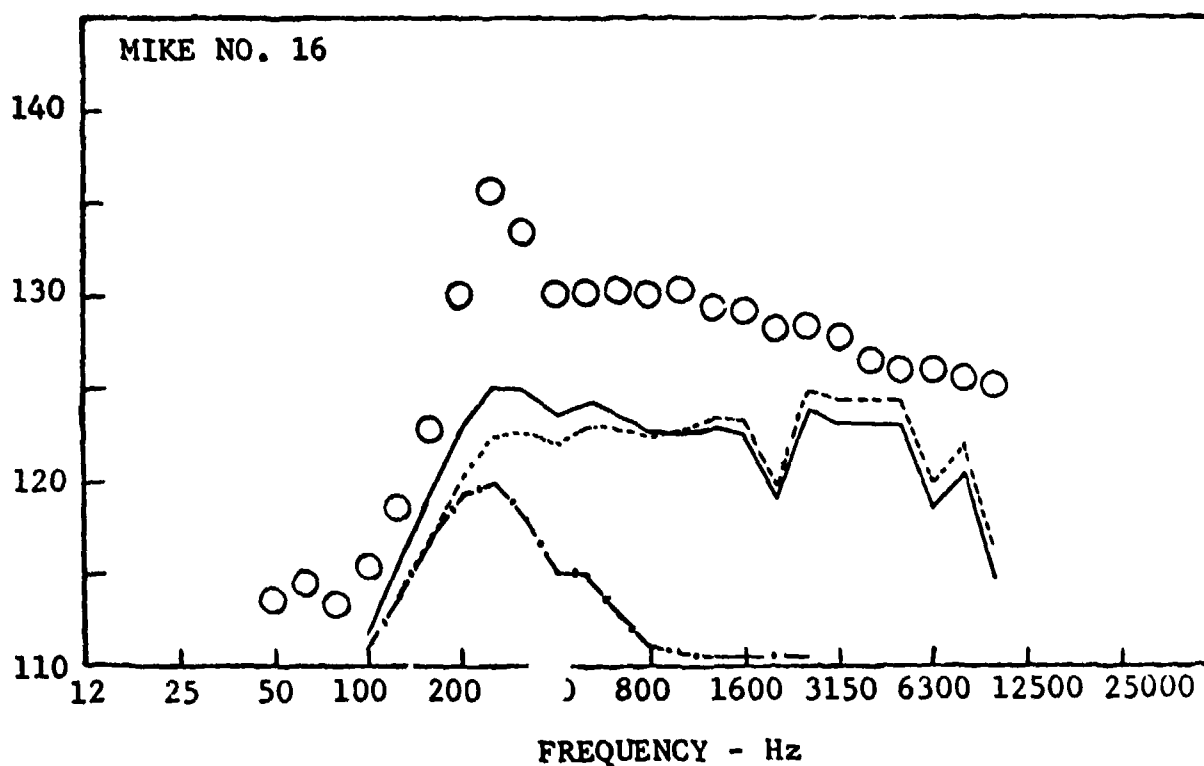
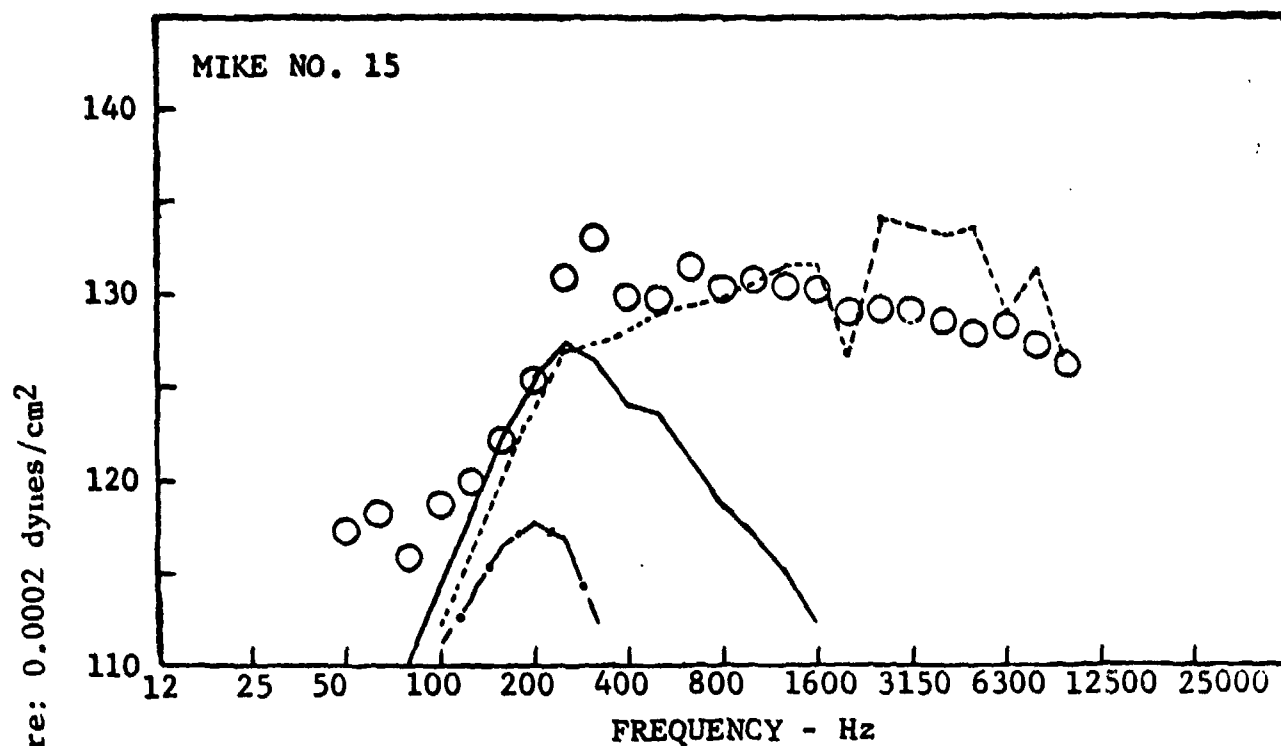
FIGURE 4(1) - 1/3 OCTAVE BAND FREQUENCY SPECTRA.  
 COMPARISON OF PREDICTION AND MEASUREMENTS.



○ MEASURED DATA  
 --- ISOTROPIC TURBULENCE  
 — LATERAL QUADRUPOLE  
 -.- LONGITUDINAL QUADRUPOLE

D = 43 INCHES  
 M = 1.4612  
 V = 3300 fps  
 T<sub>t</sub> = 3035 °R

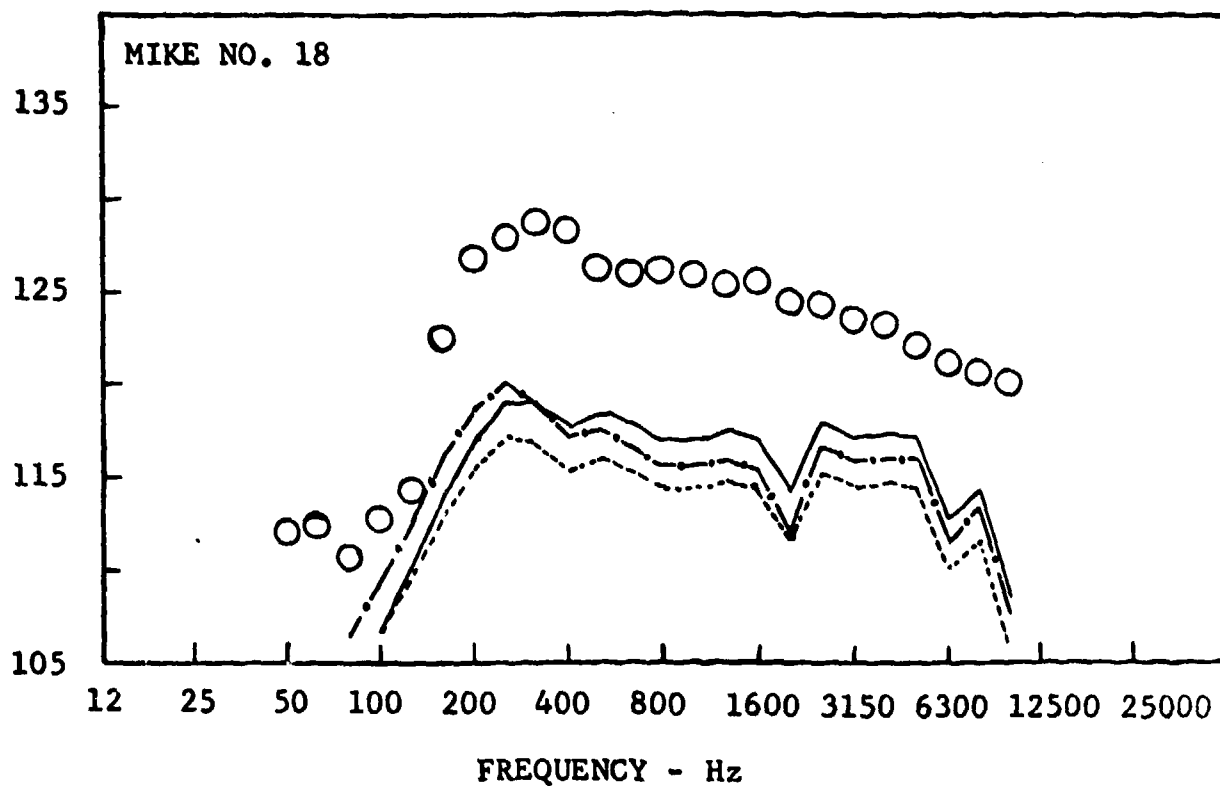
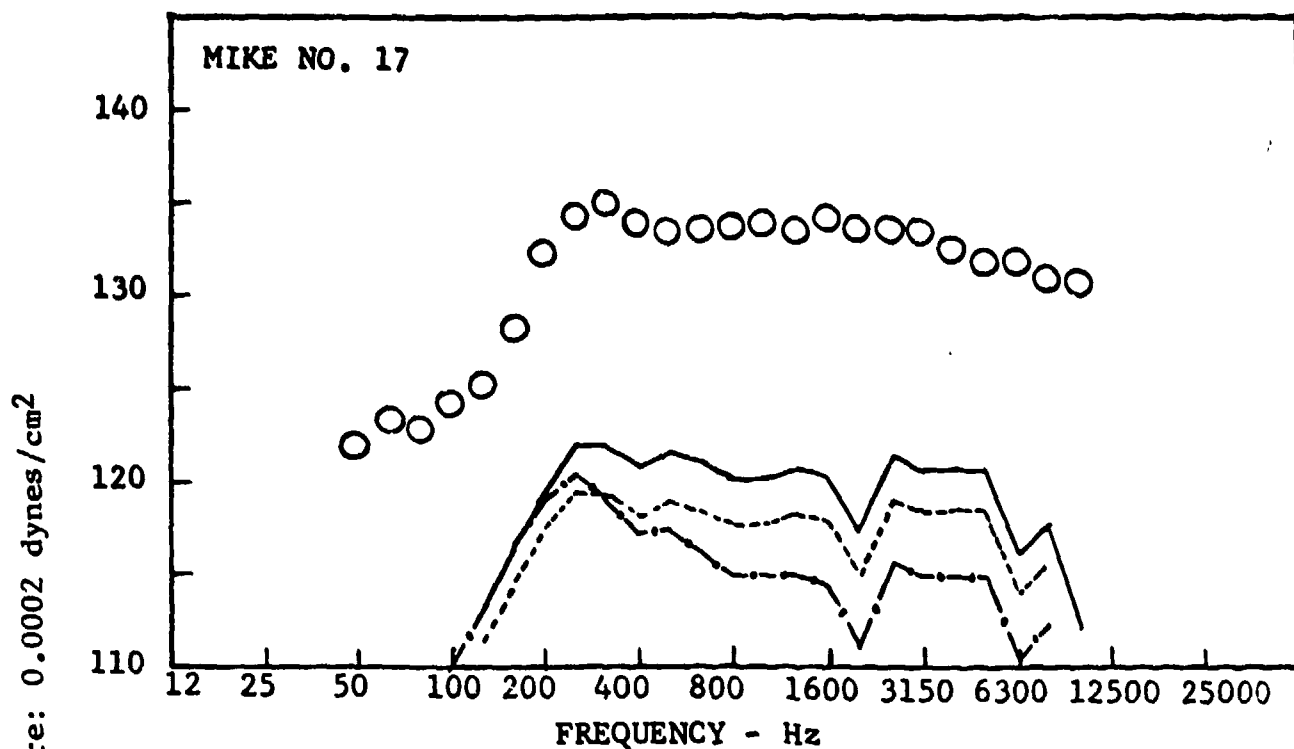
FIGURE 4(j) - 1/3 OCTAVE BAND FREQUENCY SPECTRA.  
 COMPARISON OF PREDICTION AND MEASUREMENTS.



○ MEASURED DATA  
 --- ISOTROPIC TURBULENCE  
 — LATERAL QUADRUPOLE  
 -·- LONGITUDINAL QUADRUPOLE

D = 43 INCHES  
 M = 1.4612  
 V = 3300 fps  
 T<sub>t</sub> = 3035 °R

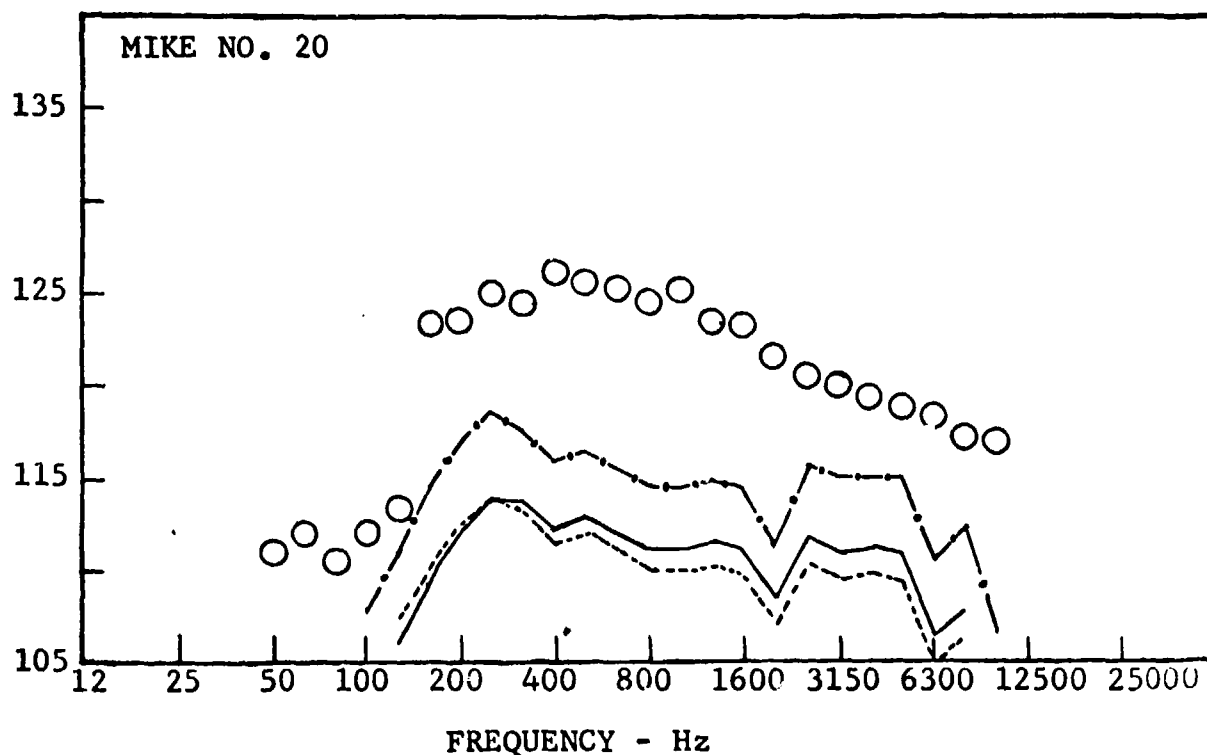
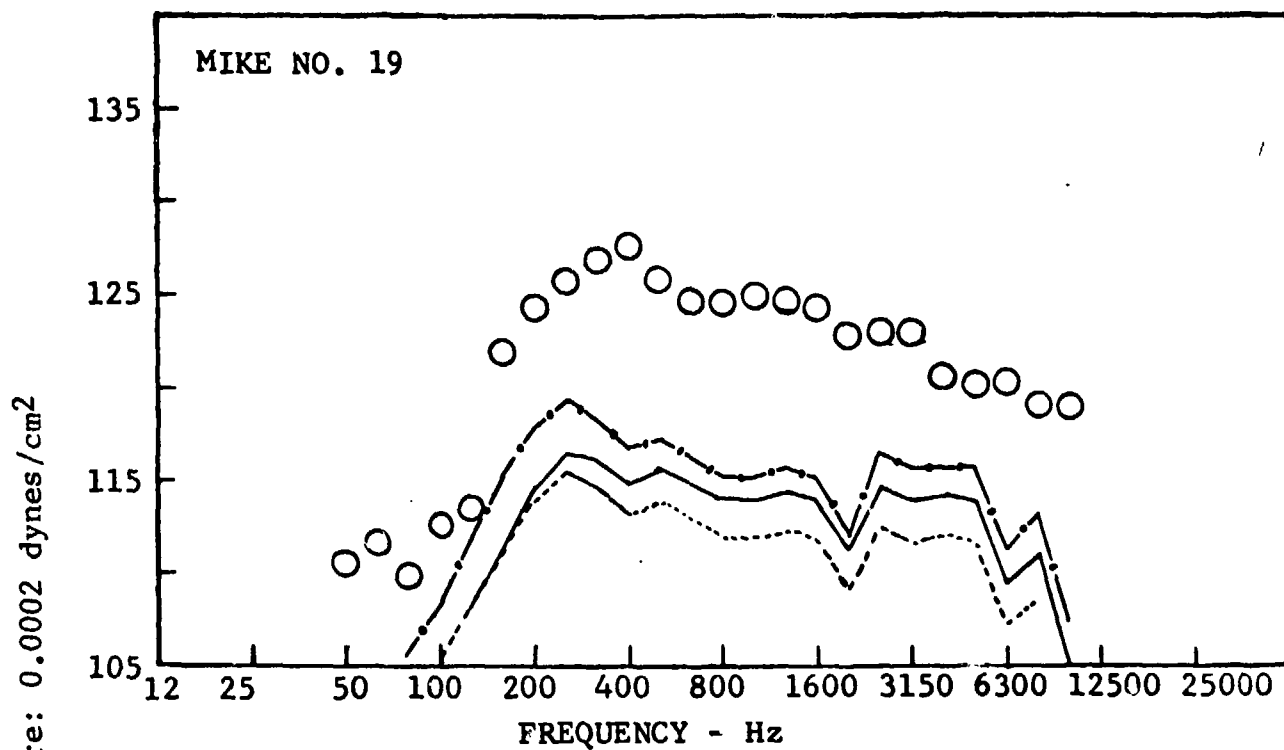
FIGURE 4(k) - 1/3 OCTAVE BAND FREQUENCY SPECTRA.  
 COMPARISON OF PREDICTION AND MEASUREMENTS.



○ MEASURED DATA  
 --- ISOTROPIC TURBULENCE  
 — LATERAL QUADRUPOLE  
 -·- LONGITUDINAL QUADRUPOLE

D = 43 INCHES  
 M = 1.4612  
 V = 3300 fps  
 T<sub>c</sub> = 3035 °R

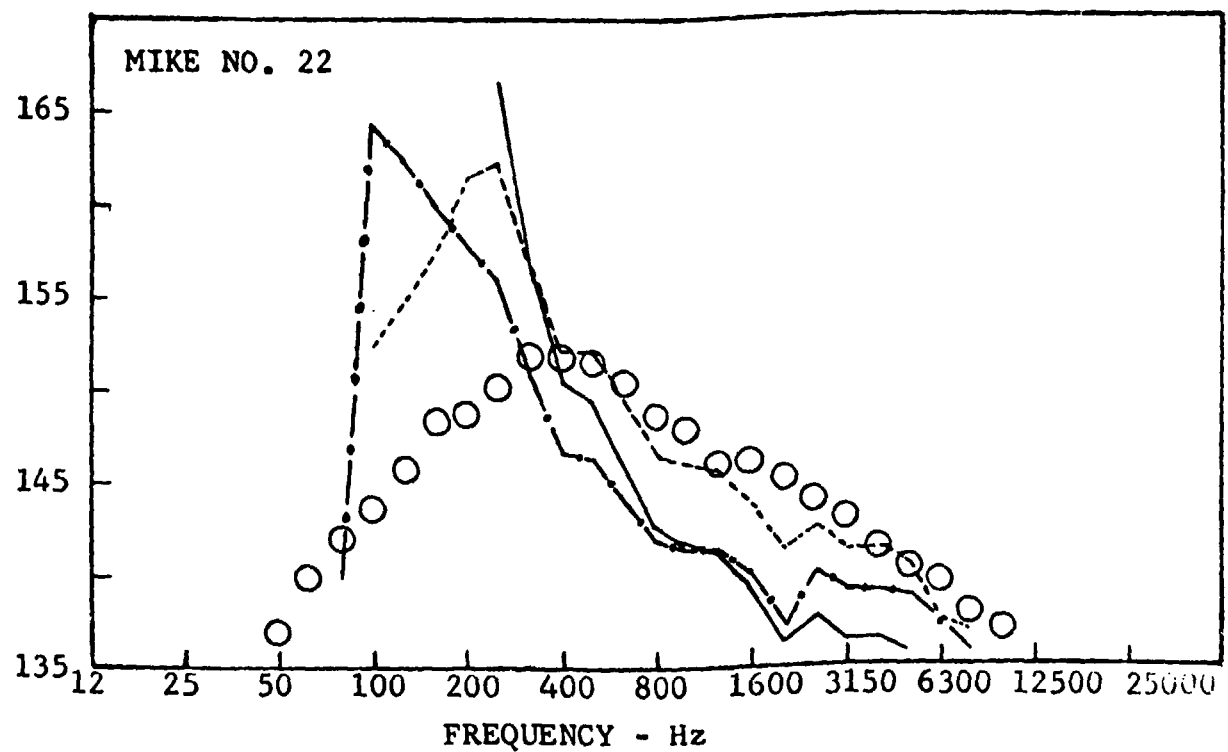
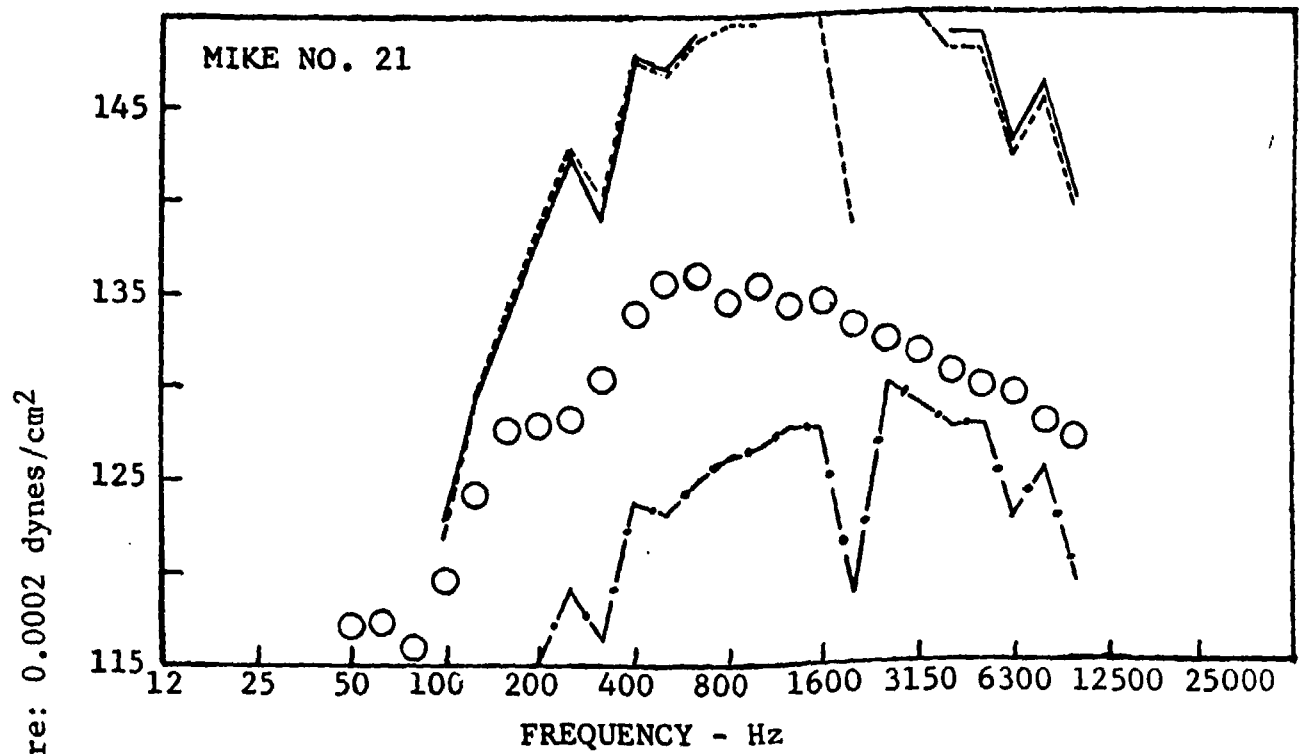
FIGURE 4(1) - 1/3 OCTAVE BAND FREQUENCY SPECTRA.  
 COMPARISON OF PREDICTION AND MEASUREMENTS.



○ MEASURED DATA  
 --- ISOTROPIC TURBULENCE  
 — LATERAL QUADRUPOLE  
 -·- LONGITUDINAL QUADRUPOLE

D = 43 INCHES  
 M = 1.4612  
 V = 3300 f<sub>ps</sub>  
 T<sub>t</sub> = 3035 °R

FIGURE 4(m) - 1/3 OCTAVE BAND FREQUENCY SPECTRA.  
 COMPARISON OF PREDICTION AND MEASUREMENTS.



○ MEASURED DATA  
 ---- ISOTROPIC TURBULENCE  
 — LATERAL QUADRUPOLE  
 - - - LONGITUDINAL QUADRUPOLE

D = 43 INCHES  
 M = 1.4612  
 V = 3300 fps  
 T<sub>t</sub> = 3035 °R

FIGURE 4(n) - 1/3 OCTAVE BAND FREQUENCY SPECTRA.  
 COMPARISON OF PREDICTION AND MEASUREMENTS.

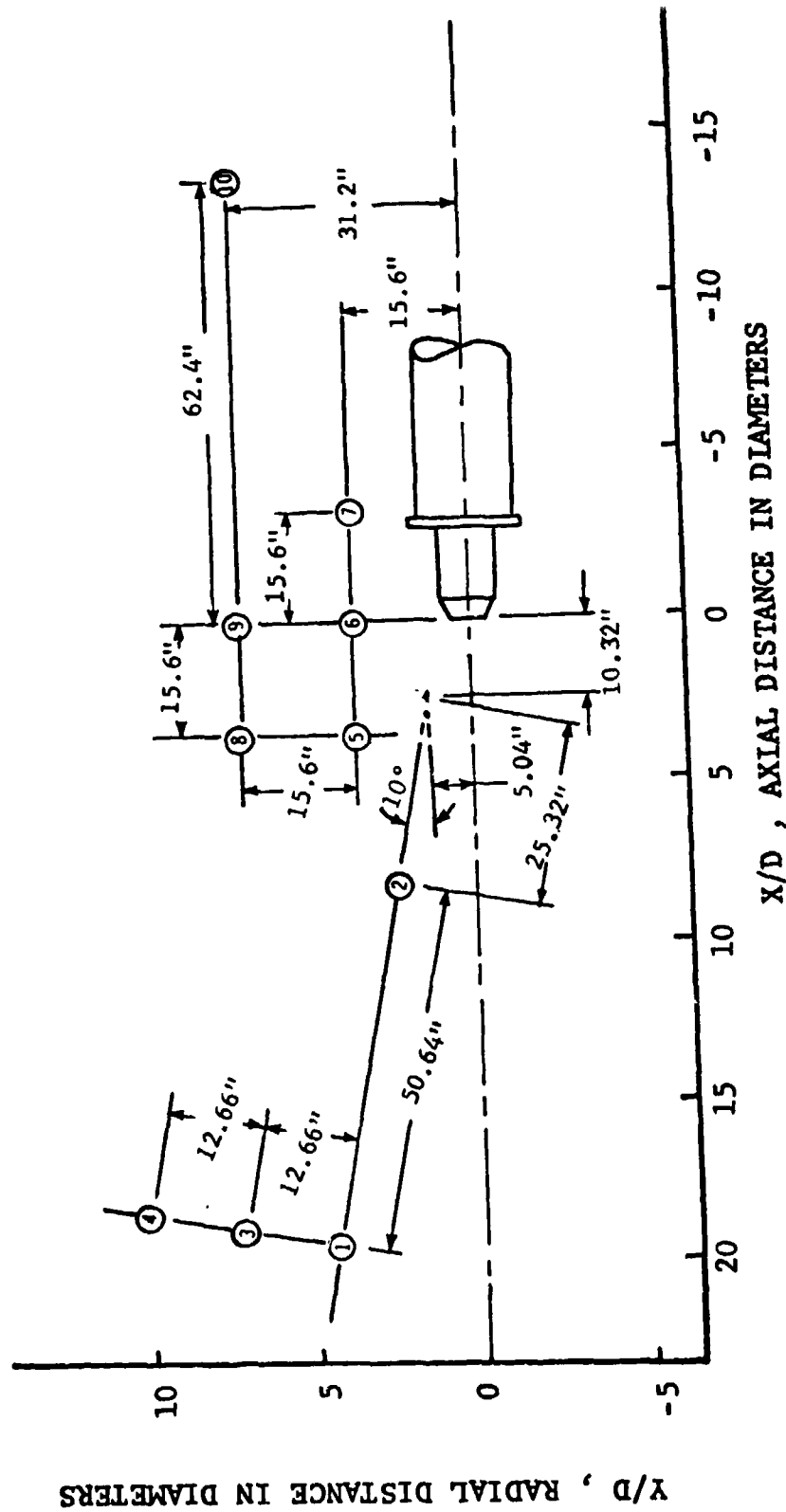
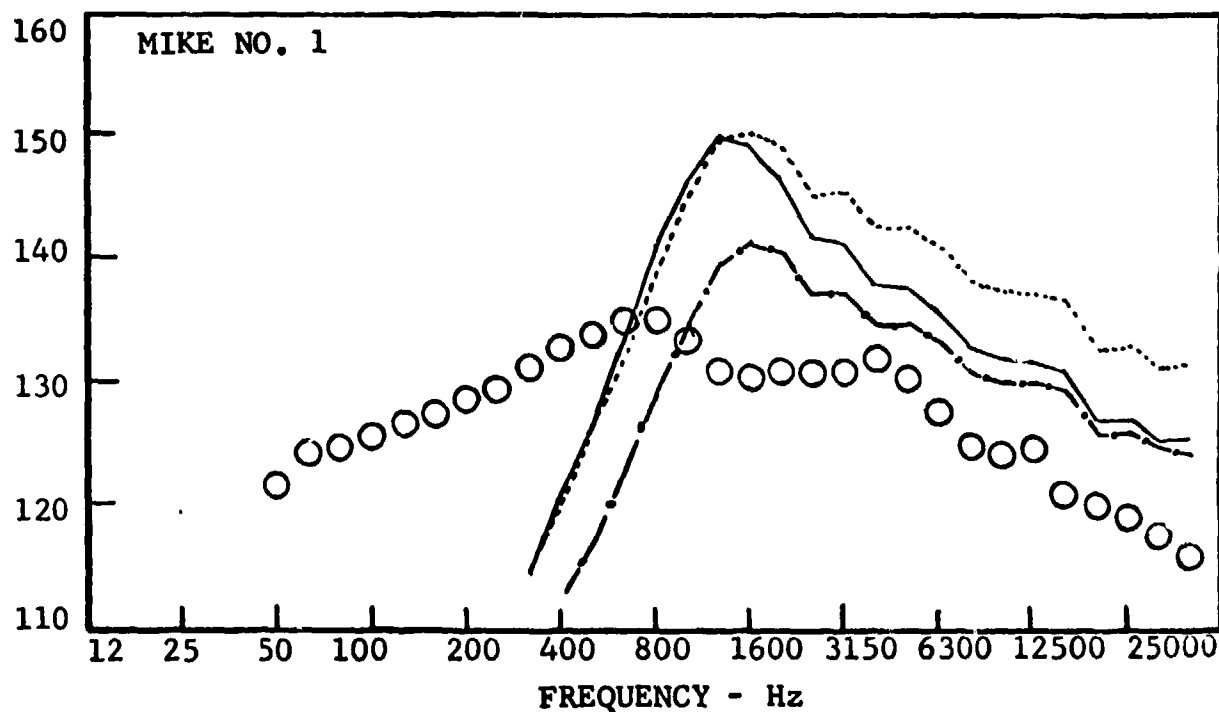
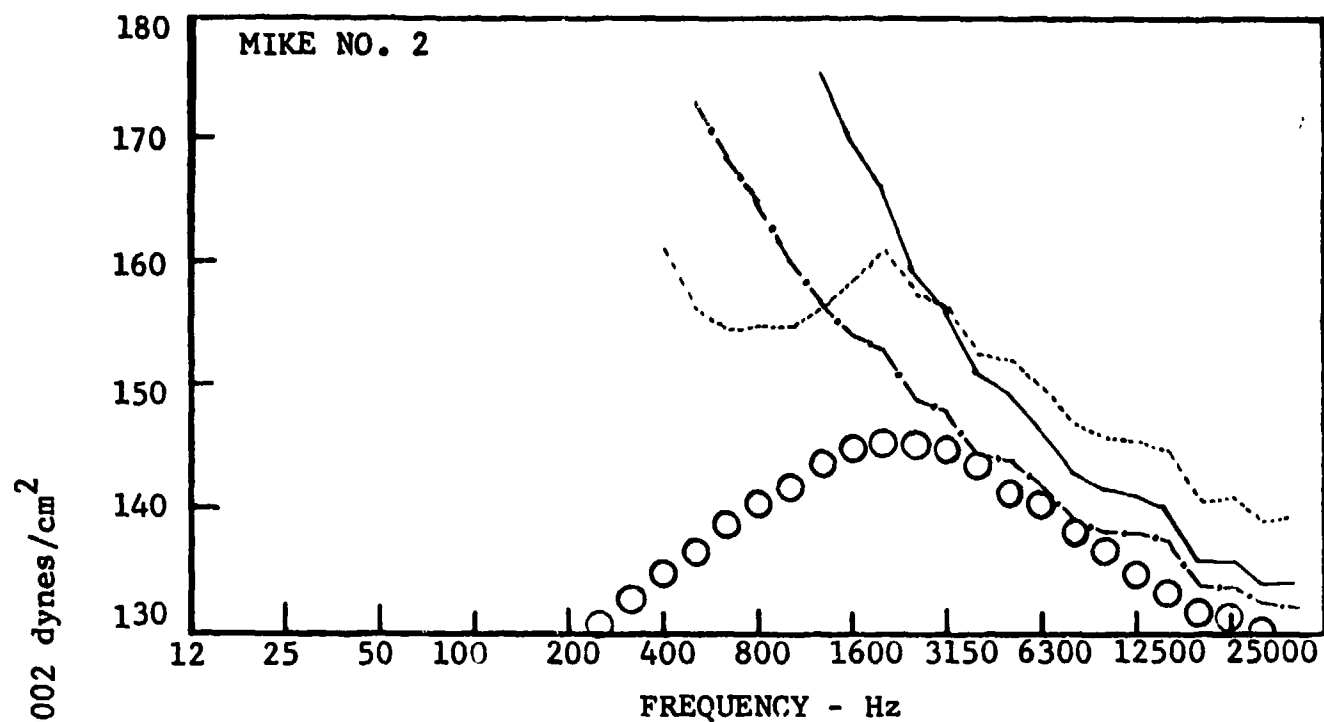


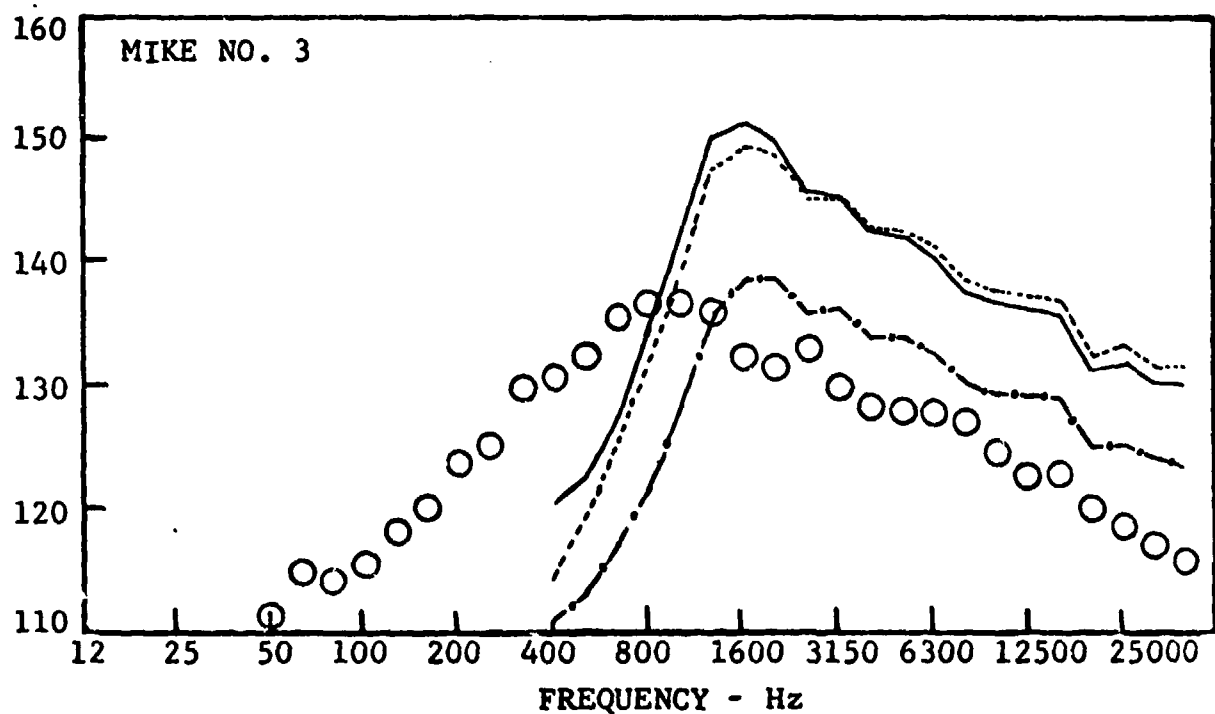
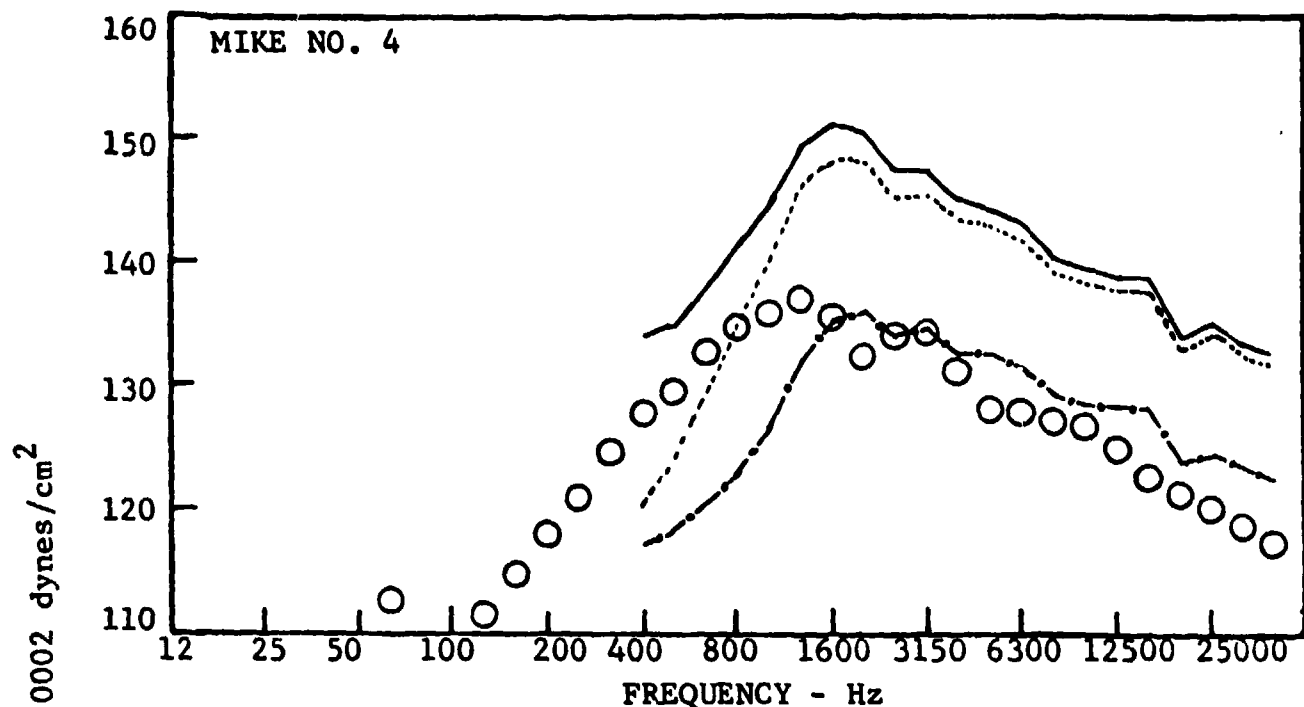
FIGURE 5 - NEAR-FIELD MICROPHONE LOCATIONS (  $D = 4.55$  in )



○ MEASURED DATA  
 --- ISOTROPIC TURBULENCE  
 — LATERAL QUADRUPOLE  
 - - - LONGITUDINAL QUADRUPOLE

$D = 4.55$  inch  
 $M = 1.3559$   
 $U_j = 2781$  fps  
 $T_t = 2407$  °R  
 $u'/U_j = .05$  (ASSUMED)

FIGURE 6(a) - 1/3 OCTAVE BAND FREQUENCY SPECTRA  
 COMPARISON OF PREDICTION AND MEASUREMENTS

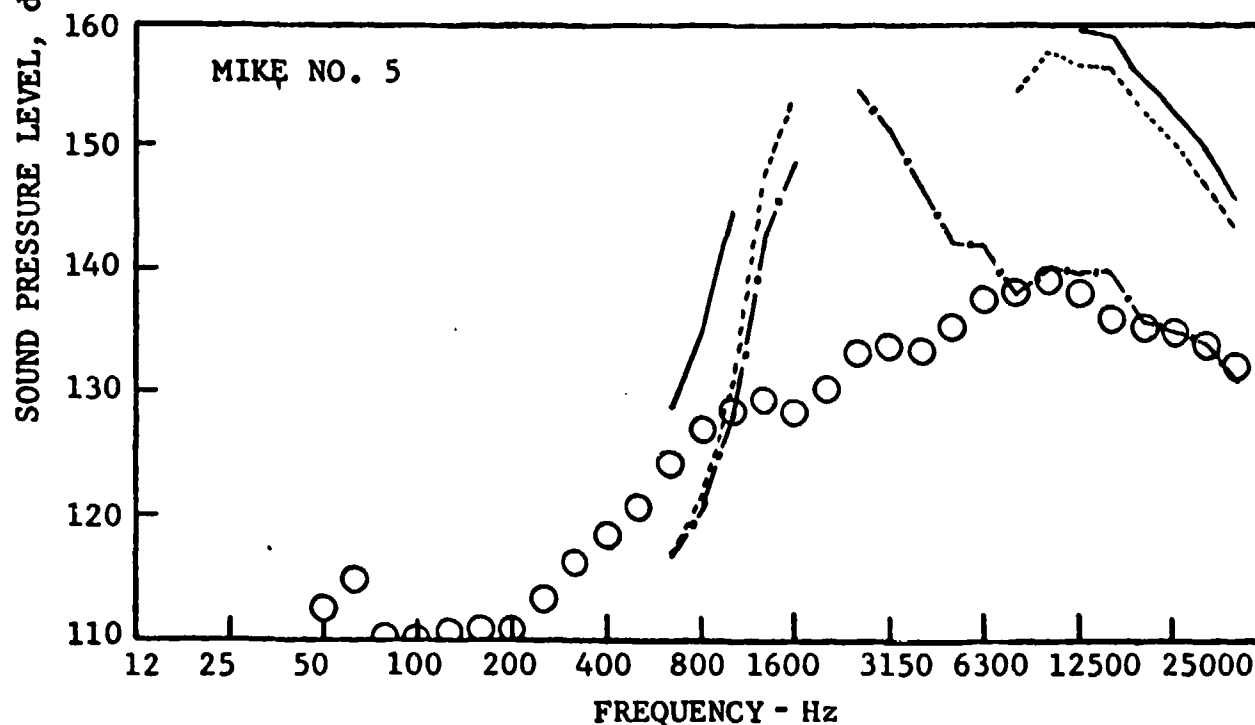
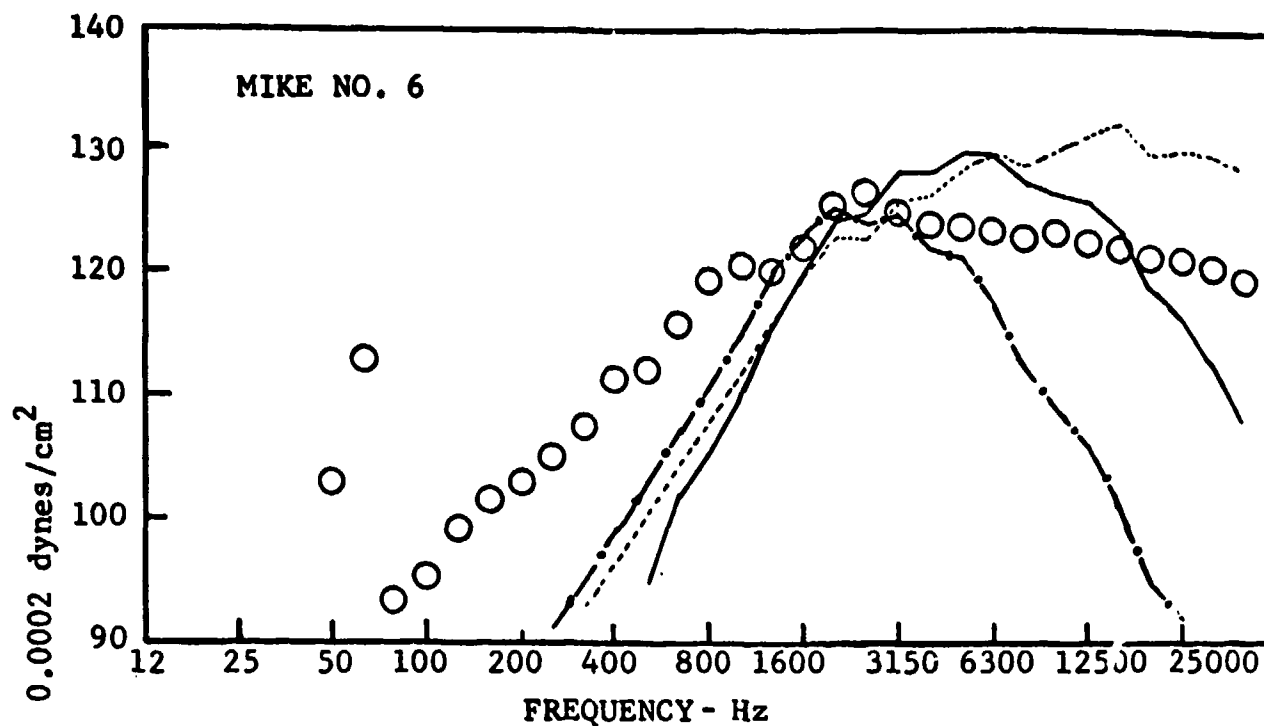


○ MEASURED DATA  
 --- ISOTROPIC TURBULENCE  
 — LATERAL QUADRUPOLE  
 - - - LONGITUDINAL QUADRUPOLE

$D = 4.55$  inch  
 $M = 1.3559$   
 $U_j = 2781$  fps  
 $T_t = 2407$  °R  
 $u'/U_j = .05$  (ASSUMED)

FIGURE 6(b)

1/3 OCTAVE BAND FREQUENCY SPECTRA  
 COMPARISON OF PREDICTION AND MEASUREMENTS



○ MEASURED DATA  
 --- ISOTROPIC TURBULENCE  
 — LATERAL QUADRUPOLE  
 -.- LONGITUDINAL QUADRUPOLE

D = 4.55 INCH  
 M = 1.3559  
 U<sub>j</sub> = 2781 fps  
 T<sub>f</sub> = 2407°R  
 u<sub>r</sub>/U<sub>j</sub> = .05 (ASSUMED)

FIGURE 6(c) - 1/3 OCTAVE BAND FREQUENCY SPECTRA  
 COMPARISON OF PREDICTION AND MEASUREMENTS

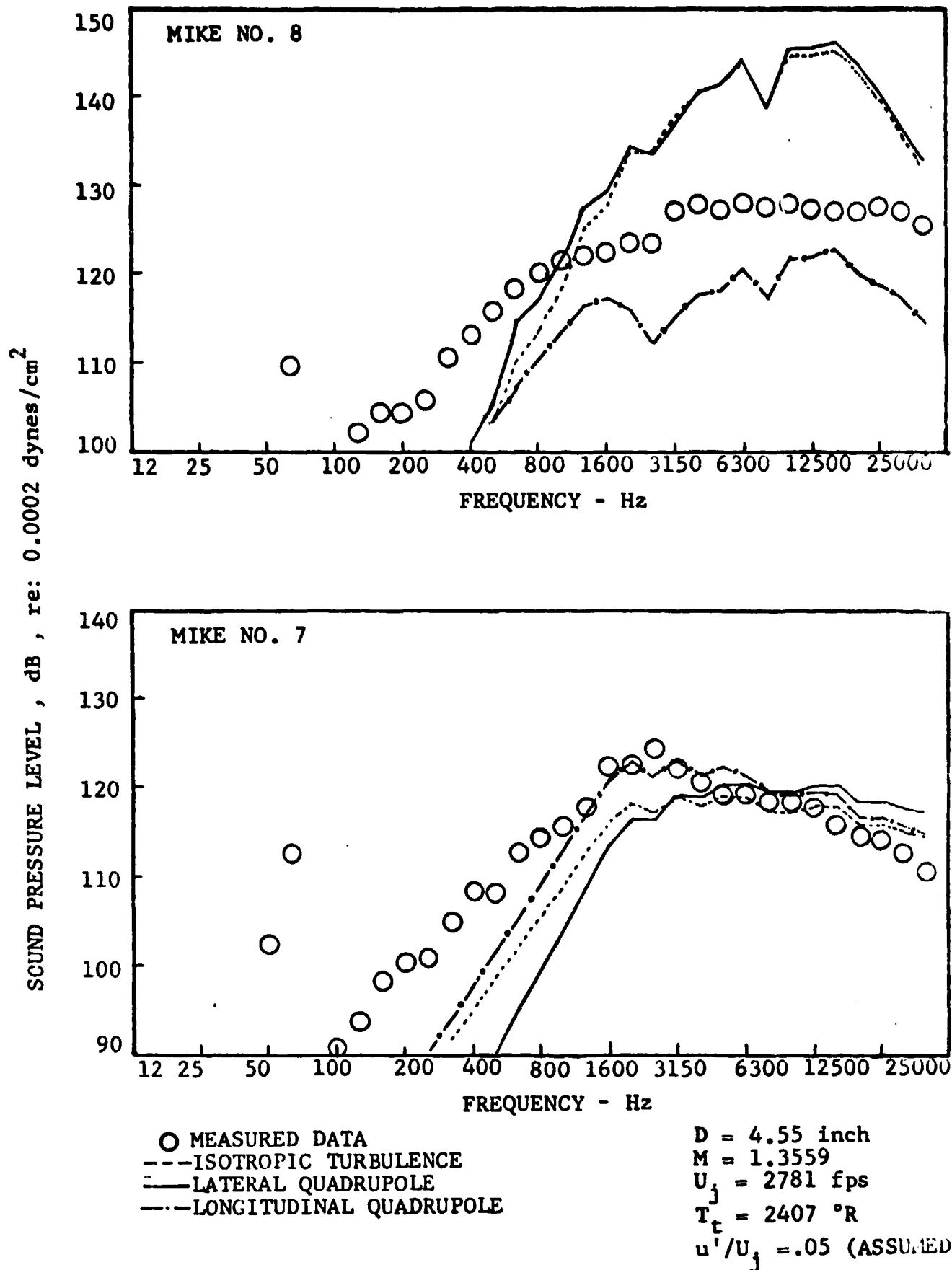
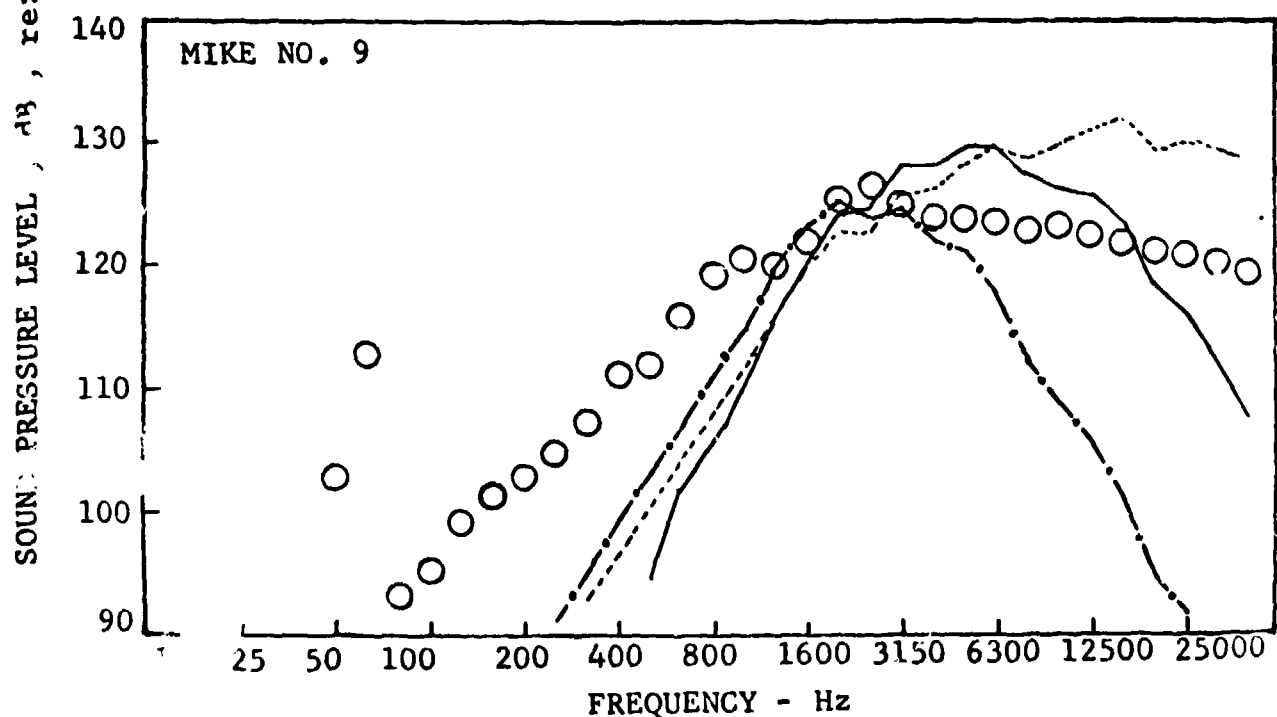
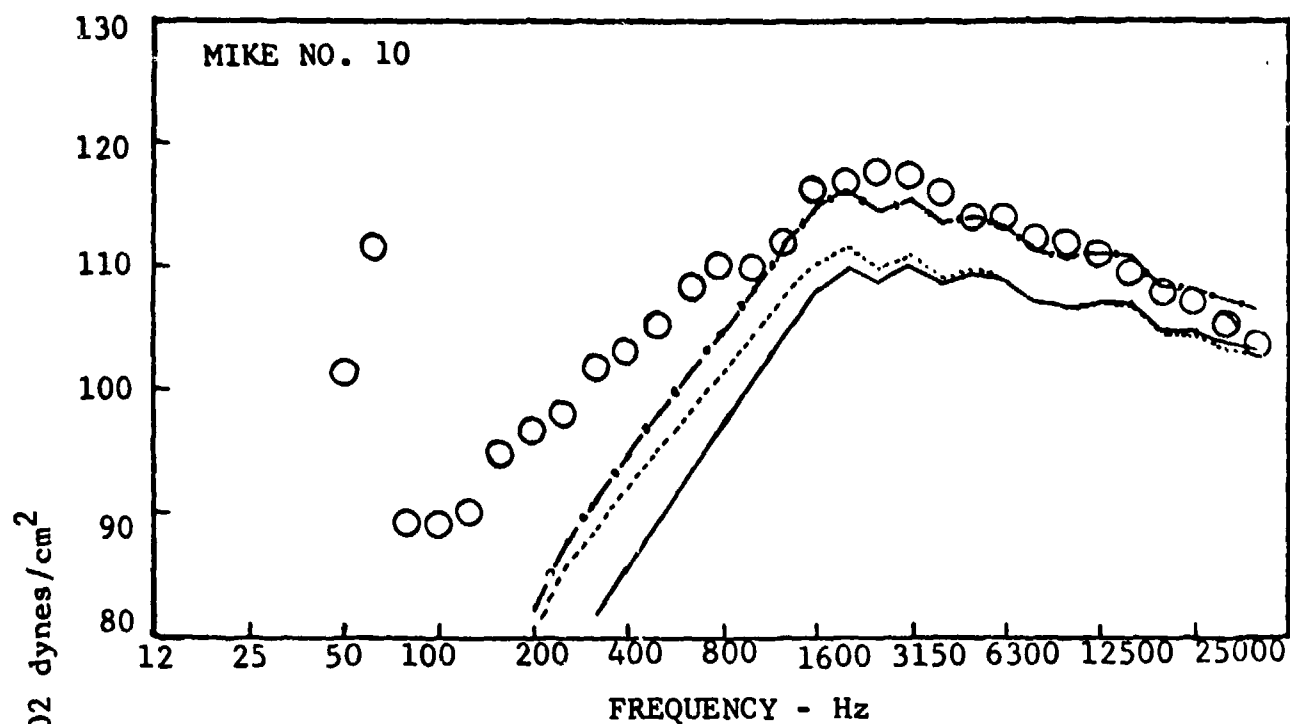


FIGURE 6(d) -

1/3 OCTAVE BAND FREQUENCY SPECTRA  
 COMPARISON OF PREDICTION AND MEASUREMENTS



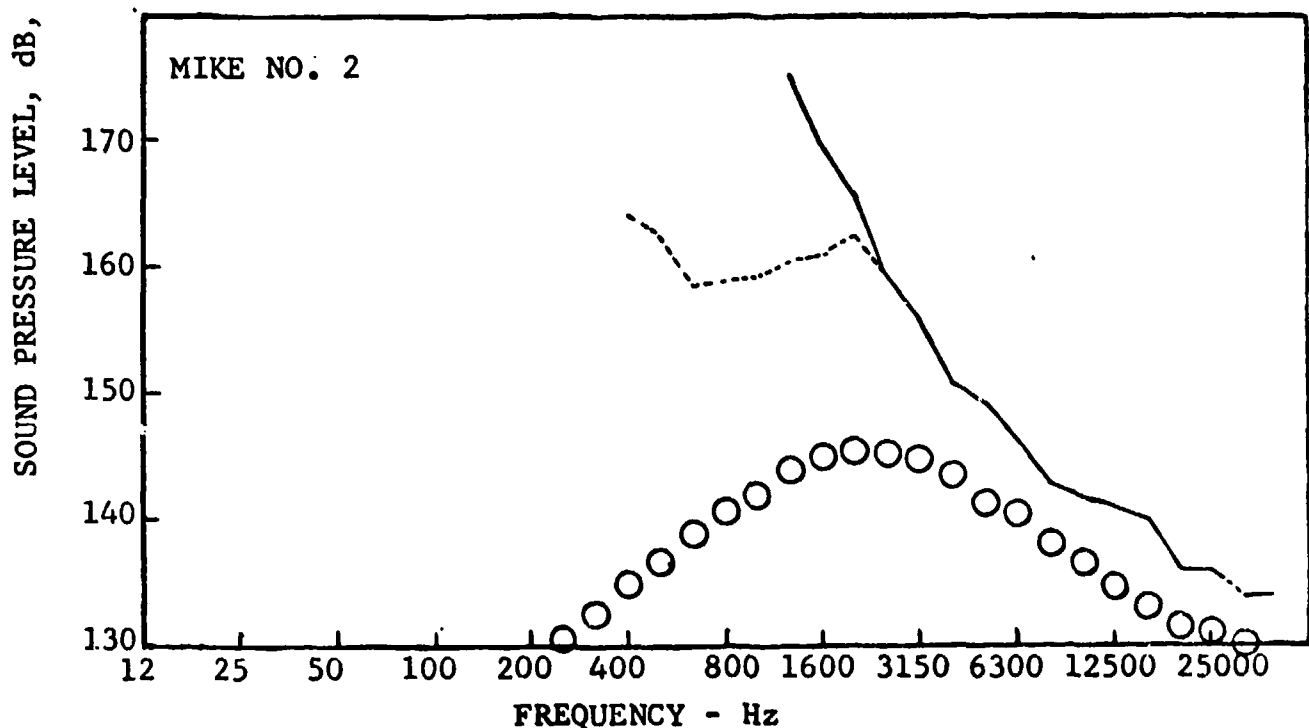
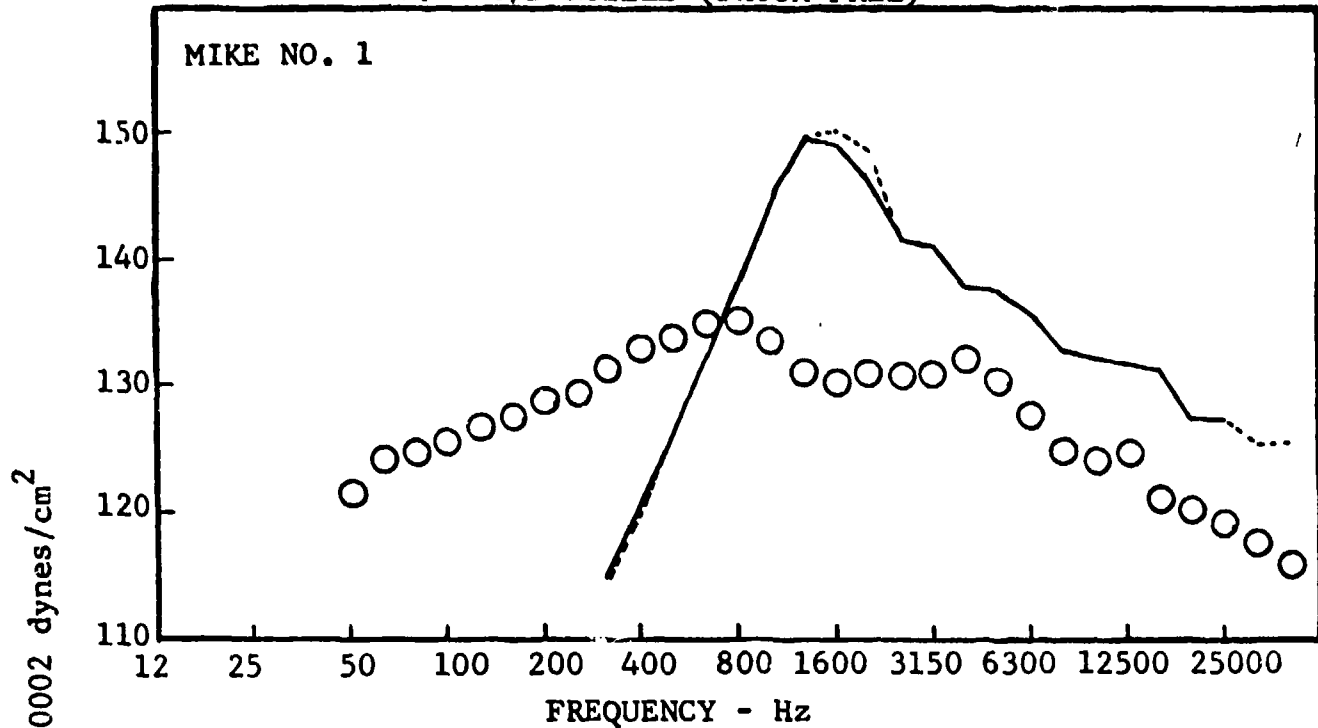
○ MEASURED DATA  
 --- ISOTROPIC TURBULENCE  
 — LATERAL QUADRUPOLE  
 -·- LONGITUDINAL QUADRUPOLE

$D = 4.55$  inch  
 $M = 1.3559$   
 $U_j = 2781$  fps  
 $T_t = 2407$  °R  
 $u'/U_j = .05$  (ASSUMED)

FIGURE 6(e)

1/3 OCTAVE BAND FREQUENCY SPECTRA  
 COMPARISON OF PREDICTION AND MEASUREMENTS

# RDG. 4 C/D NOZZLE (SHOCK FREE)

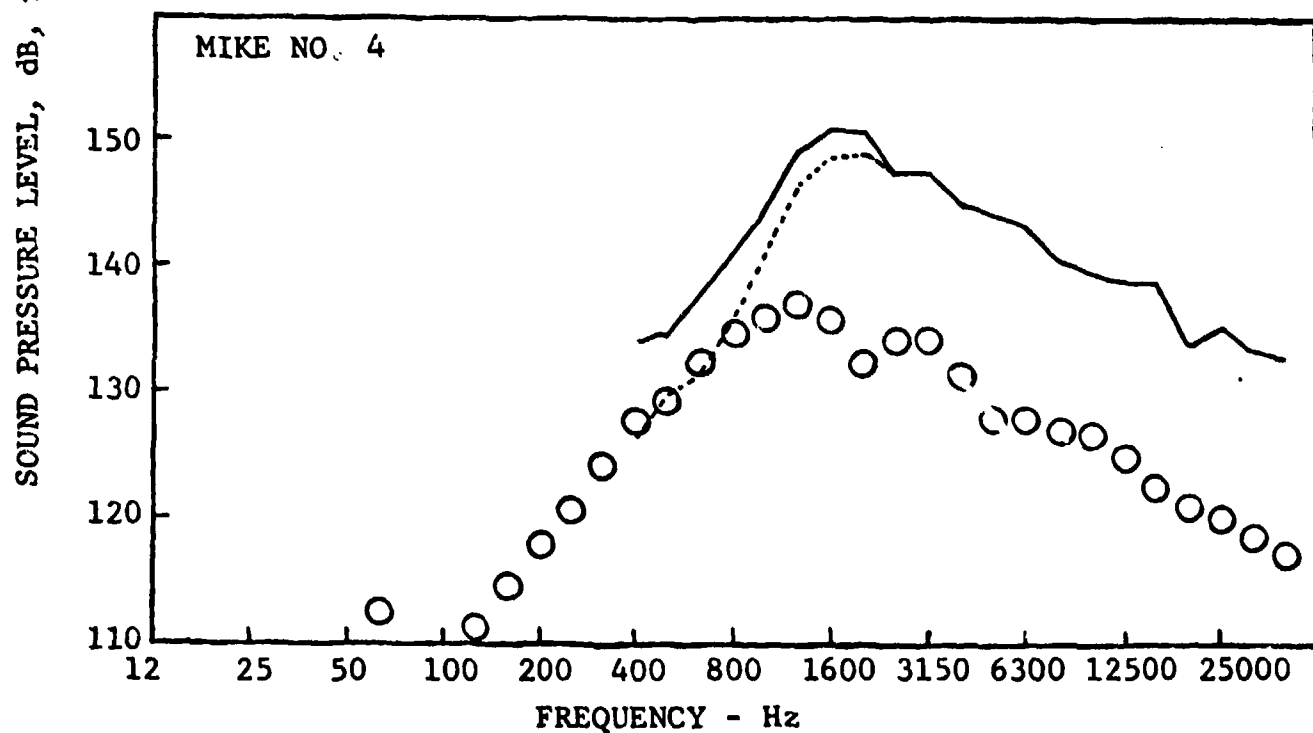
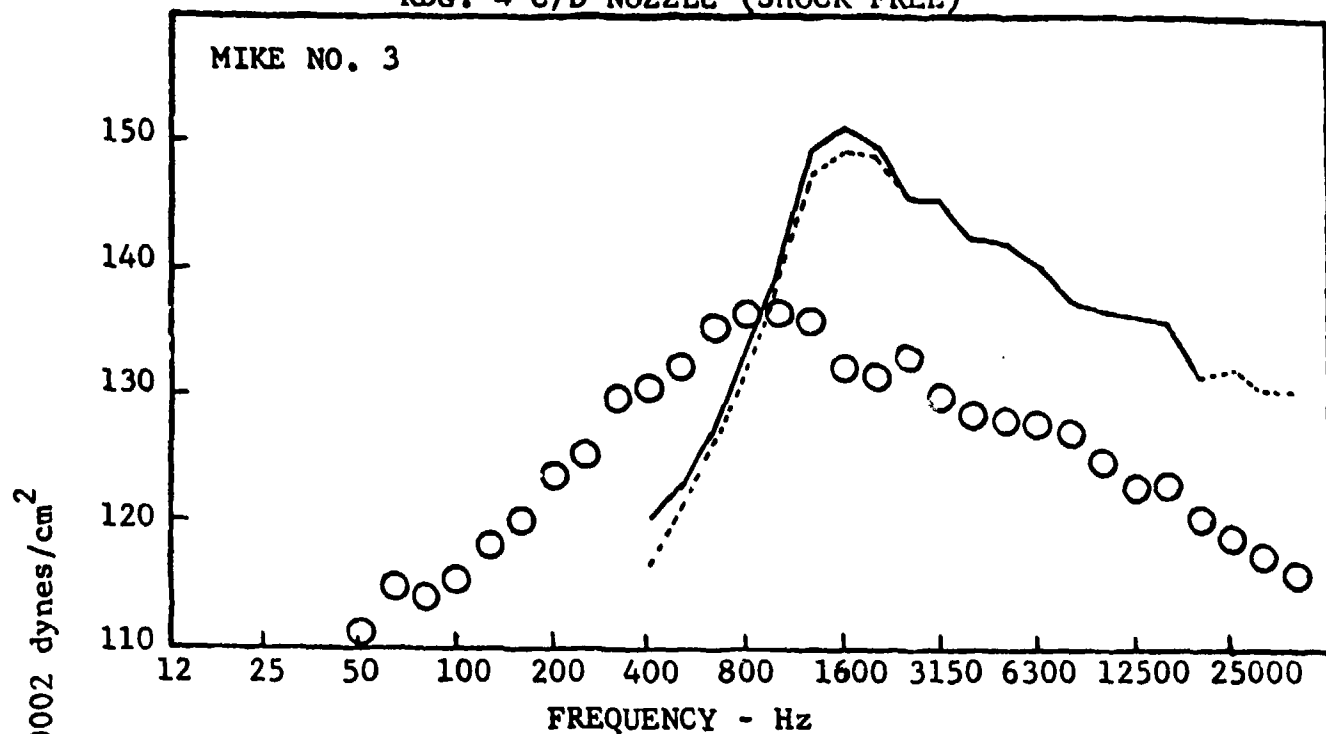


○ MEASURED DATA  
 --- COMPOSITE ACOUSTIC  
 MODEL II  
 — COMPOSITE ACOUSTIC  
 MODEL I

D = 4.55 INCHES  
 M = 1.3559  
 $U_j = 2781$  fps  
 $T_t = 2407$  °R  
 $u'/U_j = .05$  (ASSUMED)

FIGURE 7(a) - 1/3 OCTAVE BAND FREQUENCY SPECTRA.  
 COMPARISON OF PREDICTION AND MEASUREMENTS

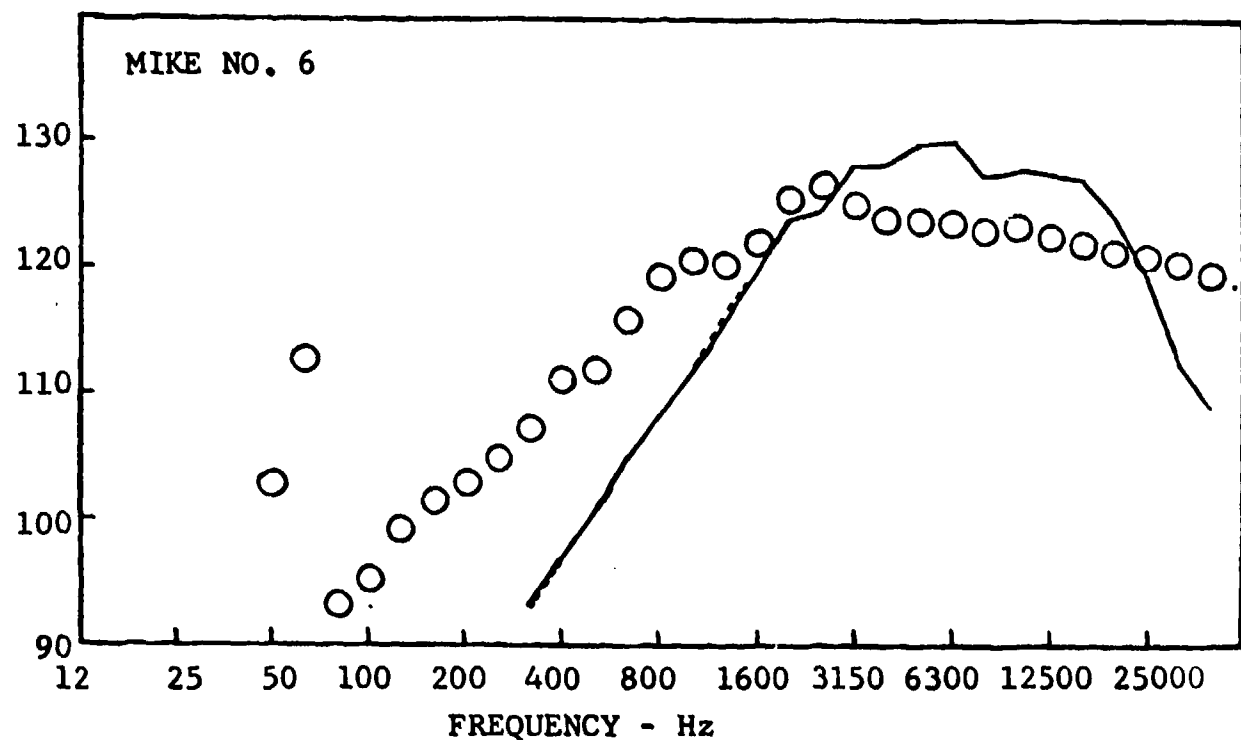
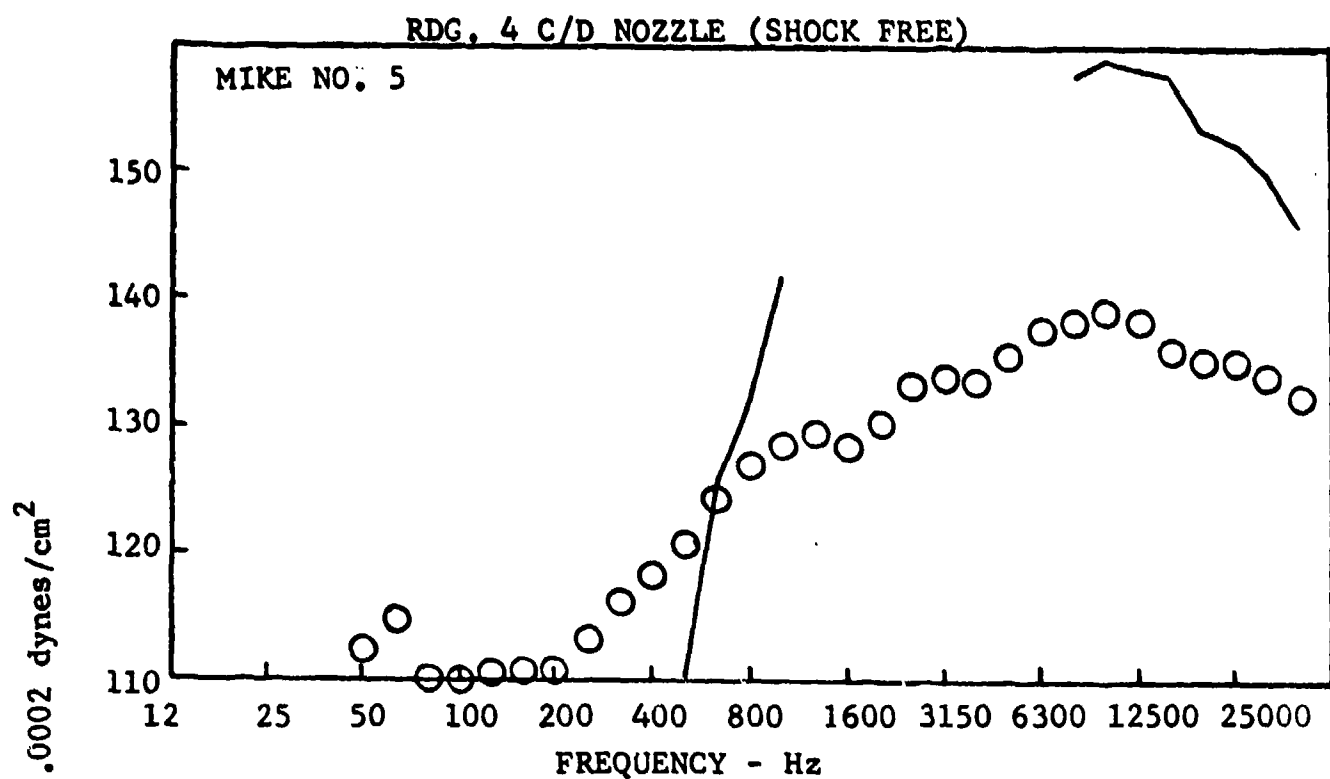
# RDG. 4 C/D NOZZLE (SHOCK FREE)



- MEASURED DATA
- COMPOSITE ACOUSTIC MODEL II
- COMPOSITE ACOUSTIC MODEL I

$D = 4.55$  INCHES  
 $M = 1.3559$   
 $U_j = 2781$  fps  
 $T_t = 2407$  °R  
 $u'/U_j = .05$  (ASSUMED)

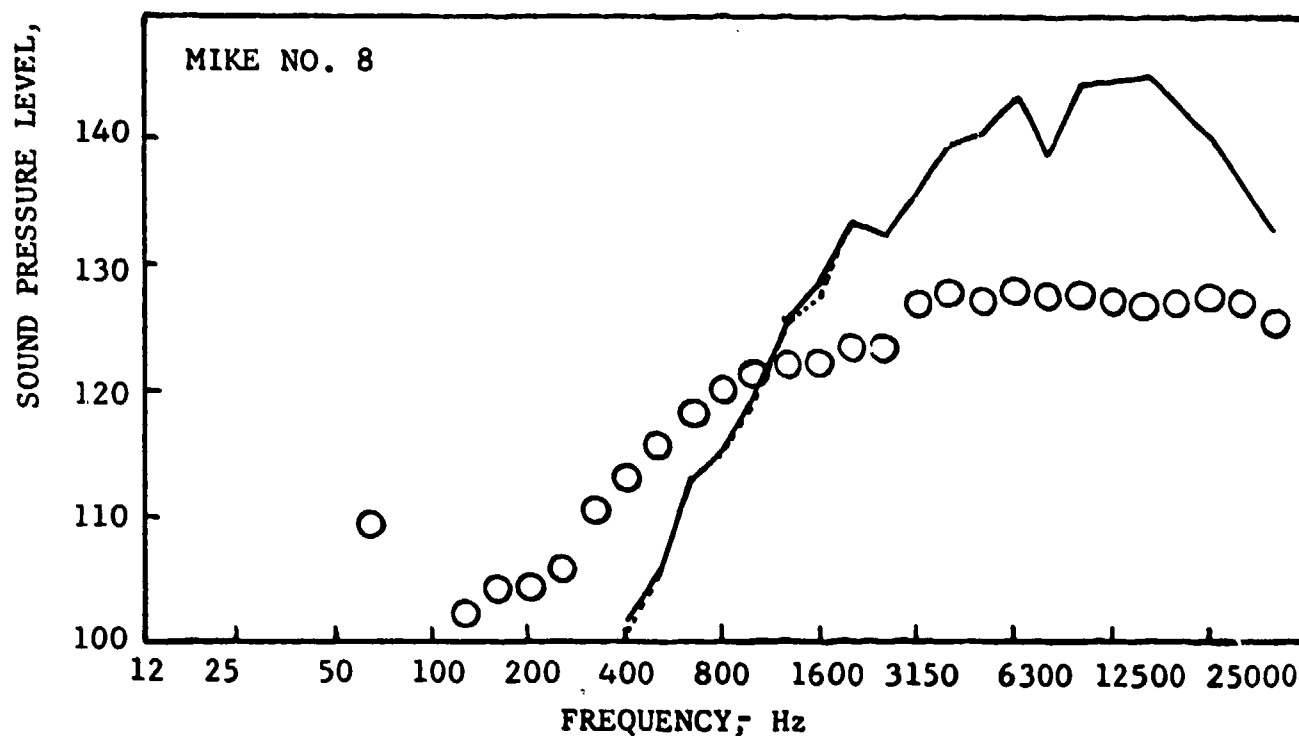
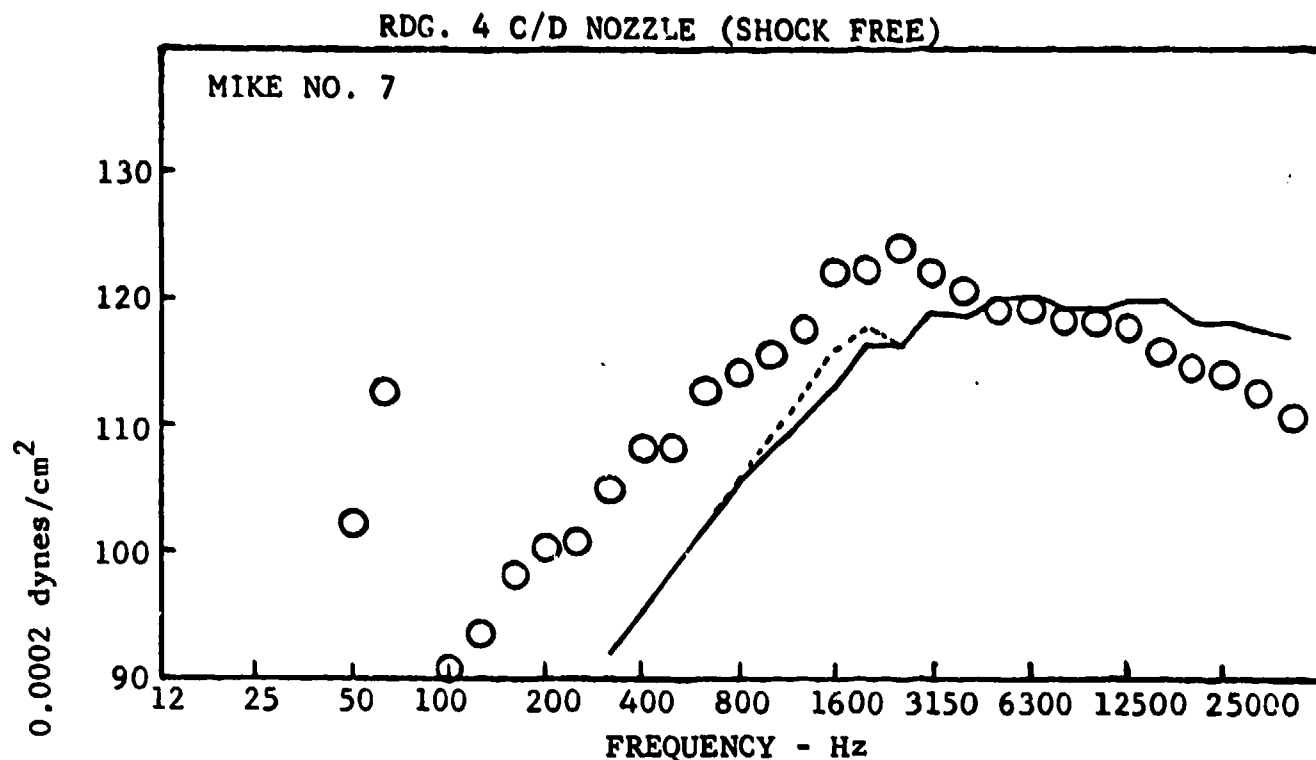
FIGURE 7(b) - 1/3 OCTAVE BAND FREQUENCY SPECTRA.  
COMPARISON OF PREDICTION AND MEASUREMENTS



- MEASURED DATA
- COMPOSITE ACOUSTIC MODEL II
- COMPOSITE ACOUSTIC MODEL I

$D = 4.55$  INCHES  
 $M = 1.3559$   
 $U_j = 2781$  fps  
 $T_t = 2407$  °R  
 $u'/U_j = .05$  (ASSUMED)

FIGURE 7(c) - 1/3 OCTAVE BAND FREQUENCY SPECTRA.  
COMPARISON OF PREDICTION AND MEASUREMENTS.



○ MEASURED DATA  
 --- COMPOSITE ACOUSTIC MODEL II  
 — COMPOSITE ACOUSTIC MODEL I

$D = 4.55$  INCH  
 $M = 1.3559$   
 $U_j = 2781$   
 $T_T = 2407^\circ R$   
 $u'/U_j = .05$  (ASSUMED)

FIGURE 7(d) - 1/3 OCTAVE BAND FREQUENCY SPECTRA.  
 COMPARISON OF PREDICTION AND MEASUREMENTS.

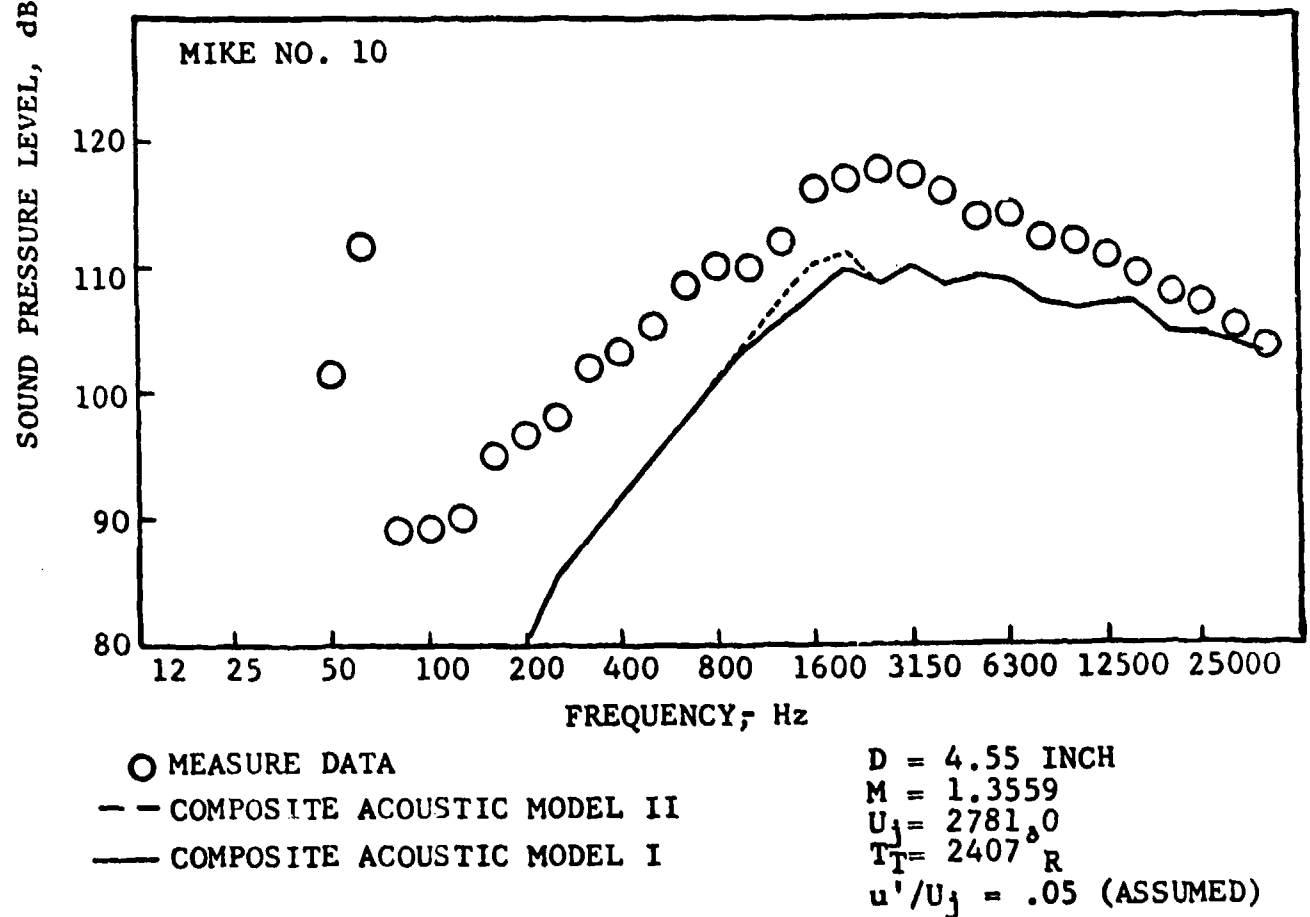
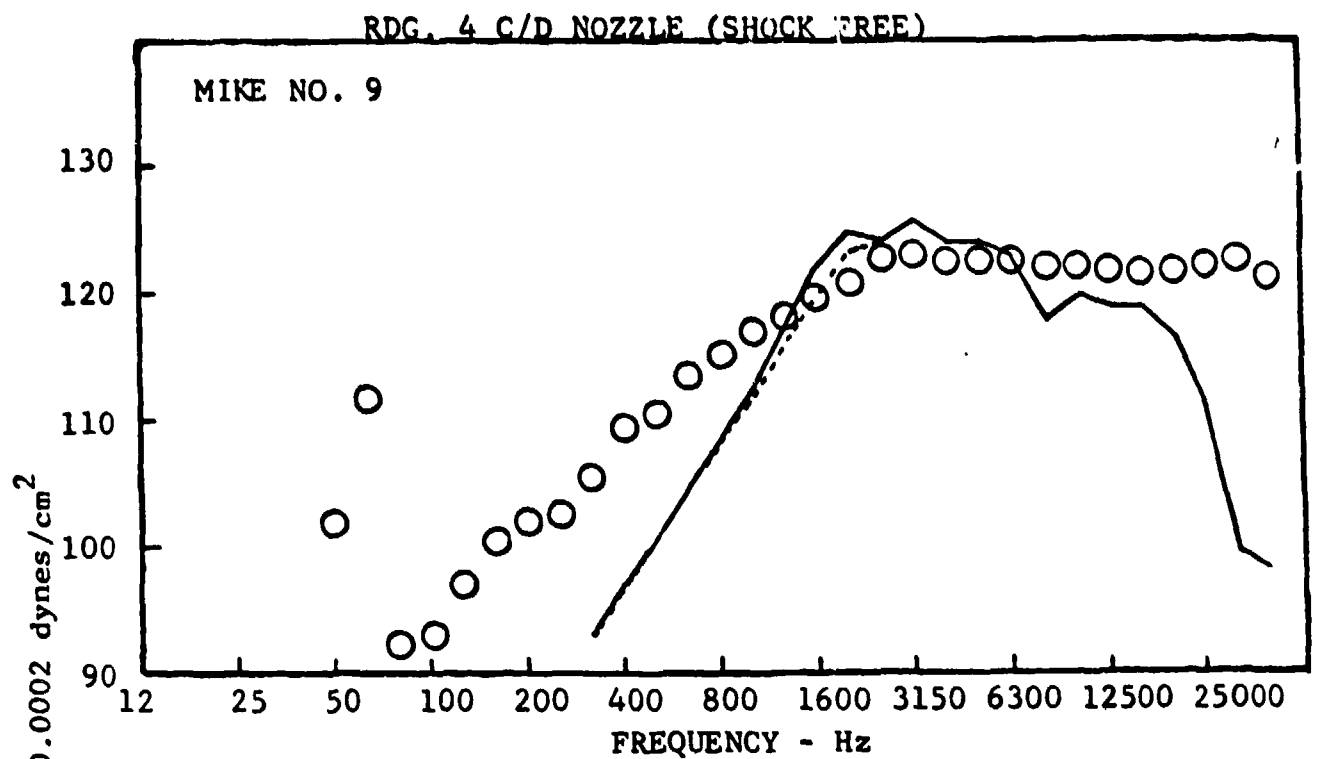
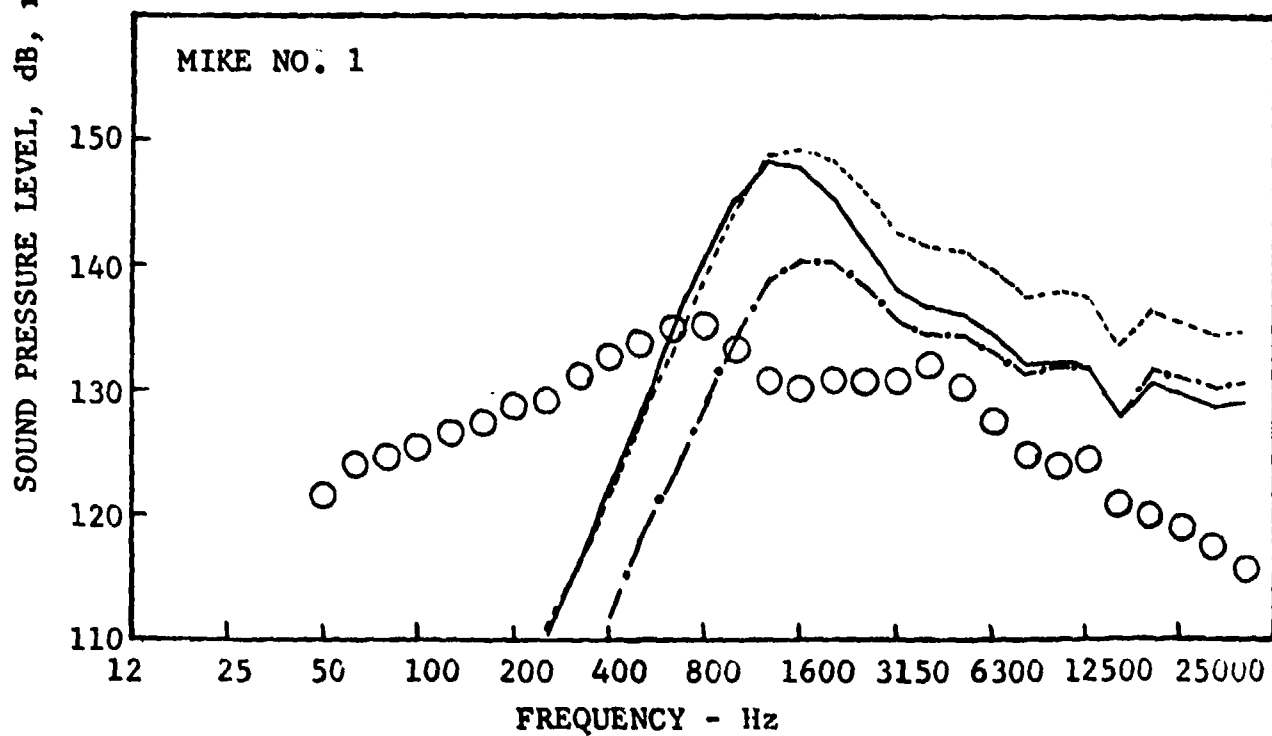
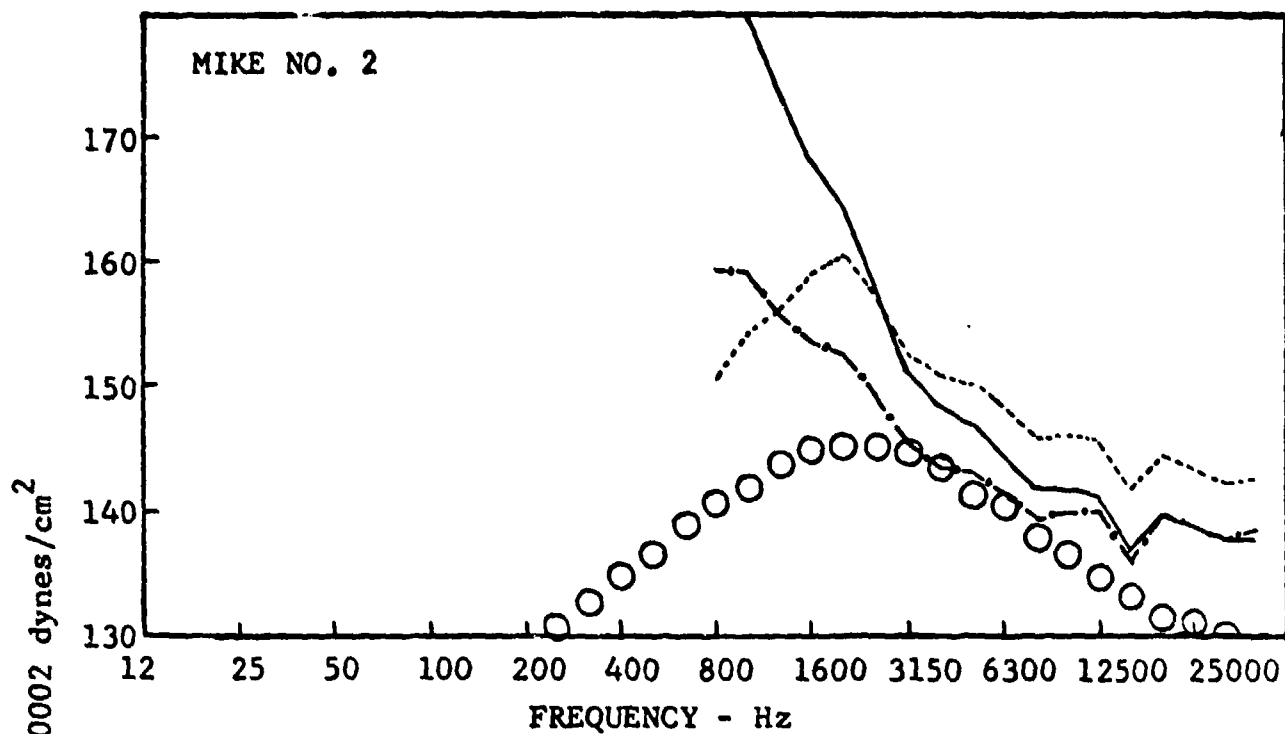


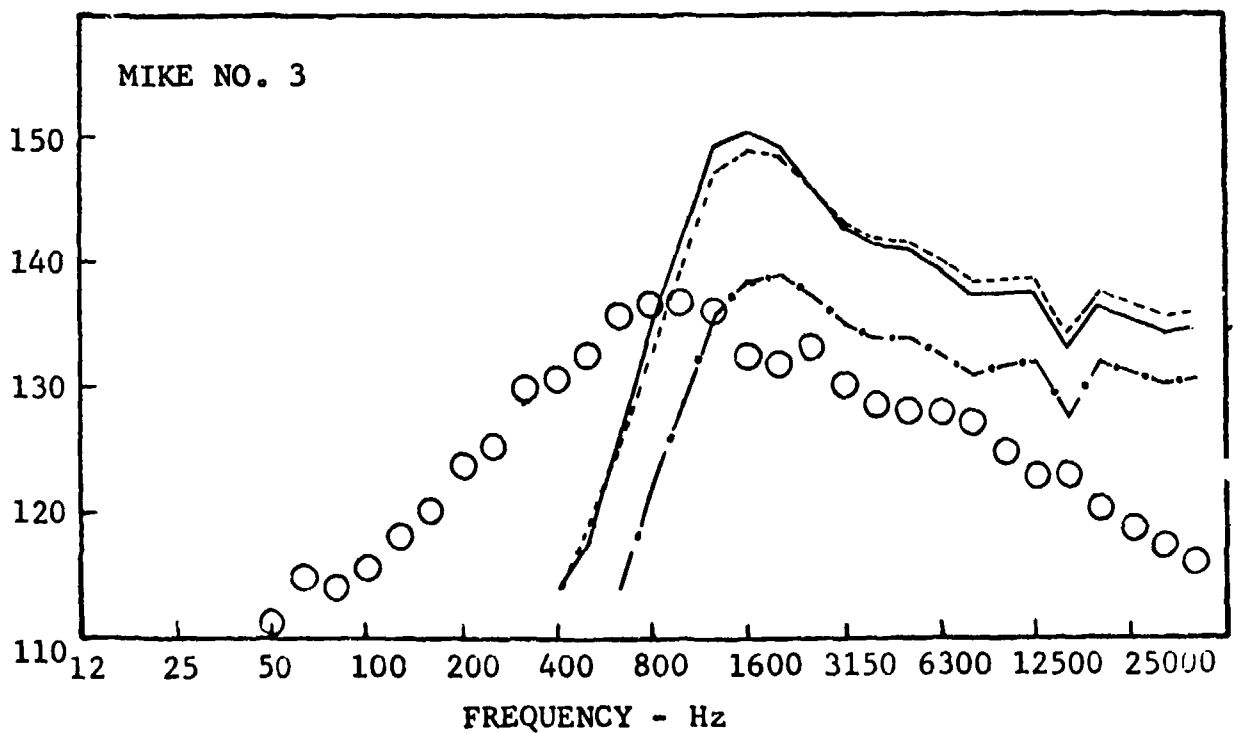
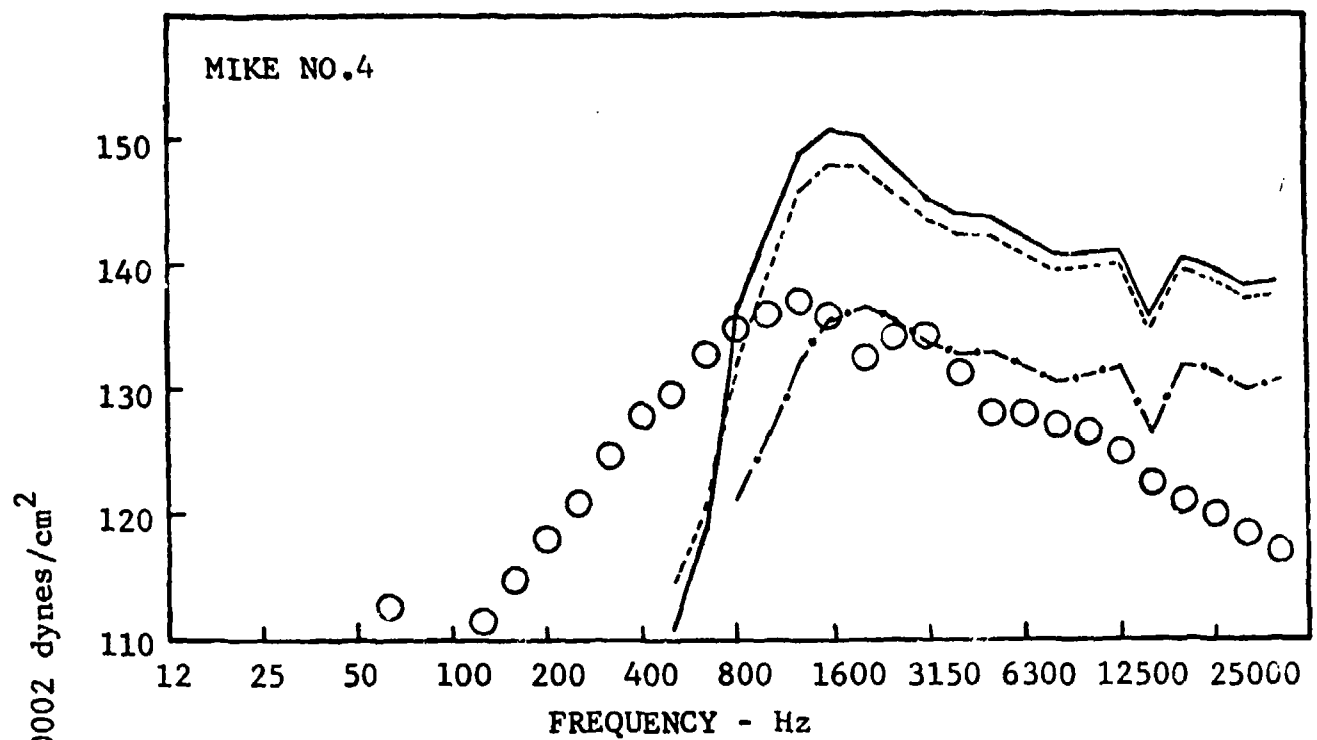
FIGURE 7(e) - 1/3 OCTAVE BAND FREQUENCY SPECTRA. COMPARISON OF PREDICTION AND MEASUREMENTS.



○ MEASURED DATA  
 -- ISOTROPIC TURBULENCE  
 — LATERAL QUADRUPOLE  
 -.- LONGITUDINAL QUADRUPOLE

D = 4.55 INCHES  
 M = 1.3559  
 U<sub>j</sub> = 2781 fps  
 T<sub>t</sub> = 2407 °R  
 u'/U<sub>j</sub> = .15 (ASSUMED)

FIGURE 8(a) - 1/3 OCTAVE BAND FREQUENCY SPECTRA.  
 COMPARISON OF PREDICTION AND MEASUREMENTS.



○ MEASURED DATA  
 --- ISOTROPIC TURBULENCE  
 — LATERAL QUADRUPOLE  
 - - - LONGITUDINAL QUADRUPOLE

D = 4.55 INCHES  
 M = 1.3559  
 U<sub>j</sub> = 2781 fps  
 T<sub>t</sub> = 2407 °R  
 u'/U<sub>j</sub> = .15 (ASSUMED)

FIGURE 8(b) - 1/3 OCTAVE BAND FREQUENCY SPECTRA.  
 COMPARISON OF PREDICTION AND MEASUREMENTS.

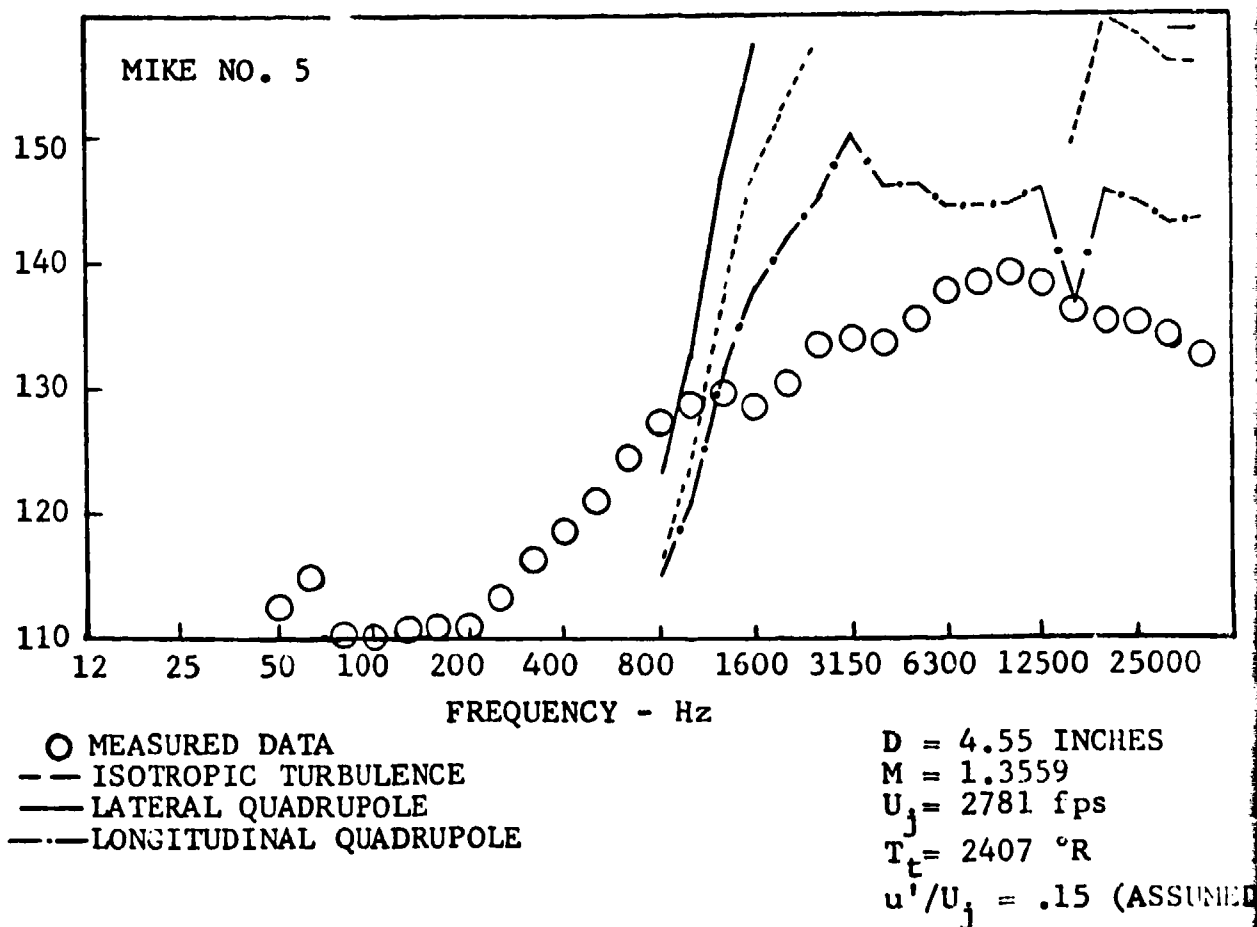
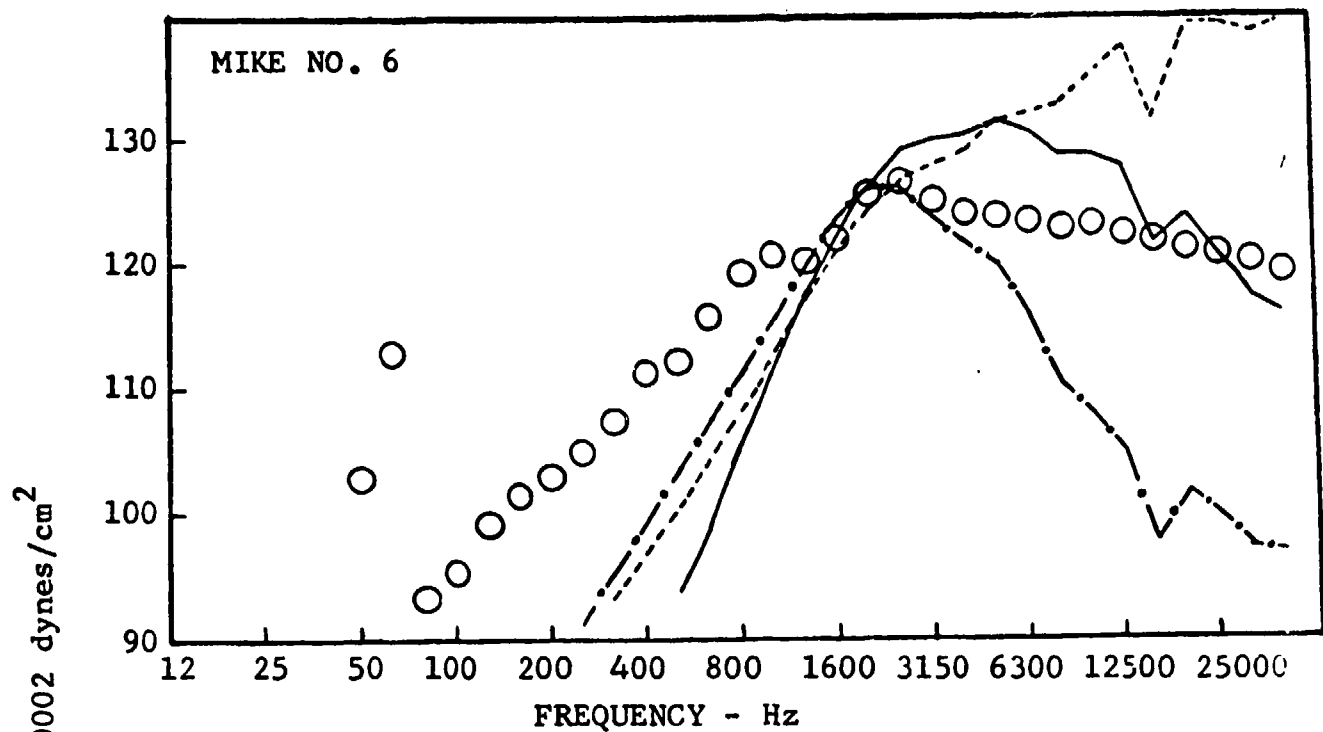


FIGURE 8(c) - 1/3 OCTAVE BAND FREQUENCY SPECTRA.  
 COMPARISON OF PREDICTION AND MEASUREMENTS.

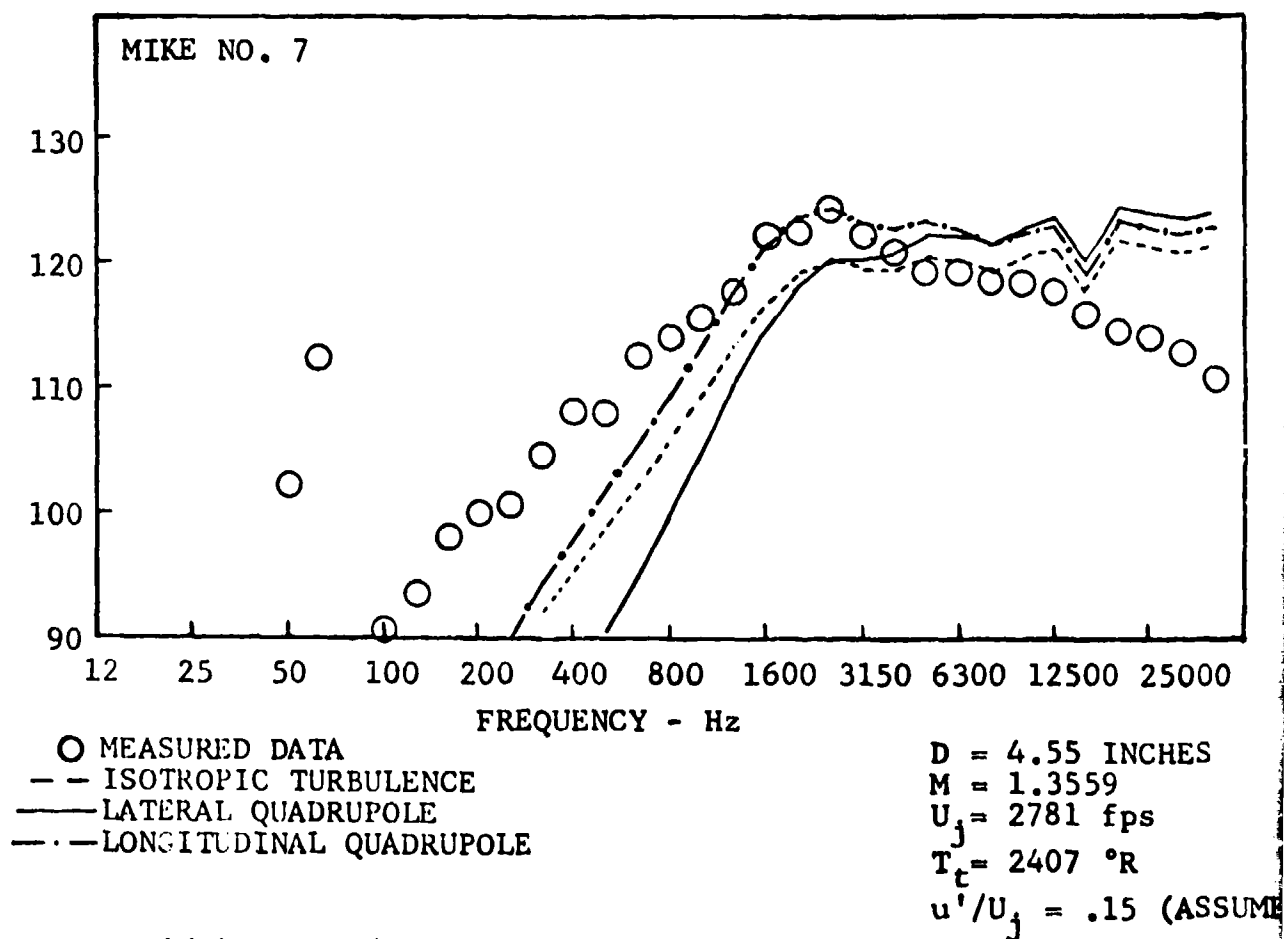
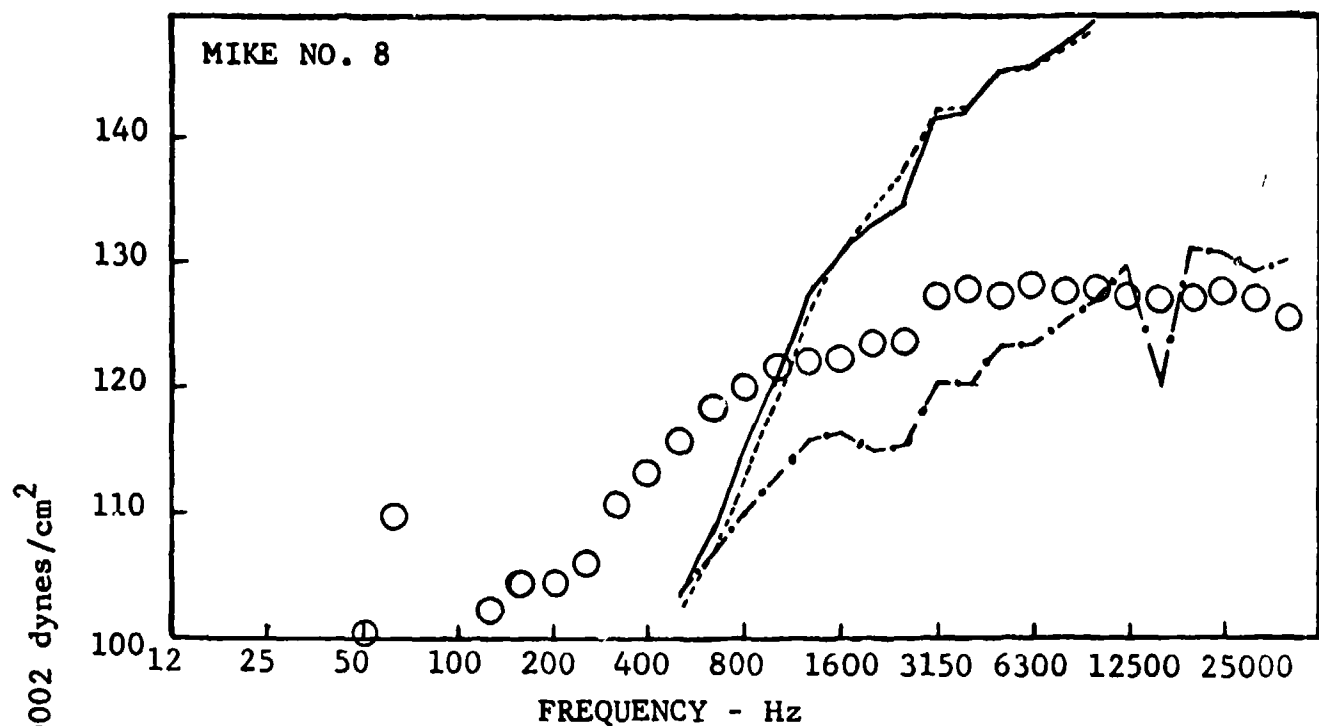


FIGURE 8(d) - 1/3 OCTAVE BAND FREQUENCY SPECTRA  
 COMPARISON OF PREDICTION AND MEASUREMENTS.

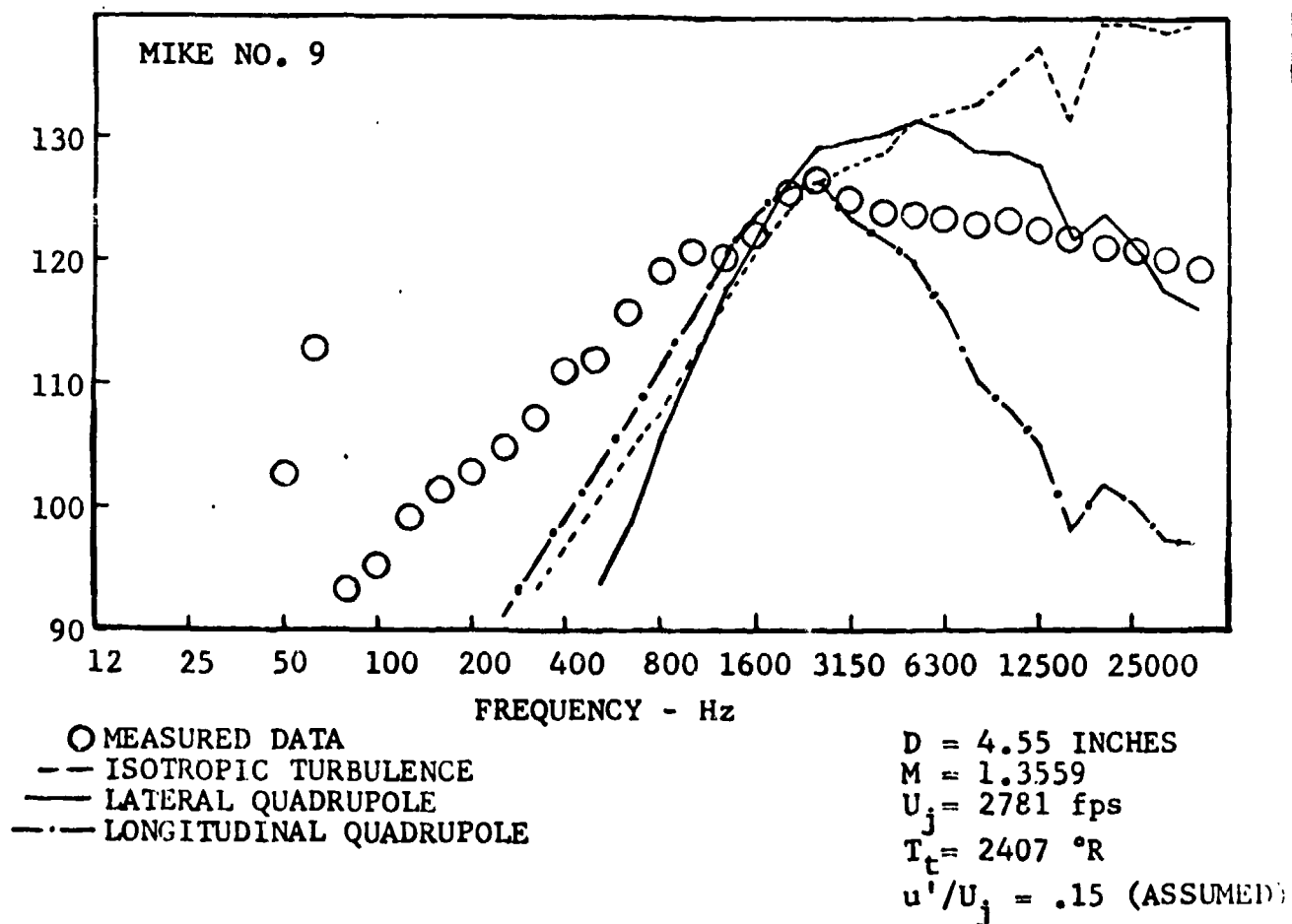
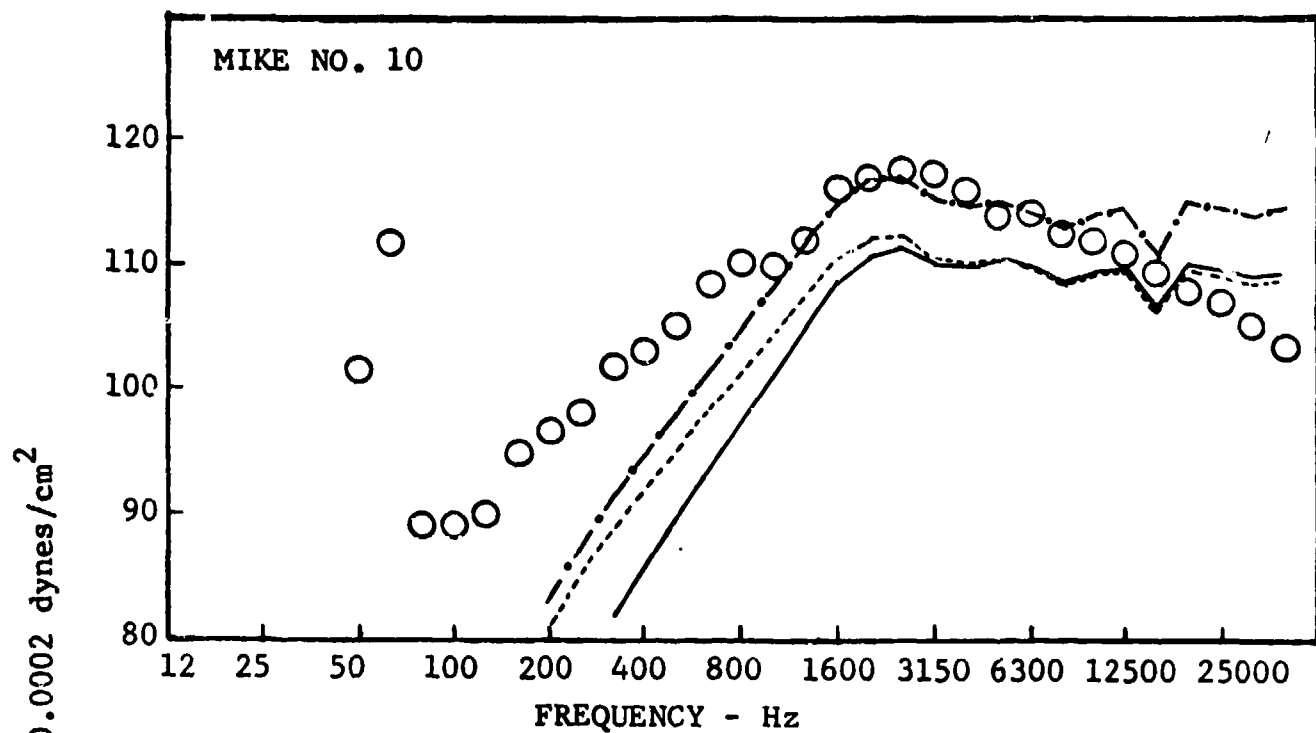


FIGURE 8(e) - 1/3 OCTAVE BAND FREQUENCY SPECTRA.  
COMPARISON OF PREDICTION AND MEASUREMENTS.

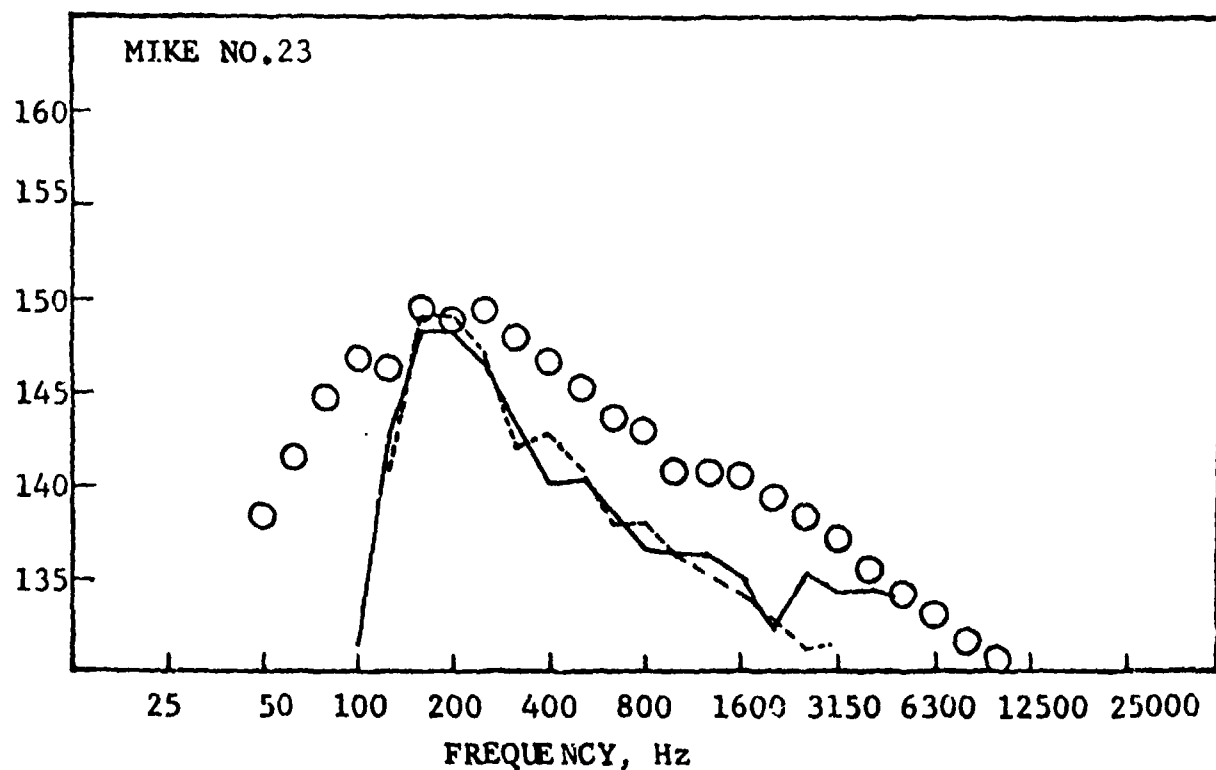
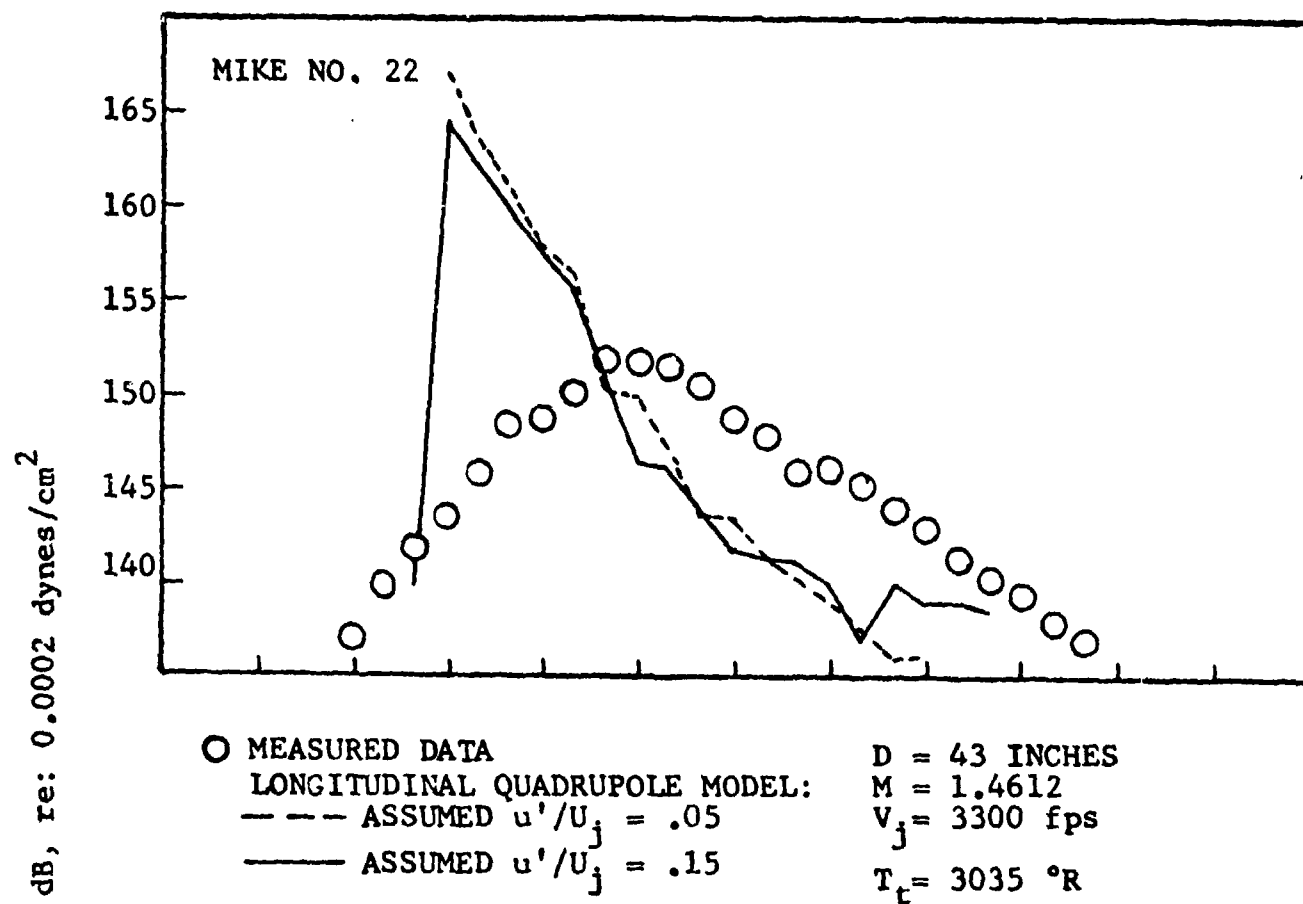


FIGURE 9(a) - EFFECT OF TURBULENCE LEVEL

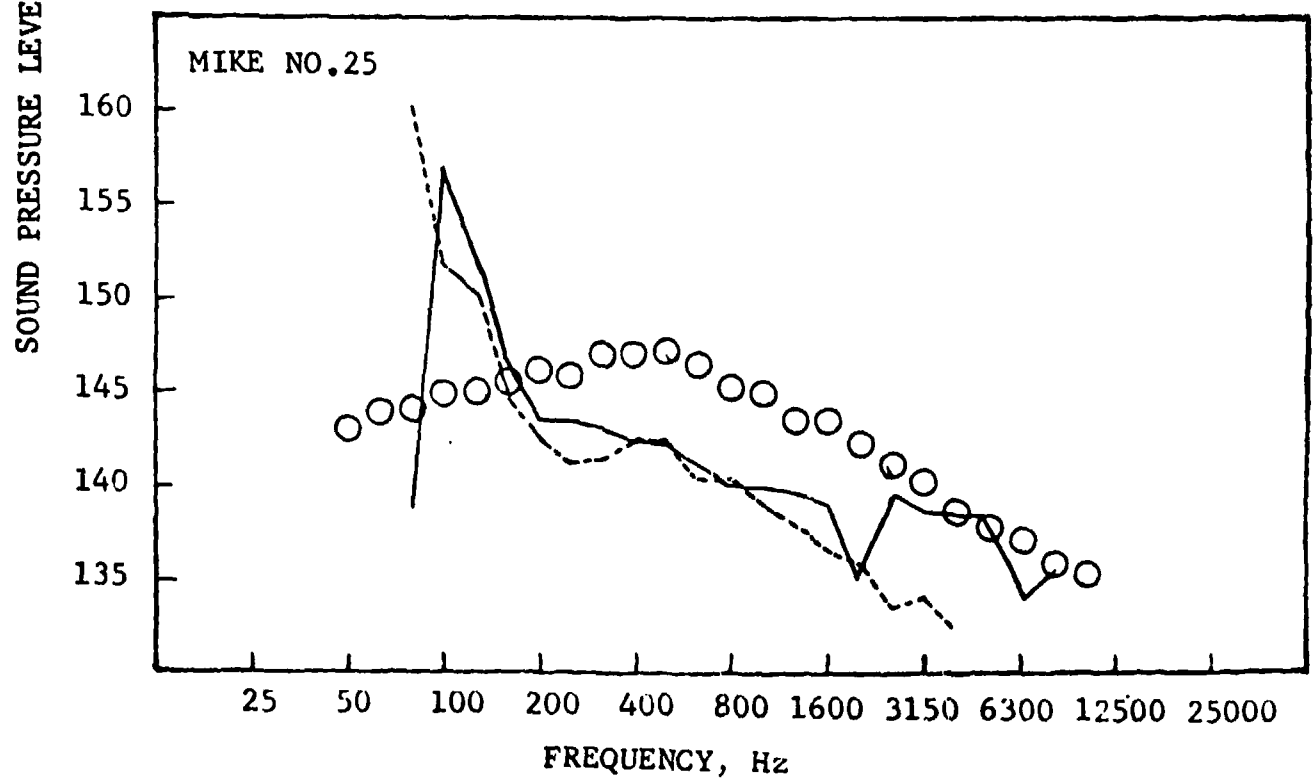
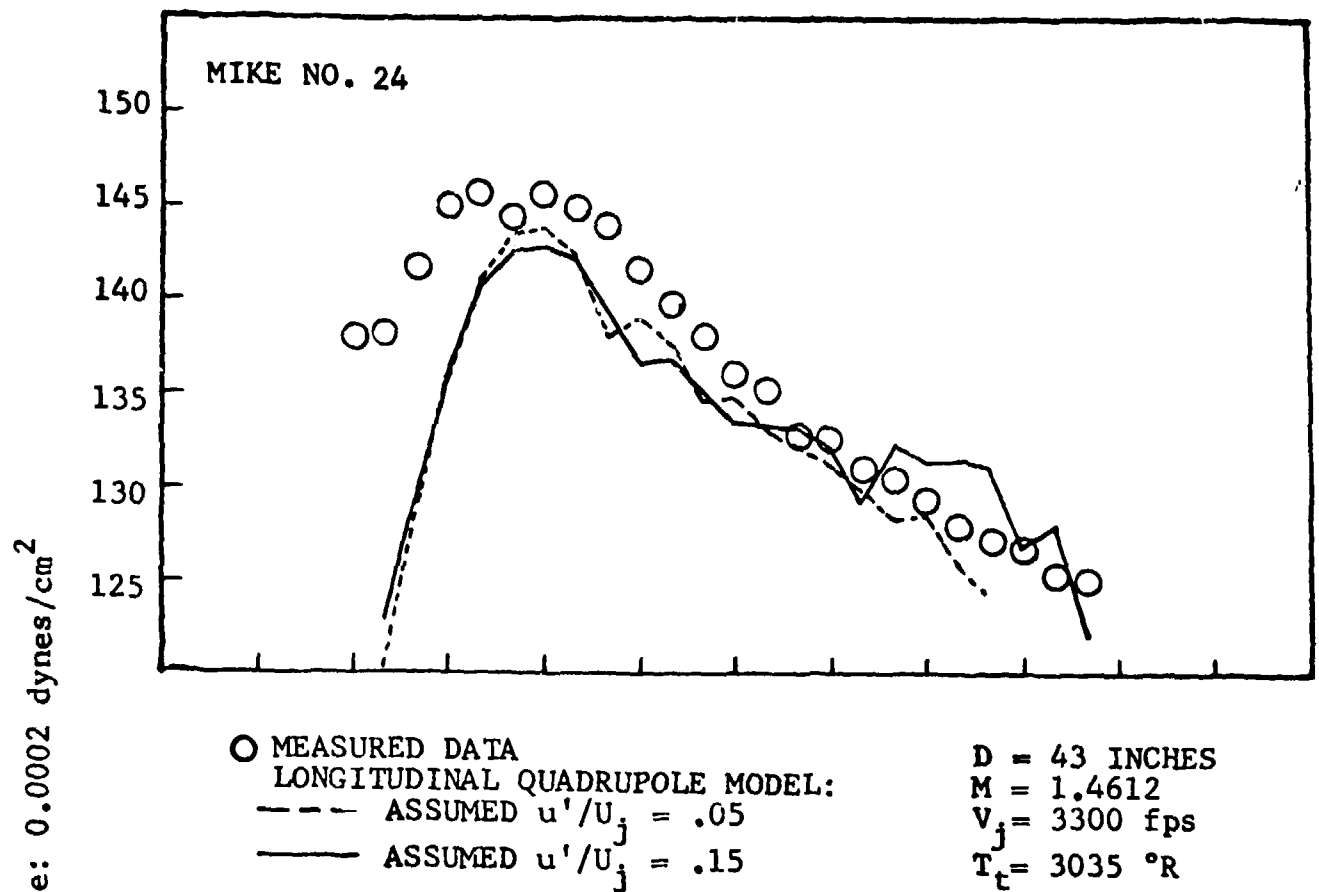


FIGURE 9(b) - EFFECT OF TURBULENCE LEVEL

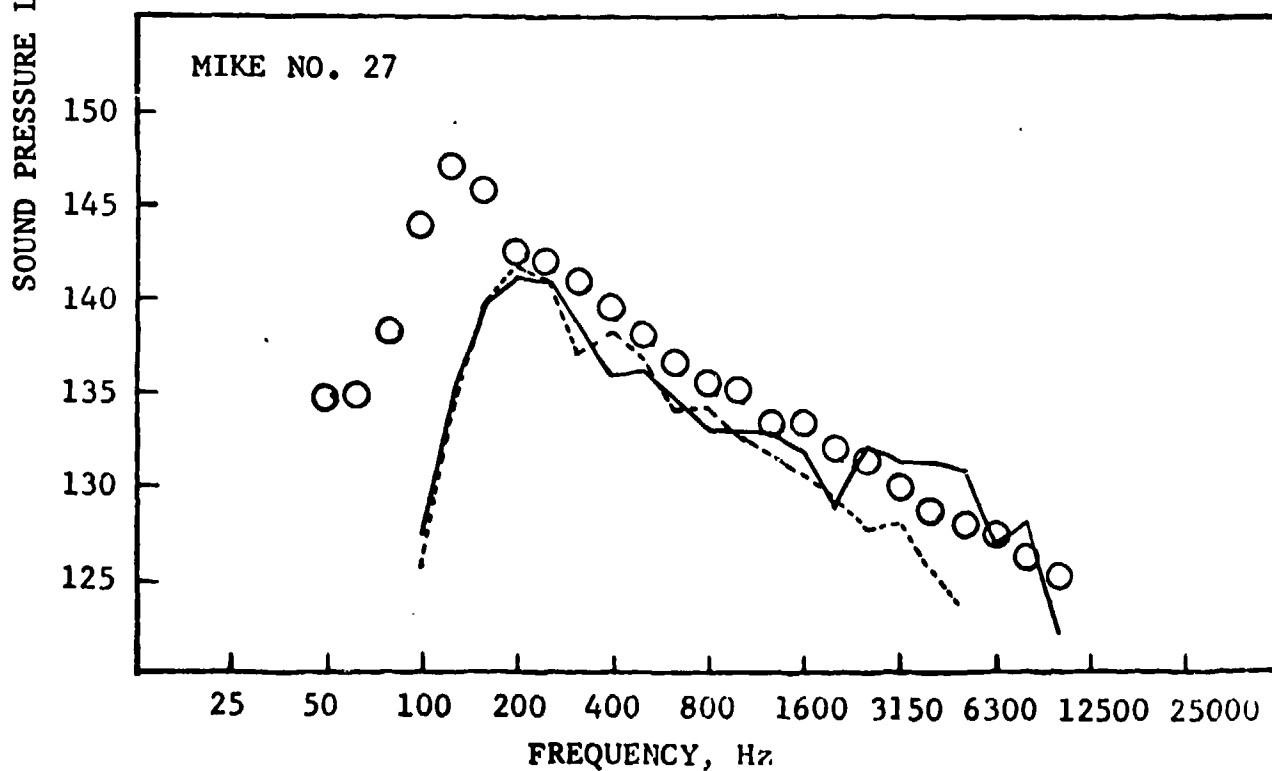
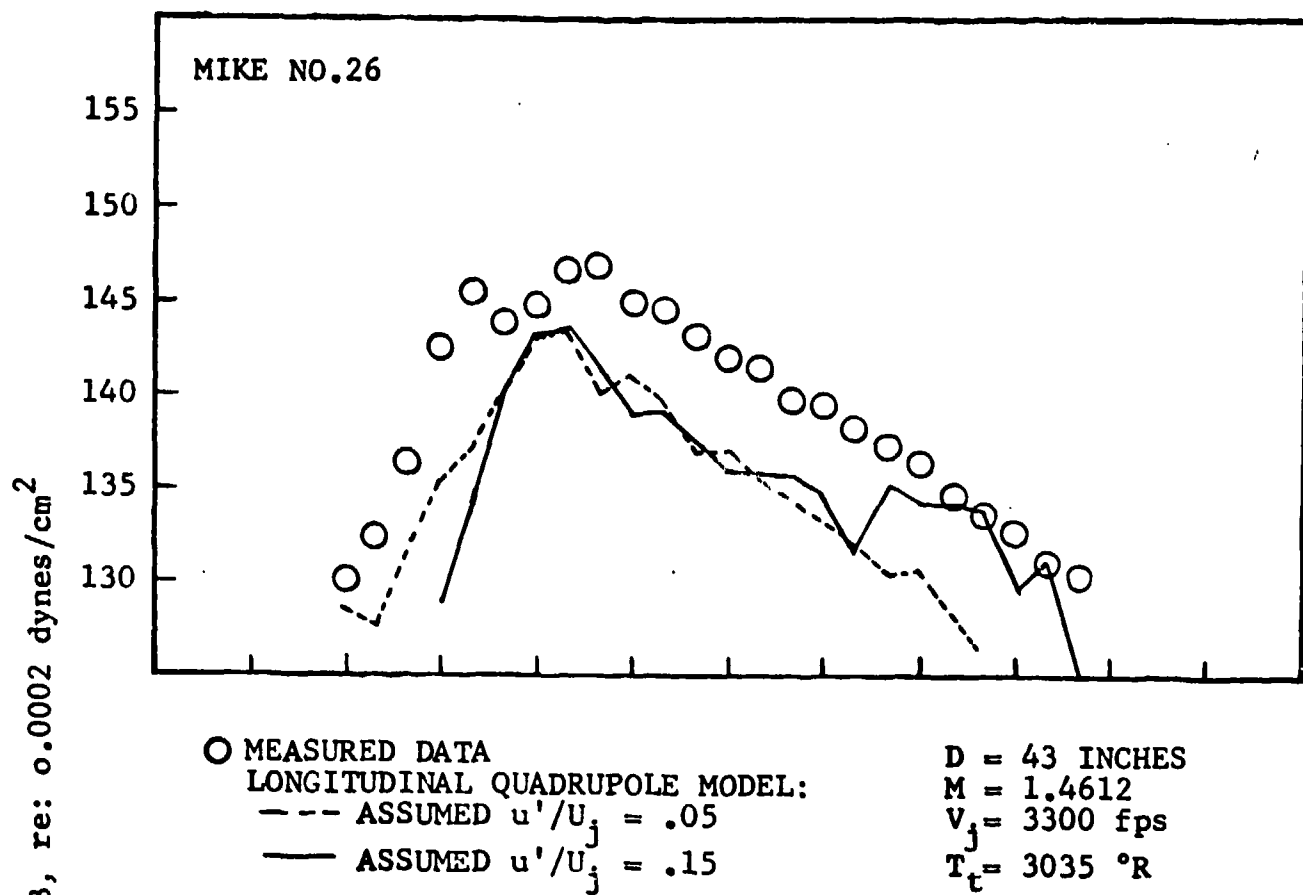


FIGURE 9(c) - EFFECT OF TURBULENCE LEVEL

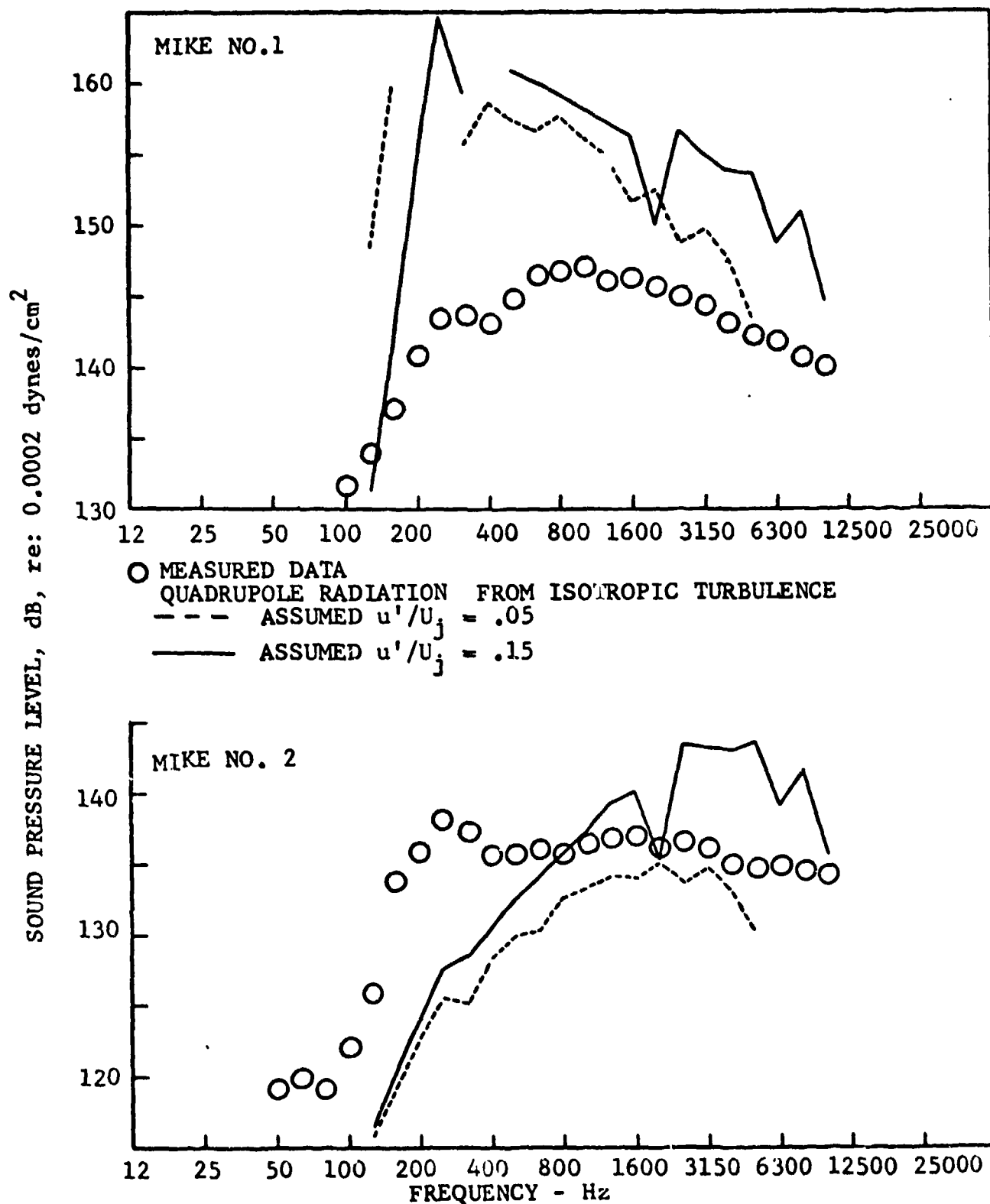


FIGURE 9(d) - EFFECT OF TURBULENCE LEVEL.

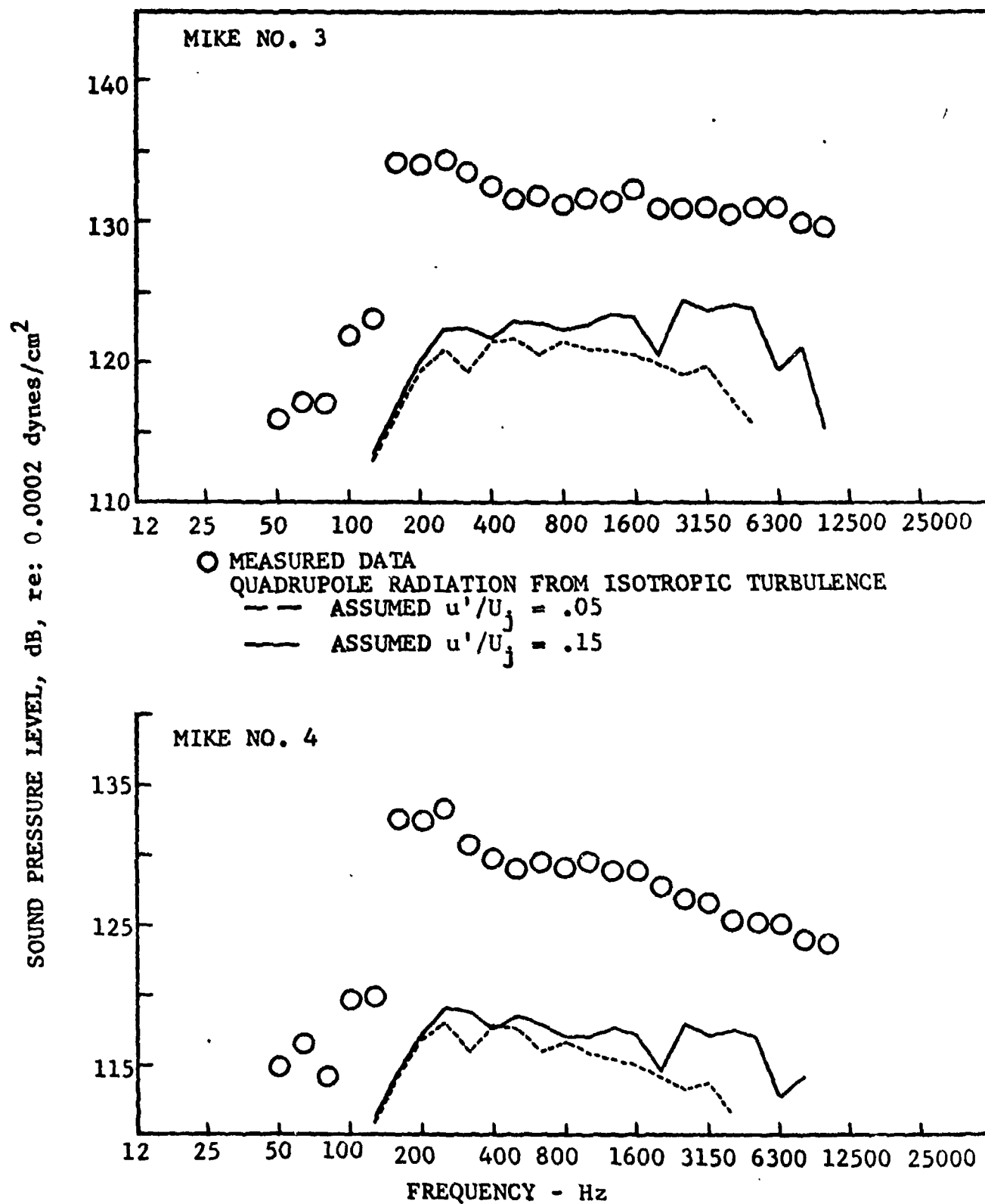


FIGURE 9(e) - EFFECT OF TURBULENCE LEVEL

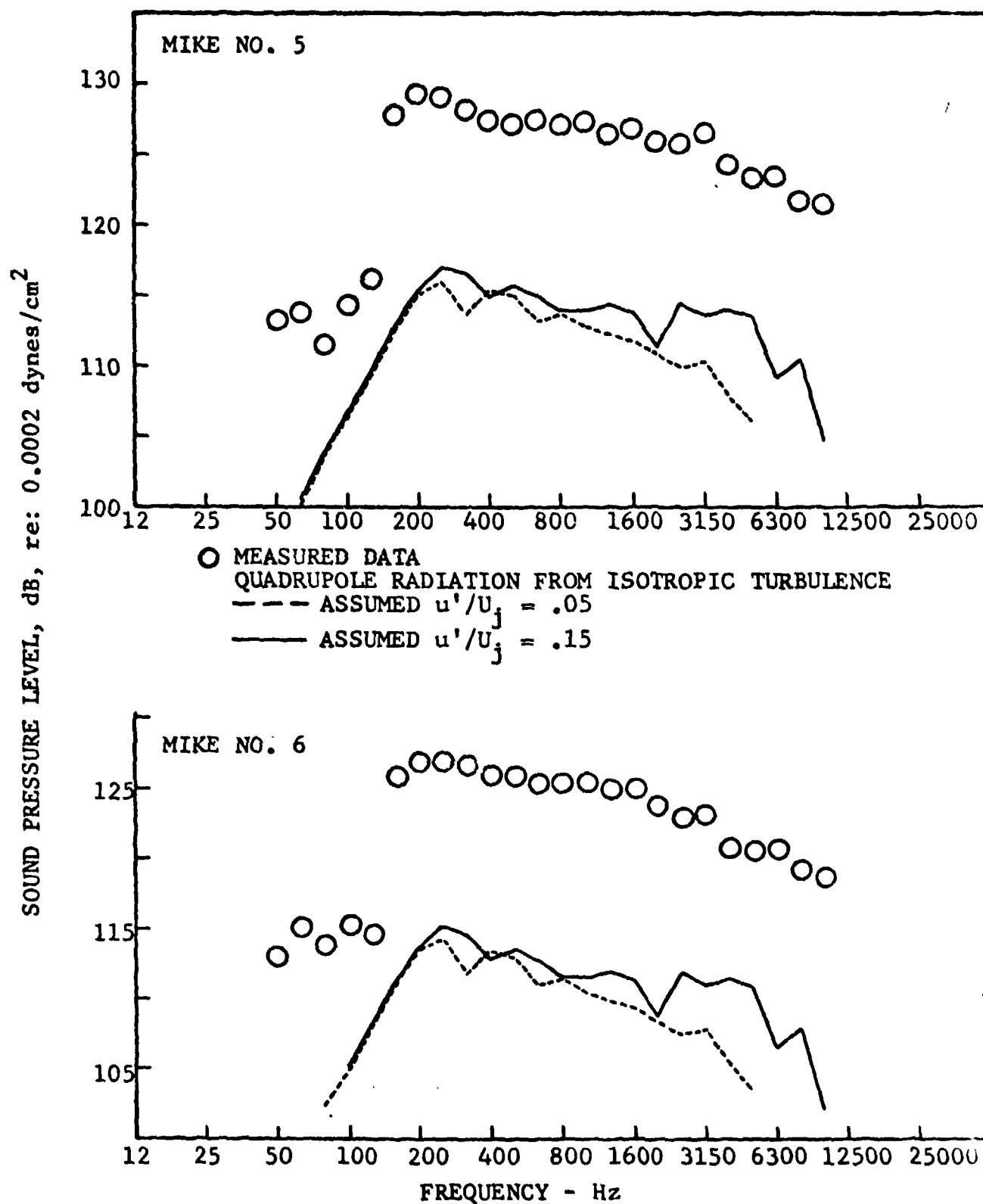


FIGURE 9(f) - EFFECT OF TURBULENCE LEVEL

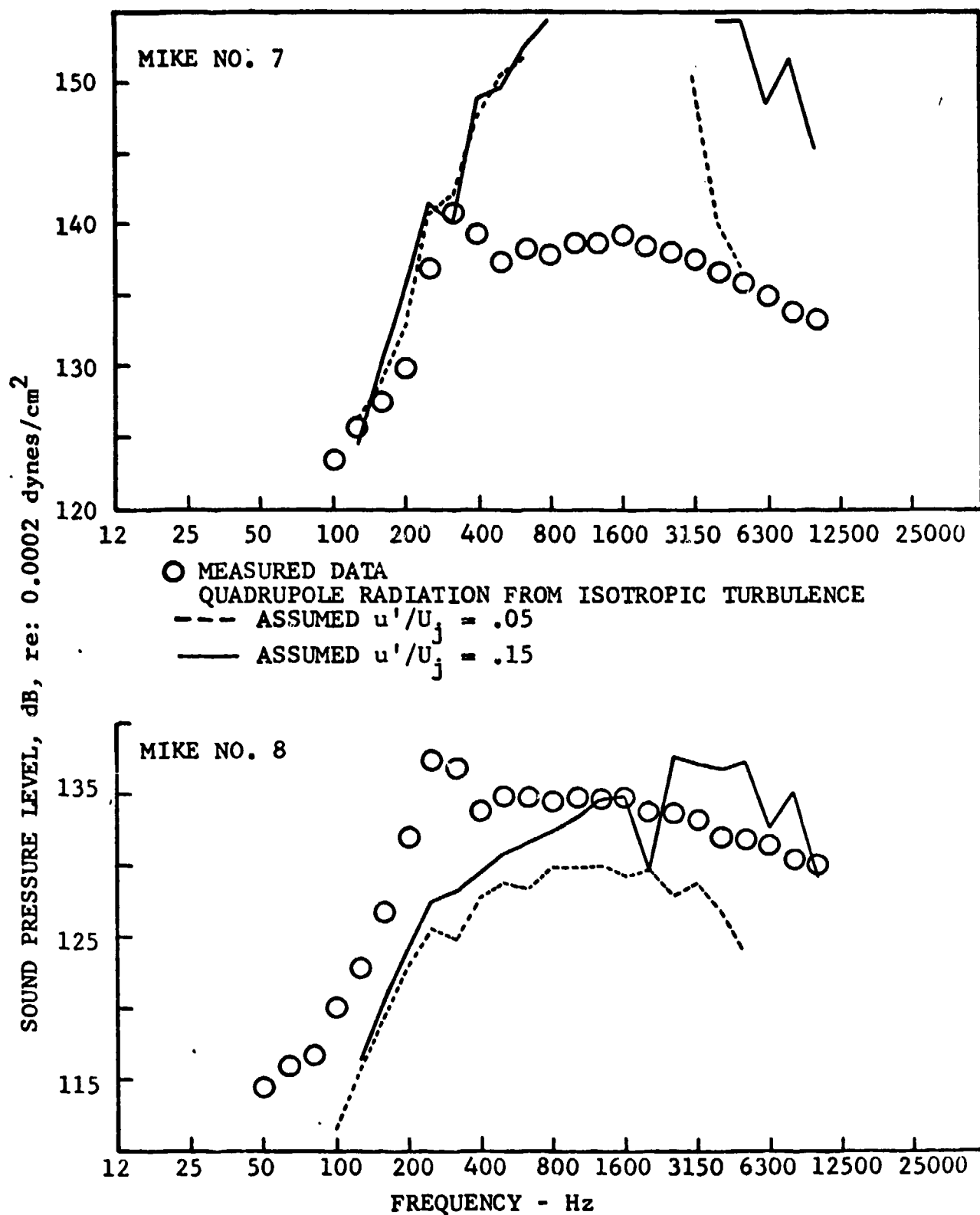


FIGURE 9(g) - EFFECT OF TURBULENCE LEVEL

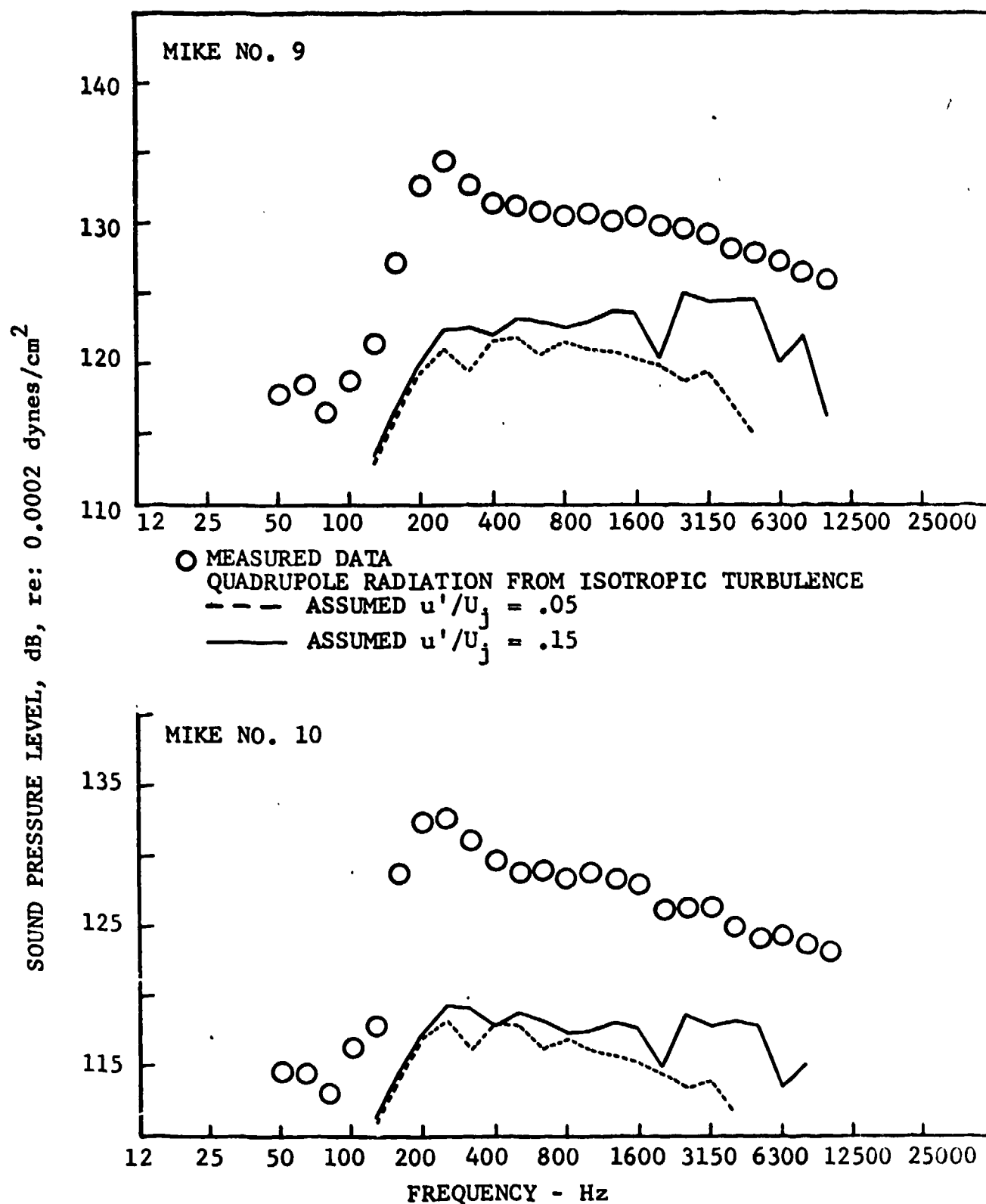


FIGURE 9(h) - EFFECT OF TURBULENCE LEVEL

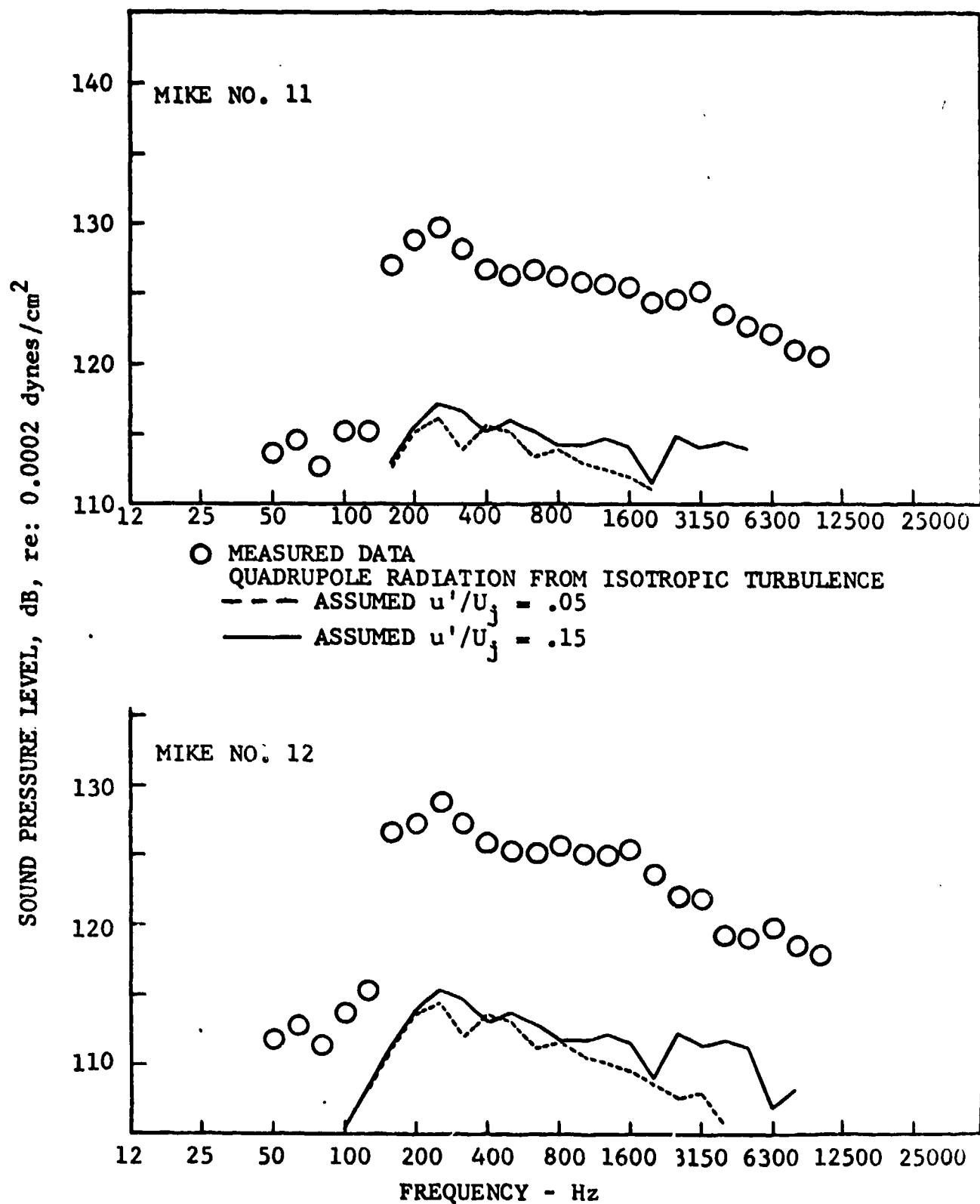


FIGURE 9(1) - EFFECT OF TURBULENCE LEVEL

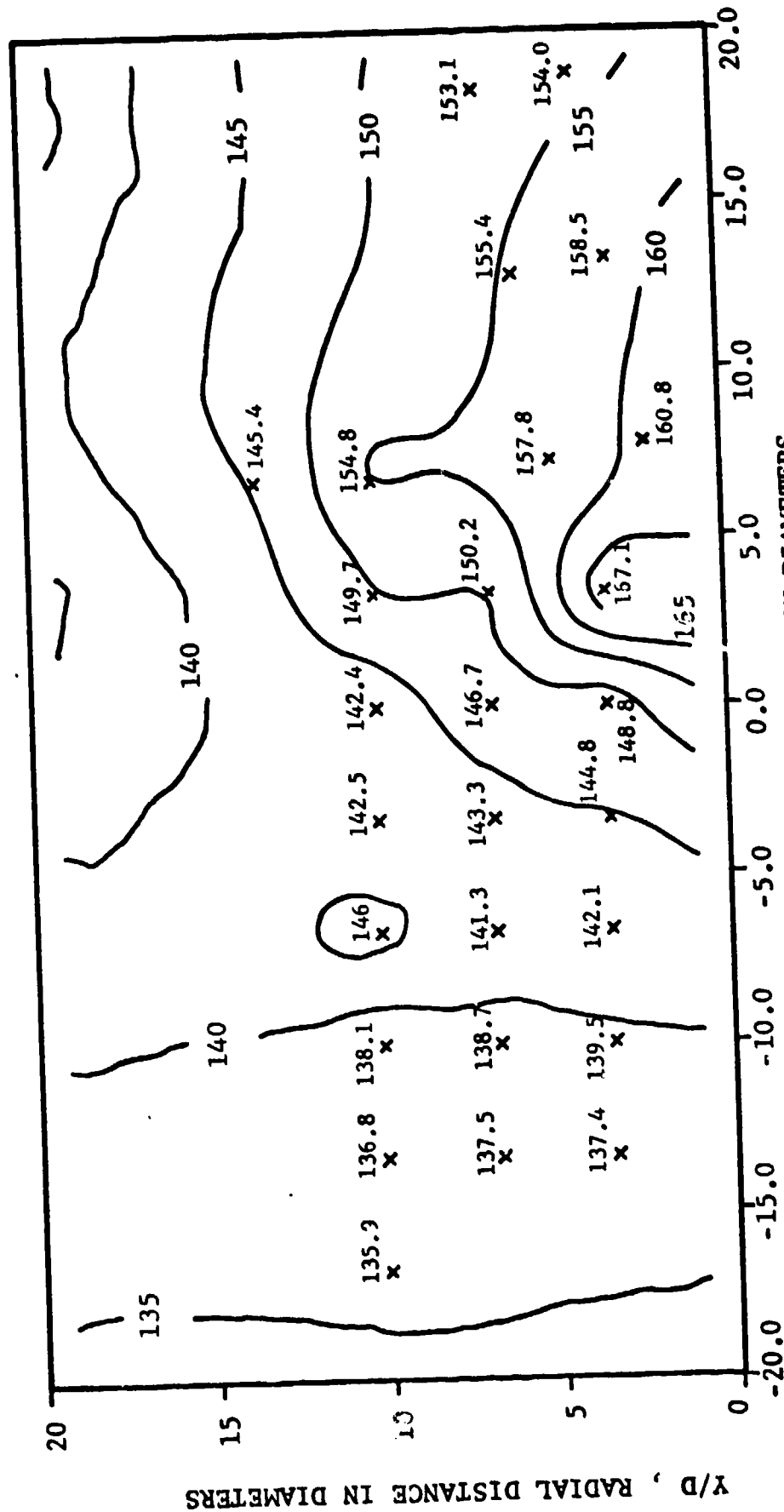
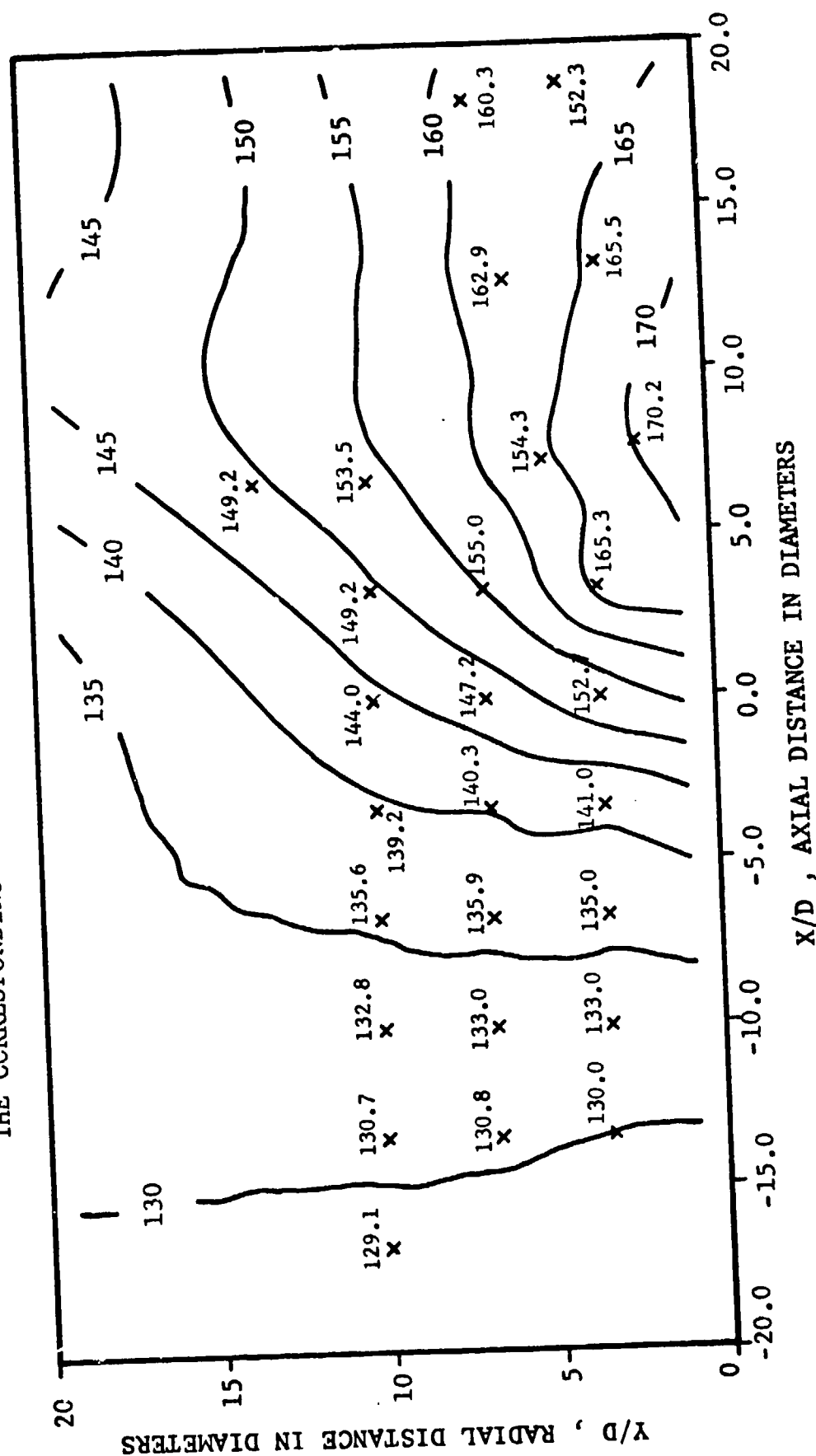


FIGURE 10 - OVERALL SOUND PRESSURE LEVEL CONTOURS FOR GE4 ENGINE  
 $M=1.46$  ;  $T_t=3000^\circ R$  ; MEASURED DATA

NOTE: THE NUMBERS BELOW DENOTE THE PREDICTED VALUES.  
THE CORRESPONDING MEASURED VALUES ARE SHOWN IN FIGURE 10.



OVERALL SOUND PRESSURE LEVEL CONTOURS FOR GE4 ENGINE  
M=1.46 ;  $T_t=3000^\circ R$  ; ISOTROPIC TURBULENCE MODEL

FIGURE 11 -

NOTE: THE NUMBERS BELOW DENOTE THE PREDICTED VALUES.  
THE CORRESPONDING MEASURED VALUES ARE SHOWN IN FIGURE 10.

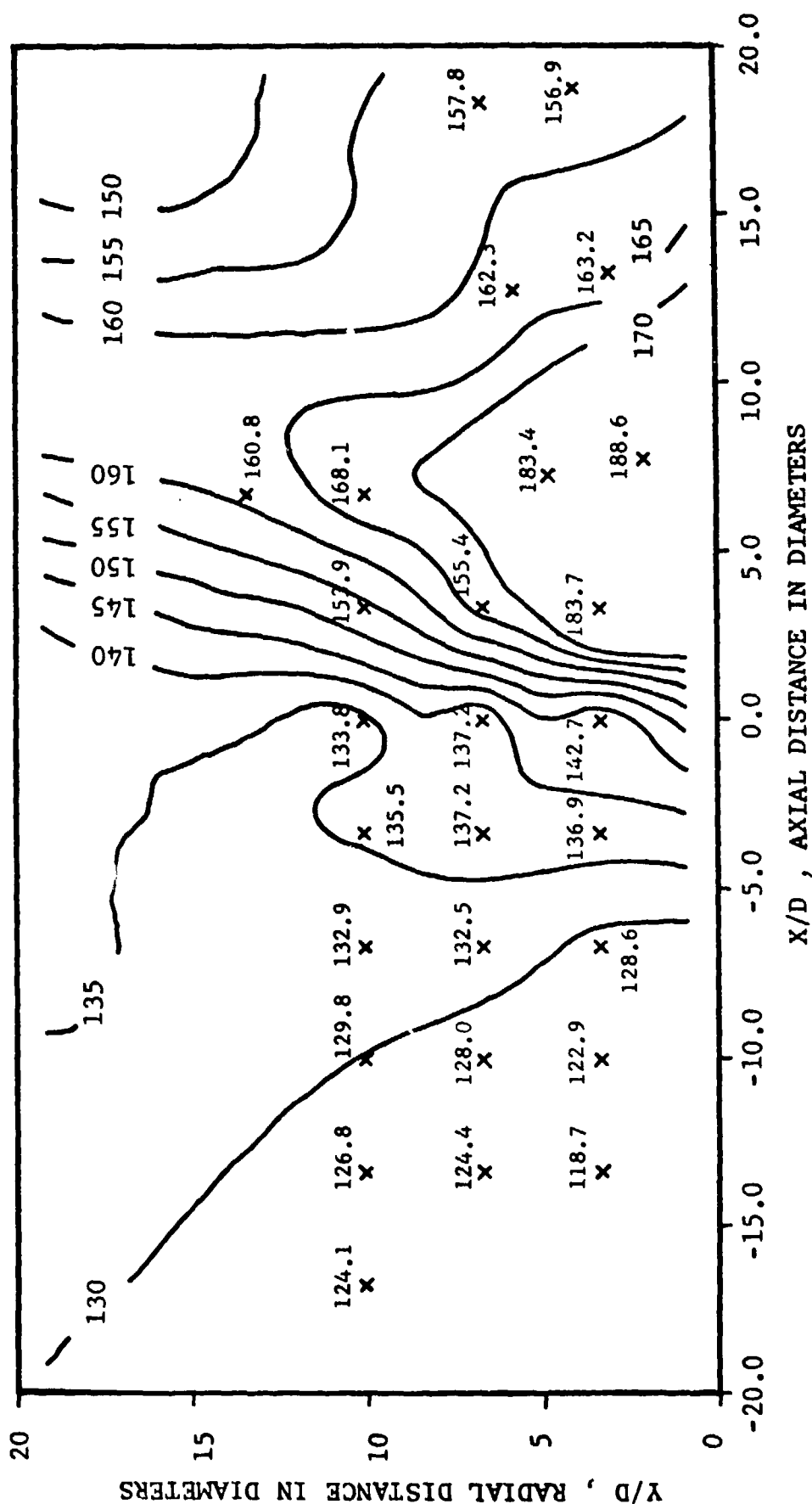


FIGURE 12 - OVERALL SOUND PRESSURE LEVEL CONTOURS FOR GE4 ENGINE  
M=1.46 ;  $T_t=3000$  °R ; LATERAL QUADRUPOLE MODEL

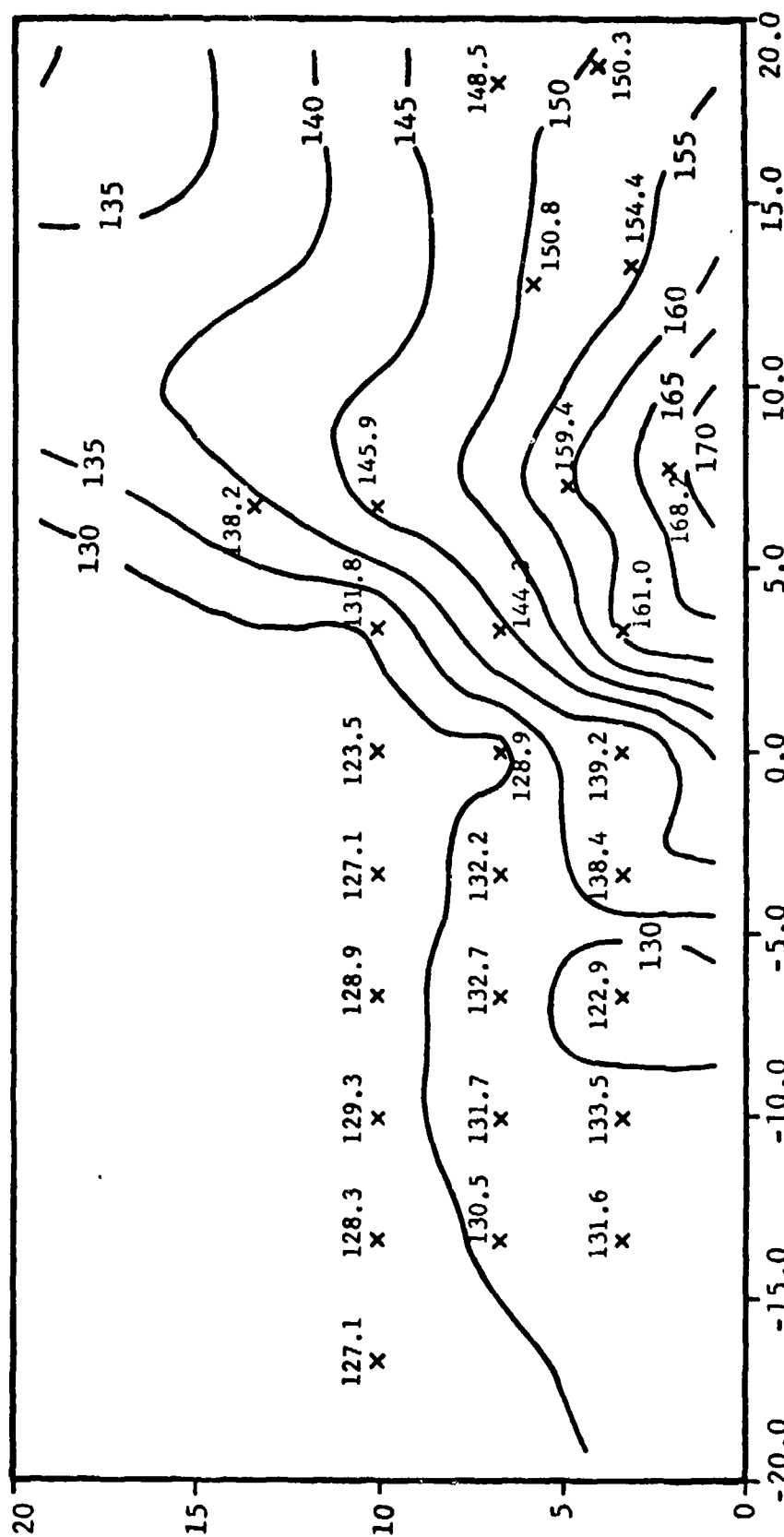


FIGURE 13 - OVERALL SOUND PRESSURE LEVEL CONTOURS FOR GE4 ENGINE  
M=1.46 LONGITUDINAL

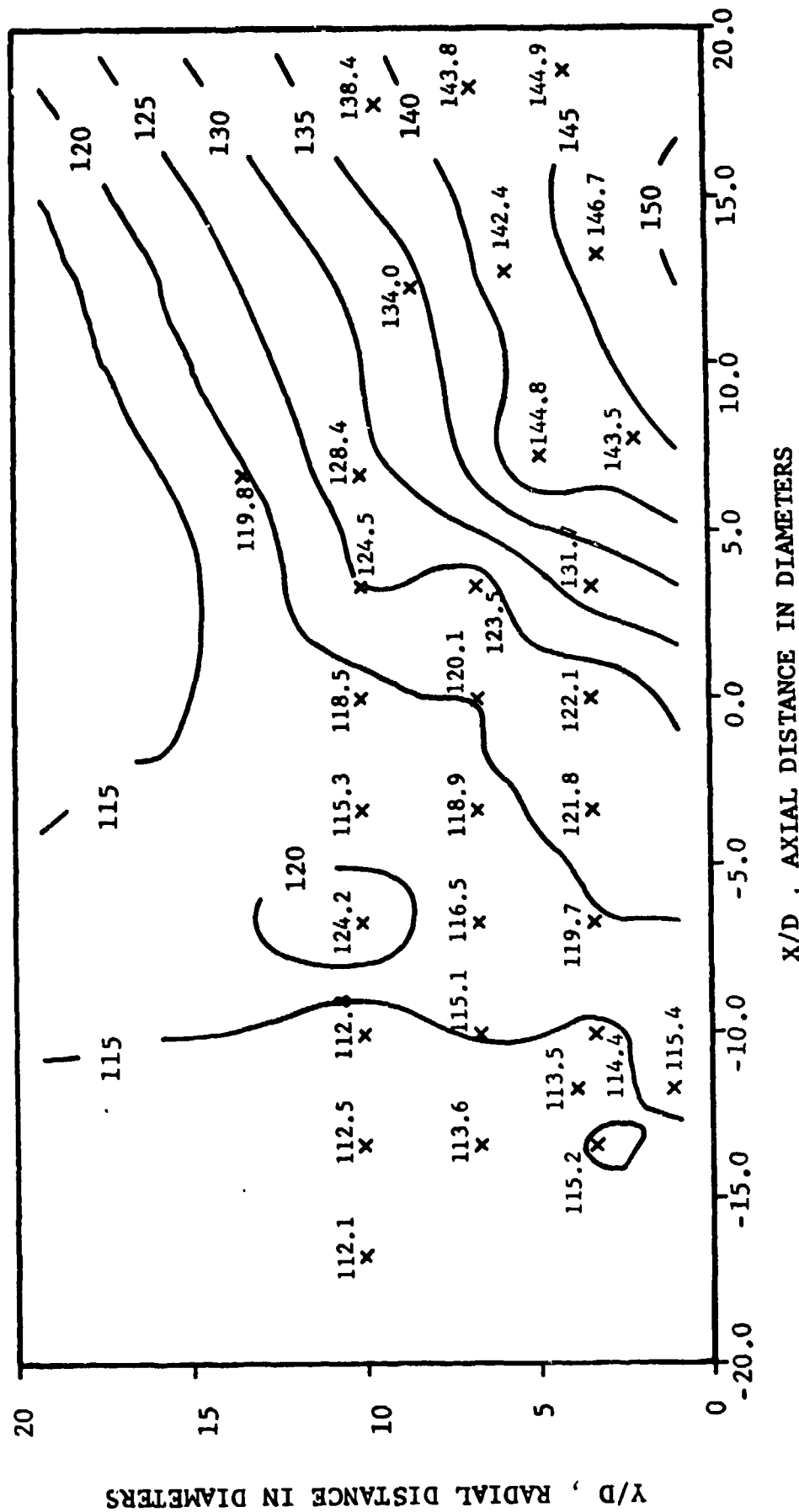


FIGURE 14 - 1/3 OCTAVE BAND SOUND PRESSURE LEVEL CONTOURS FOR GE4 ENGINE  
 $M=1.46$  ;  $T_t=3000^\circ R$  ; CENTRAL FREQUENCY=100 Hz

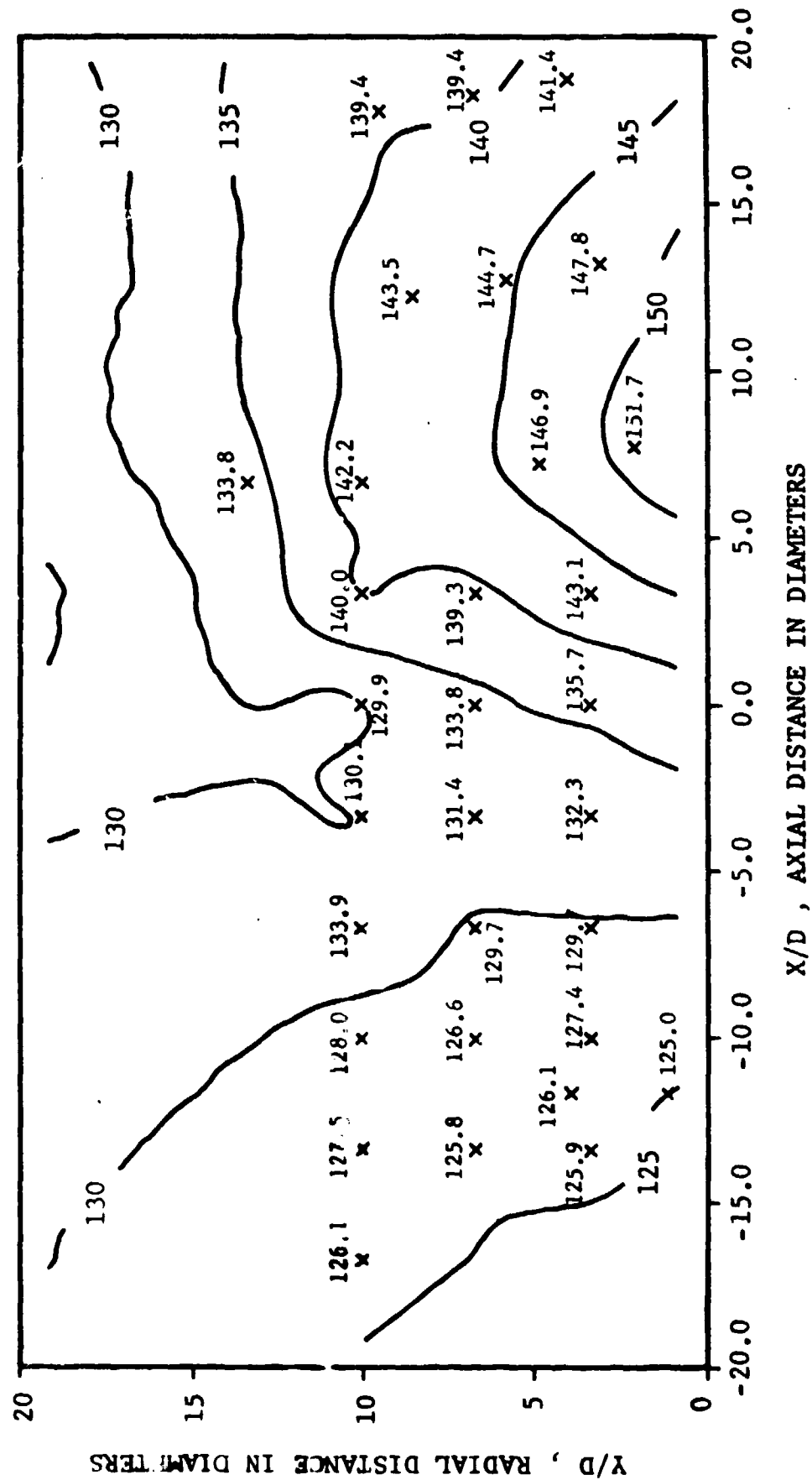
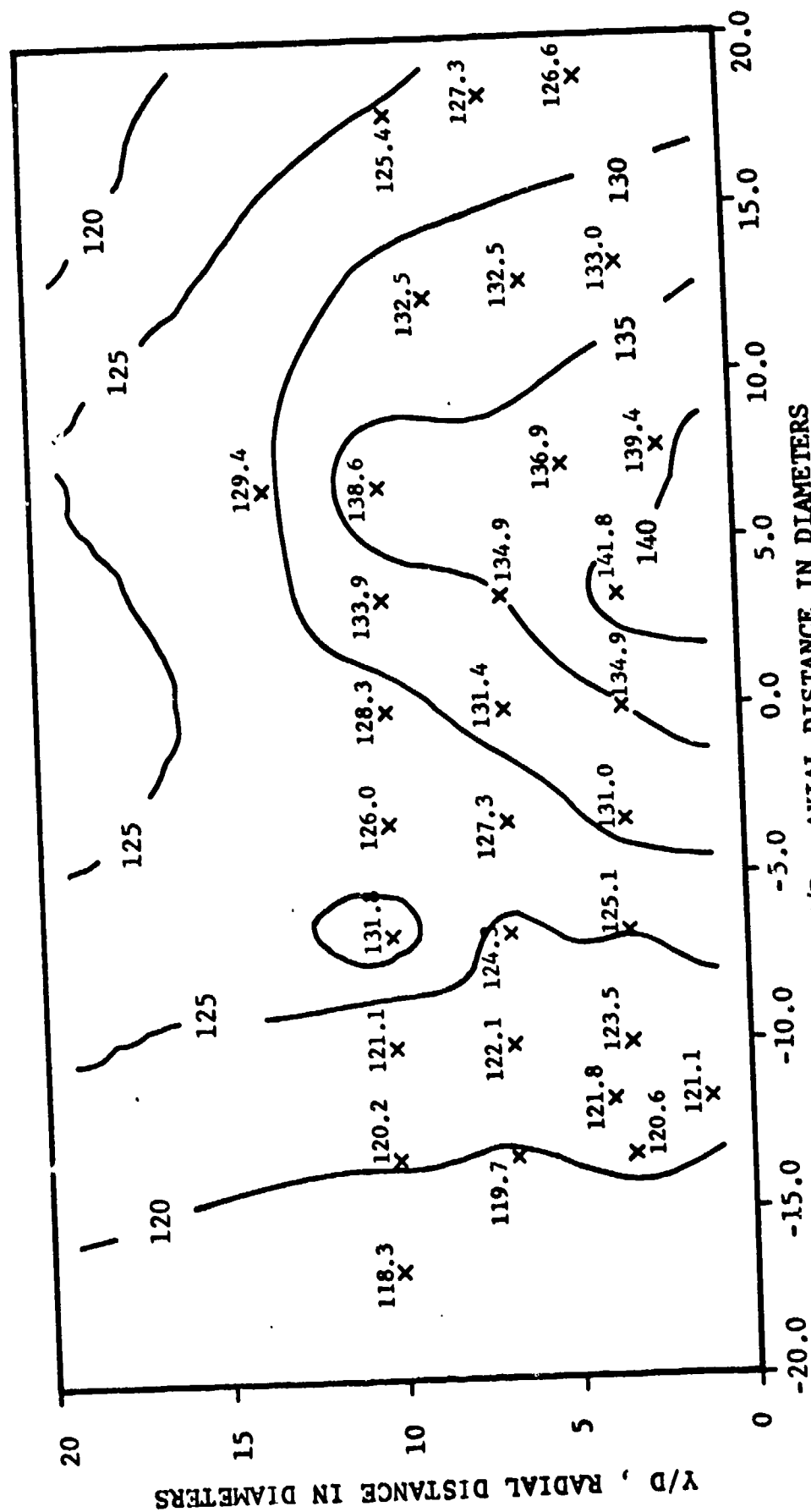


FIGURE 15 - 1/3 OCTAVE BAND SOUND PRESSURE LEVEL CONTOURS FOR GE4 ENGINE  
 $M=1.46$  ;  $T_t=3000$  °R ; CENTRAL FREQUENCY=400 Hz





X/D , AXIAL DISTANCE IN DIAMETERS  
 1/3 OCTAVE BAND SOUND PRESSURE LEVEL CONTOURS FOR GE4 ENGINE  
 $M=1.46$  ;  $T_t=3000^\circ R$  ; CENTRAL FREQUENCY=6300 Hz

FIGURE 17 -